EFFECTS OF BIOGEOCHEMICAL AND PHYSICAL PROCESSES ON THE TRANSFORMATION OF TRACE METALS AT OXIC-ANOXIC INTERFACES IN AQUATIC SYSTEMS

A Dissertation
Presented to
The Academic Faculty

by

Stephanie Stacey Chow

In Partial Fulfillment
Of the Requirements for the Degree
Doctor of Philosophy in the
School of Earth and Atmospheric Science

Georgia Institute of Technology

December 2007

EFFECTS OF BIOGEOCHEMICAL AND PHYSICAL PROCESSES ON THE TRANSFORMATION OF TRACE METALS AT OXIC-ANOXIC INTERFACES IN AQUATIC SYSTEMS

Approved by:

Dr. Martial Taillefert, Advisor
School of Earth and Atmospheric Sciences
Georgia Institute of Technology

Dr. E. Michael Perdue
School of Earth and Atmospheric Sciences
Georgia Institute of Technology

Dr. Andrew G. Stack
School of Earth and Atmospheric Sciences
Georgia Institute of Technology

Dr. George W. Luther, III
College of Marine and Earth Studies
University of Delaware

Dr. Ellery D. Ingall
School of Earth and Atmospheric Sciences
Georgia Institute of Technology

Date Approved: November 14, 2007

To my entire family

For whom my world revolves

Above all, Mike, Zack, and Natalie

ACKNOWLEDGEMENTS

This thesis has been a collaborative effort of several people I would like to recognize for their contributions and guidance for this achievement. First, I wish to thank Dr. Martial Taillefert for giving me the opportunity to work with him on all these exciting projects, for his expertise, and endless support, and most of all his friendship. I will always remember his kind and encouraging words just seconds before my first presentation at a national meeting. A special thank you goes to my committee members, Dr. George Luther, Dr. Mike Perdue, Dr. Andrew Stack, and Dr. Ellery Ingall, for their insightful comments regarding this dissertation and throughout the years. To the dedicated ladies and gentlemen of the EAS administrative and computing team, your assistance and support was invaluable. To my fellow graduate students in EAS, BIO, and CEE, as well as Meg Grantham, Dr. Stephany Rubin and Mike Mason, who made work enjoyable with their friendship and guidance in the lab and in life. To my fellow doctoral candidates, especially JFK, Jud, Steve, Rick, Arsineh, Venus, Poulomi, Tatiana, Cynthia, Rob, and Jason, you have enriched my life with your friendship and perceptive inquiries - the foundation of inspirational professors. To past and current members of the Taillefert Group, especially Beth (my guardian), NuNu (my buddy), Melanie (my sanity), Gwen (my conscience), and Morris (my interpreter), not only for your wisdom, but for your humor, empathy, and compassion - and I can not thank you enough. To my entire family - all the Chows, Knoths, Woodens, Roberts, Hoos, and significant others, I am grateful for their endless encouragement. I would like to thank my parents for always believing in my abilities and for giving me seven incredibly smart and loving siblings, who continue

to teach me by example. Mom, Dad, Mike, Lisa, Laurie, Larry, John, Stephen, and Chris- thank you for always challenging me and for loving me even when I returned the favor. To Pearl, Tommy, Iraj, Ralph, Grace, Karen, Dan, Kathy, Casey, and Sarah – thank you for your embrace, guidance, and understanding. I am so proud of my nieces and nephews, JD, Jaime, Mishi, Justin, Bobby, Garrett, Alexis, Chris, and Jade, and look forward to cheering you at your graduations. My appreciation is endless to Aunt Marylee and Uncle Mike, whose support, love, and spontaneous babysitting was crucial for managing this dissertation with a growing family. To Zack and Natalie- my perfect babies, thank you for being such wonderful kids and for putting up with all the long hours, you two make my heart smile. Last, but definitely not least, I would like to thank my husband Mike for his love, patience, encouragement, wit, and strength. He is the reason I am here, and through his unwavering faith that I belonged here, we made it through this dissertation as a family. I am lucky and forever grateful to have found someone like you.

TABLE OF CONTENTS

Page

LIST OF TABLES

Page

LIST OF FIGURES

Page

SUMMARY

Trace metals (e.g. Fe, Mn, Zn, Cu, Cd, Ni) are important micronutrients that have historically been regarded as toxic pollutants rather than essential components of riverine and estuarine environments. The toxicity and behavior of trace metals, in response to physical and biogeochemical processes, are determined by their individual physico-chemical properties. In this dissertation, the vertical transformation of trace metals across oxic-anoxic interfaces was investigated at two sites, a Fe-rich freshwater river with minimal sulfide and an estuary with elevated Mn and $\sum H_2S$ concentrations.

Sediment profiles obtained from the Chattahoochee River showed that dissolved arsenic, present as As(V) only, is scavenged by Fe-oxides and accumulates directly below the sediment-water interface. Depth profiles also indicate that As(V) fluxes into the overlying water during baseflow conditions as well as after storm events. The significant correlation between Fe(II) and As(V) suggest that As(V) is released from Fe-oxides during their microbial reduction. By implementing a series of sediment incubations under increasing As(V) loads, it was determined that adsorption onto Fe-oxides and microbially mediated reductive dissolution of these mineral phases drive arsenic cycling in this sediment. These incubations also reveal for the first time that arsenic, even in low concentrations, impacts iron cycling by stimulating anaerobic respiration of Fe-oxides and promoting recrystallization of authigenic Fe-oxides, up to a toxicity threshold up to a few micromolar in concentrations.

A combination of *in situ* measurements with discrete water sampling was utilized to determine the effects of tidal cycling on the distribution of trace metals under changing redox conditions during two consecutive tidal cycles at Station 858 in the Chesapeake

Bay. Estuarine circulation patterns driven by tidal oscillations, a defined pycnocline, and the shallow sill (~20 m) of the Chesapeake Bay promoted bottom water anoxia during the summer months that allowed dissolved sulfide and reduced manganese to accumulate below the oxycline. The distribution of barium (conservative freshwater tracer) and uranium (conservative seawater tracer) across the pycnocline over the two tidal cycles indicated that the source of dissolved species was surficial sediments. During ebb and flood tides, the shear stress from the bottom waters flowing over the sediment seems to episodically promote the advection of porewaters enriched in dissolved sulfide, manganese, uranium, barium, lead, chromium, and copper. The selective enrichment of these trace metals appears to be controlled by their reactivity with sulfide. In turn, cobalt and nickel are retained in sediments by adsorbed or incorporated in FeS and FeS_2, while arsenic co-precipitates with sulfide or iron sulfide minerals. Overall, this study demonstrates that natural aquatic systems are complex environments where the interplay between biological, chemical, and physical processes affects the distribution of trace metals over short time scales. While a great wealth of knowledge can be obtained by laboratory experiments with synthetic solutions or pure cultures of organisms, a combination of *in situ* measurements and incubations with real samples is necessary to characterize the processes regulating the cycling of trace metals in aquatic systems.

CHAPTER 1

INTRODUCTION

1.1 Trace Metals in Aquatic Environments

Trace metals are potential contaminants that are often toxic in low concentrations, yet some (for example, cobalt, copper, zinc, nickel, and molybdenum) are nutrients. The toxicity, fate, and transport of trace metals are determined by their individual physico-chemical properties. Therefore, it is important to understand the interdependence of physical, chemical, and biological processes on trace metal transformations across oxic-anoxic interfaces in order to predict their behavior and define remediation strategies. Several studies characterize trace metal distribution, uptake, and transport in natural aquatic systems (e.g. Matisoff et al., 1975; DeGroot et al., 1976; Li et al., 1984; Kuwabara and Baker, 1993; Knight and Pasternack, 2000; Turner and Millward, 2002).

Dissolved and particulate trace metals are introduced into aquatic systems by atmospheric deposition, runoff and riverine inputs (Figure 1.1). In the dissolved phase, trace metals are mainly in the form of free metal ions as well as inorganic and organic complexes. In oxic waters, trace metals are typically scavenged by particles of both biogenic (phytoplankton and biological debris) and inorganic (e.g. aluminum, manganese and iron oxides) composition. When particles settle to the sediment-water interface (SWI), trace metals are efficiently removed from surface waters (Kuwabara and Baker, 1993; Knight and Pasternack, 2000; Turner and Millward, 2002). In both freshwater and

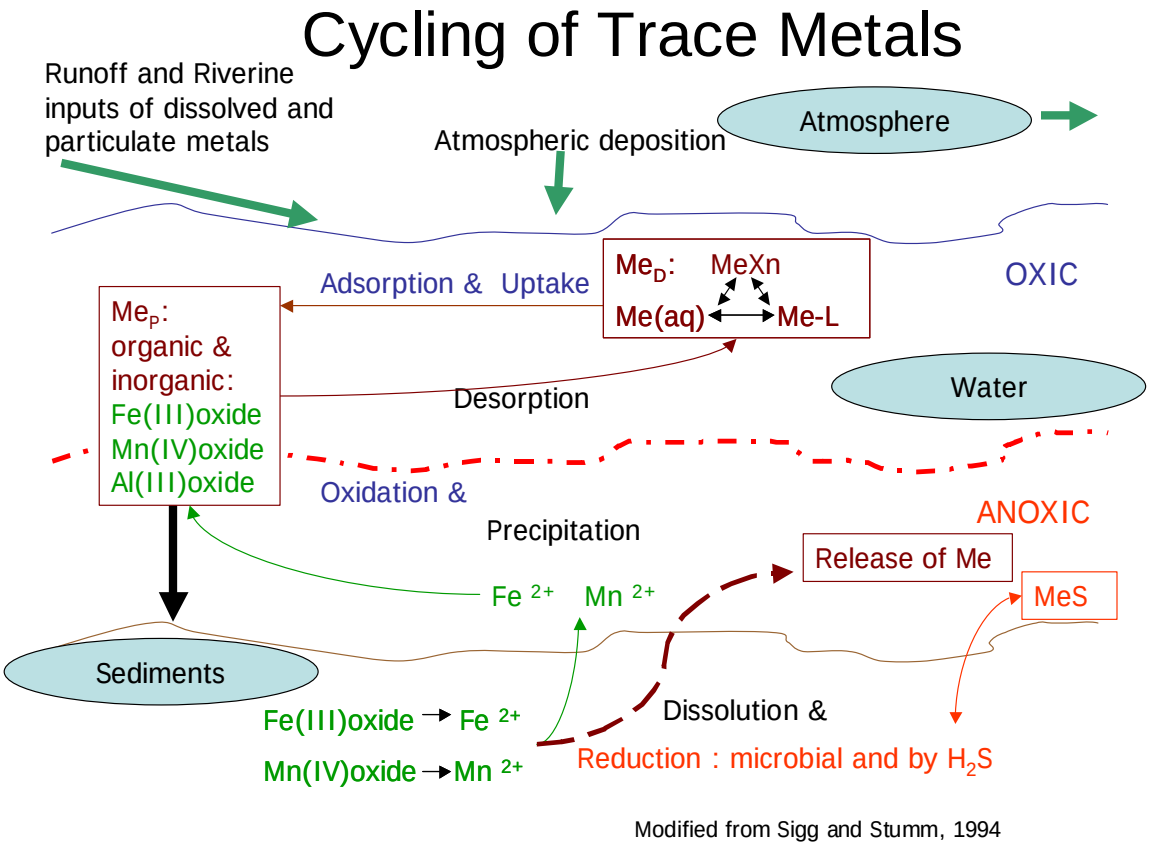

Figure 1.1- Schematic of the general trace metal cycle. Trace metals may enter aquatic systems from atmospheric deposition, runoff, and riverine inputs as dissolved or particulate metals. Dissolved trace metals can be adsorbed onto metal oxides or uptaken by organisms. As particulate metals, they may settle through anoxic conditions to sediments where trace metals may be released by reductive dissolution, then available for precipitation or recycling.

marine systems, biological and chemical consumption of oxygen with depth typically results in the formation of a vertical oxycline when waters are stagnant or stratified. In response to this redox change, the microbial community composition shifts to take advantage of the reduction of a characteristic sequence of chemical substrates coupled with organic matter oxidation (NO_3^-/NO_2^-, Mn(IV)/Mn(III), Fe(III), SO_4^{2-}) (Froelich et al., 1979). As a result, under anoxic conditions, iron and manganese oxides may undergo microbial or chemical reductive dissolution. As their geochemical carriers undergo this transformation, trace metals may be released which are then free to precipitate or complex with sulfides, if sulfidic conditions have developed. Large reservoirs of these potentially toxic metals are stored in underlying sediments and may be mobilized depending upon composition and hydrology of overlying waters.

This dissertation explores the vertical transformation of redox-sensitive trace metals across oxic-anoxic interfaces in response to physical and biogeochemical processes in both a freshwater sediment and an estuarine water column. At these dynamic interfaces, the chemical and biological processes described above are intertwined with physical processes (advection, dispersion, and coagulation), often controlling temporal and spatial (vertical and horizontal) distribution of both chemical and biological species (Matisoff et al., 1975; Harris et al., 1975; DeGroot et al., 1976; Li et al., 1984; Bruland et al., 1991; Cutter, 1991; Kuwabara and Baker, 1993; Jonas, 1997; Cooper and Morse, 1998; Jones et al., 1998; Breitburg et al., 1999; Knight and Pasternack, 2000; Turner and Millward, 2002, Caccia et al., 2003; Bratton et al., 2003; Kemp et al., 2005; Li et al., 2005).

A major challenge for trace metal research in natural aquatic environments is the development of quantitative tools to predict changes in trace metal speciation in response to chemical, physical, and biological variations over a wide range of spatial and temporal scales. Improving the state of knowledge about trace metals in shifting redox transitions located within water columns and sediments requires the development of innovative data acquisition, analysis, and modeling techniques. In both studies, depth profiles of redox species were measured voltammetrically using a combination of *in situ* and *ex situ* techniques. These data were utilized to determine redox zonation at high (mm) spatial resolution and target chemically significant strata for discrete analyses of porewater in freshwater sediments, as well as water and suspended particulate matter (SPM) in an estuarine water column. Depending on the nature of the study, complementary analytical tools such as Ion-Chromatography (anions), Inductively Couple Plasma-Mass Spectroscopy (dissolved and particulate trace metals), and Hanging Mercury Drop Electrode (arsenic speciation) were used to assess biogeochemical processes. This chapter (Chapter 1) provides background information and motivations for the two different investigations compiled as part of this dissertation. Chapters 2 and 3 focus on the redox transformation of iron and arsenic in the sediment of the Chattahoochee River (GA). Chapter 4 investigates the effect of tidal forcing on the dynamics of trace metals in Northern Chesapeake Bay. Chapter 5 synthesizes and concludes on the effects of biogeochemical and physical processes on the transformation of trace metals at the oxic-anoxic interfaces in aquatic systems.

1.2 Arsenic Diagenesis at the Sediment-Water Interface of a Recently Flooded Freshwater Sediment

The poisonous effects of arsenic have been known for several centuries, yet when an estimated 80 million people in West Bengal India and Bangladesh were subjected to elevated doses (10-5,000 μg/L) in their drinking water, The Arsenic Crisis[1] raised global concerns regarding its toxicity and possible carcinogenic effects (Feeney and Kounaves, 2000). Even today, elevated arsenic levels in drinking and irrigation water remain an issue for many citizens, rich and poor, living in this region as well as many others throughout the globe. Arsenic can be present in water, soils, and sediments, and in the atmosphere. Reported regions impacted by elevated arsenic are Bangladesh, China, India, England, Thailand, and within the United States (i.e., Florida, New Hampshire, New Mexico, Massachusetts, Maine, Michigan, California, and Oregon). This worldwide concern about arsenic in natural environments triggered years of debates in the US that led to lowering the drinking water standard for total dissolved arsenic from 50 ppb to 5 ppb and forcing all US public drinking water systems to comply to 10 ppb (133 nM) (www.epa.gov/safewater). Nonetheless, regions where water recharge and storage are within geologic terrains containing arsenic-bearing minerals still report enrichments. For instance, an Aquifer Storage and Recovery system (pumping during low demand periods into groundwater for extraction during peak season) in Florida recently triggered the dissolution and oxidation of arsenic bearing minerals, a similar mechanism that caused

[1] *The Arsenic Crisis*-West Bengal and Bangladesh, over the last two decades untreated tube well water was heavily promoted and developed as a safe and environmentally acceptable alternative to microbiologically unsafe untreated surface water. In the 1980s, scientists began finding evidence of arsenic contamination. The origin of the arsenic pollution is geological in this case - the arsenic is released to groundwater under naturally occurring aquifer conditions. (http://bicn.com/acic/)

the crisis in West Bengal and Bangladesh. Clearly, arsenic is a drinking water contaminant of major concern, and its fate in aquatic systems has recently been the subject of intense research (Oremland and Stolz, 2003; Horneman et al., 2004; O'Day et al., 2004; Oremland and Stolz, 2005). The toxicity of arsenic is related to its oxidation state (Slotnick et al., 2006), and its mobility in reduced conditions is controlled by the biogeochemical cycling of iron and sulfide (O'Day et al., 2004). Figure 1.2 depicts the dominant arsenic and iron forms over changing pH and pE assuming equilibrium, a total arsenic concentration of 1×10^{-4} M, and total iron concentration of 2×10^{-3} M. In natural environments, arsenite (As(III)) is not only more mobile but can be greater than 60 times more toxic than arsenate (As(V)) salts, or organoarsenic compounds (Feeney and Kounaves, 2000; Ryu et al., 2002). The presence of these species in the environment is due to both natural and anthropogenic sources. In general, arsenic may be removed from water through adsorption onto solid surfaces (i.e., metal oxides), and released from sediments through reductive dissolution of the host geochemical carrier or through competitive ligand exchange reactions (Figure 1.3). If co-ions (i.e., phosphate and carbonate) are present, the residence time of arsenic is shortened when it is released (desorbed) in the aqueous phase. Phosphorous and arsenic are both Group 5A elements and thus they form species that have similar chemical properties. For example, phosphate and arsenate both have similar structures and affinities for protons. The affinity of phosphate and arsenate for mineral surfaces (e.g. metal oxide surfaces) depends on the electrostatic interaction with the charged surface as well as the complexing capacity of the anion, which allows binding to surface groups by ligand

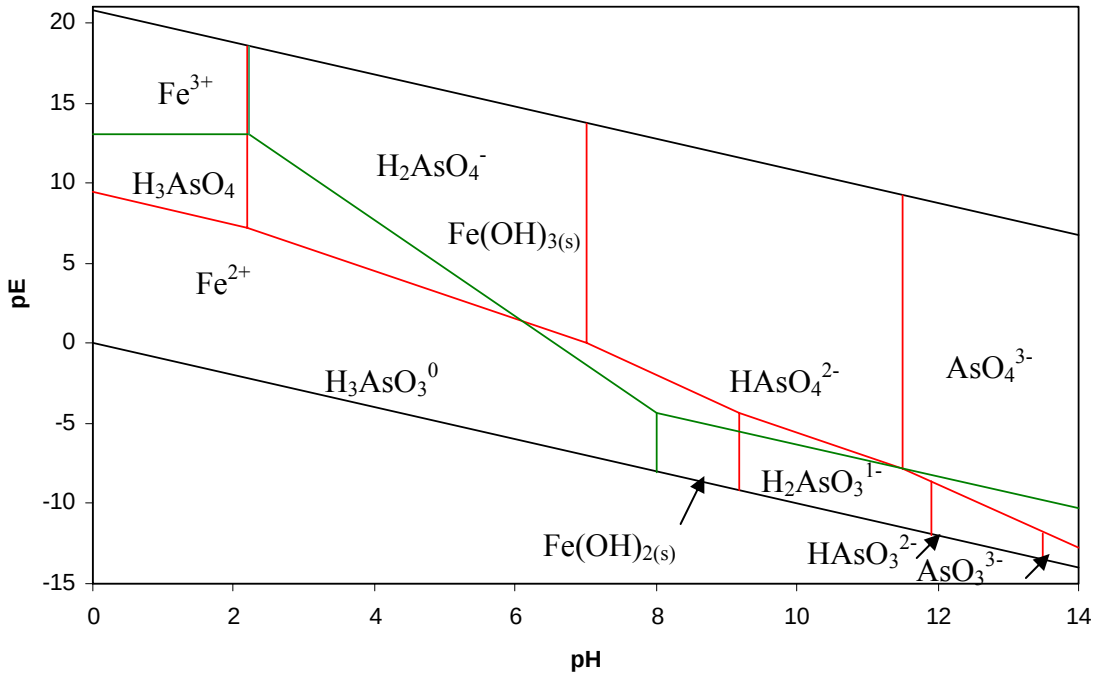

Figure 1.2- pE-pH diagram for As-Fe-H_2O systems (25°C). Total As = 1 x 10^{-4} M and total Fe = 2 x 10^{-3} M. As (red) and Fe (green) lines refer to the equilibria calculated using equations listed in Table 1.1.

Table 1.1 Thermodynamic data for arsenic and iron species

Reaction	log K	notes	ref.
Aqueous arsenic species			
$H_2AsO_3^- + 0.5\ O_{2(aq)} = H_2AsO_4^-$	30.53		1
$H_3AsO_{4(aq)} = H_2AsO_4^- + H^+$	-2.30	a	1
$H_2AsO_4^- = HAsO_4^{2-} + H^+$	-6.99	a	1
$HAsO_4^{2-} = AsO_4^{3-} + H^+$	-11.50	a	1
$H_3AsO_{3(aq)} = H_2AsO_3^- + H^+$	-9.17	a	1
$AsO_4^{3-} + 2\ H^+ = H_2AsO_4^-$	18.80	a	1
$HAsO_3^{2-} + H^+ = H_2AsO_3^-$	14.1	a	1
$AsO_3^{3-} + 2\ H^+ = H_2AsO_3^-$	29.1	a	1
$AsS(OH)(SH)^- + 2\ H_2O = H_2AsO_3^- + 2\ HS^- + 2\ H^+$	-27.19		1
$As_3S_4(SH)_2^- + 9\ H_2O = 3\ H_2AsO_3^- + 6\ HS^- + 8\ H^+$	-99.78		1
Arsenic and iron redox reactions			
$H_3AsO_4^0 + 2H^+ + 2e^- = H_3AsO_3^0 + H_2O$	18.92	a	1
$H_2AsO_4^- + 3H^+ + 2e^- = H_3AsO_3^0 + H_2O$	21.12	a	1
$HAsO_4^{2-} + 4H^+ + 2e^- = H_3AsO_3^0 + H_2O$	28.12	a	1
$HAsO_4^{2-} + 3H^+ + 2e^- = H_2AsO_3^- + H_2O$	18.94	a	1
$AsO_4^{3-} + 4H^+ + 2e^- = H_2AsO_3^- + H_2O$	30.44	a	1
$Fe^{3+} + e^- = Fe^{2+}$	13.04	a	3
$Fe(OH)_{3(s)} + 3H^+ + e^- = Fe^{2+} + 3H_2O$	16.58	a	3
$Fe(OH)_{3(s)} + H^+ + e^- = Fe(OH)_{2(s)} + H_2O$	3.68	a	3
Arsenic and iron surface complexation			
$>FeO^- + H^+ = >FeOH$	8.93		2
$>FeOH_2^+ = >FeOH + H^+$	-7.29		2
$>FeH_2AsO_3 + H_2O = >FeOH + H_3AsO_{3(aq)}$	-5.41		2
$>FeH_2AsO_4 + H_2O = >FeOH + AsO_4^{3-} + 3\ H^+$	-29.31		2
$>FeHAsO_4^- + H_2O = >FeOH + AsO_4^{3-} + 2\ H^+$	-23.51		2
$>FeOHAsO_4^{3-} = >FeOH + AsO_4^{3-}$	-10.58		2
Arsenic and iron solids			
$As_{(s)} + 1.5\ H_2O + 0.75\ O_{2(aq)} = H^+ + H_2AsO_3^-$	42.80		1
Arsenolite (As_2O_3) + $3\ H_2O = 2\ H_2AsO_3^- + 2\ H^+$	-19.72		1
Claudetite (As_2O_3) + $3\ H_2O = 2\ H_2AsO_3^- + 2\ H^+$	-19.75		1
$As_2O_{5(s)} + 3\ H_2O = 2\ H^+ + 2\ H_2AsO_4^-$	3.65		1

Realgar (AsS) + 2.5 H_2O + 0.25 $O_{2(aq)}$ = $H_2AsO_3^-$ + 2 H^+ + HS^-	-7.8		1
Orpiment (As_2S_3) + 6 H_2O = 2 $H_2AsO_3^-$ + 3 HS^- + 5 H^+	-64.6		1
$As_2S_{3(am)}$ + 6 H_2O = 2 $H_2AsO_3^-$ + 3 HS^- + 5 H^+	-63.2		1
Fe^{3+} + 3H_2O = $Fe(OH)_{3(s)}$ + 3H^+	-3.54	a	3
Fe^{2+} + 2H_2O = $Fe(OH)_{2(s)}$ + 2H^+	-12.9	a	3

Reactions were written in terms of the basic species $H_2AsO_3^-$, $H_2AsO_4^-$, Fe^{2+}, Fe^{3+}, H^+, $O_{2(aq)}$, SO_4^{2-}, HS^-, >FeOH, and H_2O, and equilibrium constants at 25°C.

(a) equations and log K used to calculate equilibria lines for Figure 1.2.

1. Nordstrom, D. K. and Archer, D. G. (2003) in *Arsenic in Groundwater*, eds. Welch, A. H. and Stollenwerk, K. G. (Kluwer, Boston), 1–25.

2. Dzombak, D. A. and Morel, F. M. M. (1990) *Surface Complexation Modeling* (Wiley, New York).

3. Stumm, W. and Morgan, J.J. (1996) *Aquatic Chemistry* (Wiley, New York).

exchange reactions. The competitive adsorption of phosphate and arsenate on synthetic goethite (α-Fe-OOH) has been compared in a few articles (Manning and Goldberg, 1996; Gao and Mucci, 2001; Violante and Pigna, 2002; Antelo et al, 2005), with mixed conclusions. The adsorption of phosphate and arsenate on goethite decreased in 0.7 M NaCl solutions between the pH ranges of 3 to 10 (Gao and Mucci, 2001). In 0.1 M NaCl solutions, however, the affinity of As(V) was lower than that of phosphate for goethite, especially in the circum-neutral and alkaline pH range (Manning and Goldberg, 1996). In general, phosphate is more sensitive to changes in pH and ionic strengths resulting in lower phosphate adsorption in basic pH ranges and solutions of low ionic strengths, yet higher adsorption is acidic solutions. Meanwhile, As(V) adsorption is almost independent on the electrolyte concentrations. While As(V) may compete with phosphate for adsorption sites, it is important to investigate arsenic speciation under reducing conditions due to the mobility and toxicity of As(III).

In rivers and lakes, particle reactivity impacts the persistence and mobility of arsenic (e.g., Bose and Sharma, 2002). In iron-dominated systems, arsenic is removed by adsorption onto iron oxides (Pierce and Moore, 1982) and is generally released in solution during the reductive dissolution of iron oxides (Guo et al., 1997). As a consequence, a strong correlation is evident between the dissolution of iron oxides and the release of arsenic in freshwater sediment (Aggett and O'Brien, 1985). When dissolved sulfide concentrations dominate in anoxic waters, sulfide precipitates arsenic-sulfide minerals. However, if iron concentrations are much higher than sulfide levels, sequestration of arsenic is controlled by iron because aqueous sulfide is rapidly depleted during the formation of FeS and pyrite (Rochette et al., 2000).

The following is a schematic of arsenic redox cycling at circum-neutral pH:

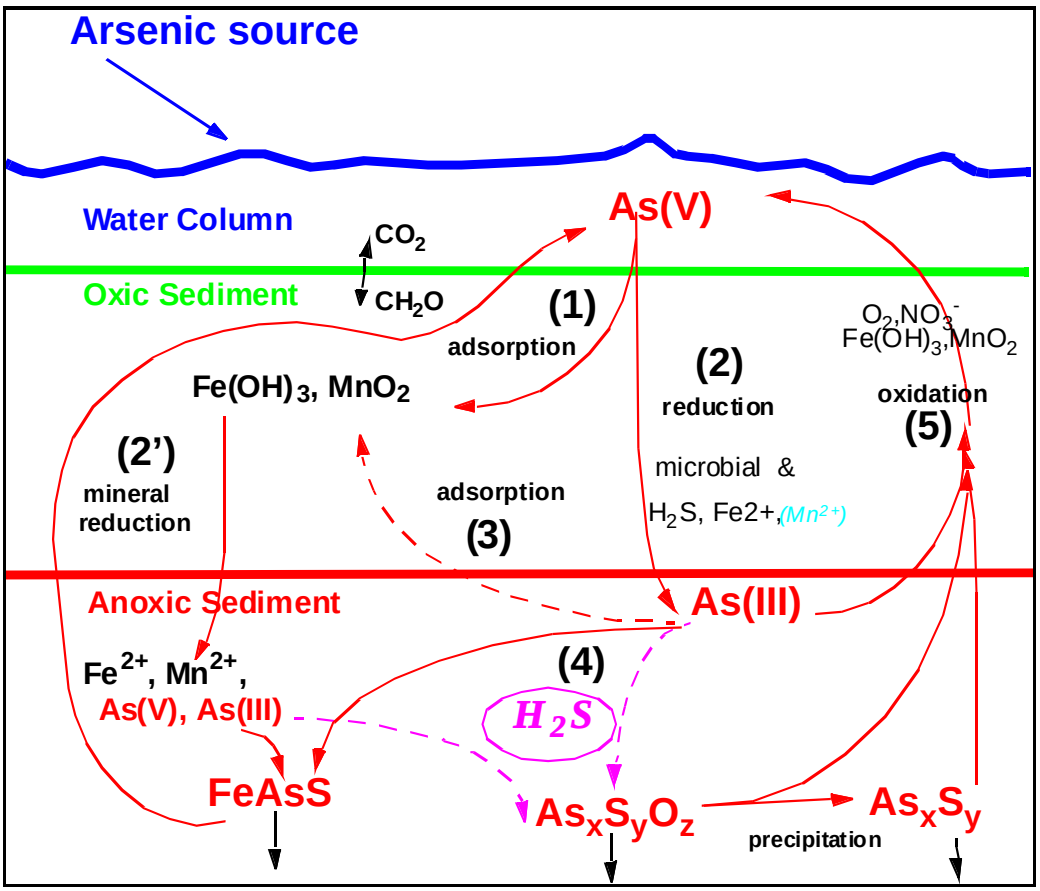

Figure 1.3- General Arsenic Cycle: As(V) can be adsorbed onto metal oxides (1) or reduced by H_2S, or microorganisms (2). The metal oxides, with the sorbed As(V), may undergo reduction (2') and release Fe^{2+}, Mn^{2+}, and arsenate. The arsenate may then be reduced microbially or by H_2S to As(III). As(III) could then be adsorbed onto metal oxides (3) or arsenite may encounter dissolved sulfide (4) and may precipitate to As_xS_y after forming an intermediate As-S-O complex. If the arsenic-bearing complex or mineral is oxidized (5), As(III) is remobilized, and As(V) may be re-cycled.

The investigation of the biogeochemical cycling of arsenic began after a study characterizing transport of coal constituents in the Chattahoochee River demonstrated elevated total As concentrations upstream of a local drinking water reservoir in Westpoint Lake (GA) (Lesley, 2002). Although arsenic levels in the water column are below the public drinking water standards, chronic exposure to sub-acute levels (Jain and Ali, 2000), potentially ingested via water supplies, may represent a danger for local residents.

Depth profiles in the sediment porewaters of the Chattahoochee River (Georgia) suggest that iron oxides scavenge arsenate in the water column and settle to the sediment-water-interface (SWI) where they are reduced by iron reducing bacteria. During their reduction, these particles seem to release arsenic to the porewaters under the form of arsenate only, even though thermodynamic calculations suggest arsenite should be dominant (Figure 1.2). These results suggest either the system was not in equilibrium, common of a natural setting, or the system lacked a suitable microbial or chemical reductant. Arsenate is usually not reduced chemically by any other reductant than sulfide (O'Day et al., 2004), and the presence of arsenite in anoxic, but sulfide-depleted, freshwaters has been attributed to microbial arsenate reduction (Newman et al., 1998; Stolz and Oremland, 1999).

Various biotic pathways have been proposed for dissimilatory arsenate reduction, such as reduction and alkylation (McBride and Wolfe, 1971) and anaerobic respiration coupled to oxidation of natural organic matter or hydrogen, typically observed in the presence of high concentrations of arsenate (Newman et al., 1998; Stolz and Oremland, 1999). For example, the sulfate reducing bacteria, *Desulfotomaculum*, has been found to co-reduce SO_4^{2-} to HS^-, and AsO_4^{3-} to AsO_3^{3-} during respiration. This process promotes

the spontaneous precipitate of a mineral complex of arsenic and sulfide, As_2S_3, both intracellularly and extracellularly (Madigan et al, 2003). In a system with high As(V) concentrations, a decrease in As(V) and As(III) may also indicate assimilation (Newman et al., 1998). Living organisms transport As(V) into cell tissue for assimilation. The dissimilatory microbial reduction of arsenate may occur via a respiratory process. Alternatively, microbial reduction of arsenate may occur through a detoxification process during which organisms do not acquire energy for growth (Saltikov et al., 2005). The structural similarity of arsenate to phosphate has been linked to ATP depletion through the formation of the labile arsenylated compound ADP-As (Mukhopadhyay et al, 2002). So far, it has been shown with a pure culture that arsenate reduction as a detoxification process (e.g. Ars pathway) does not occur below a threshold of around 100 μM arsenate (Saltikov et al., 2005), however As respiration (e.g. Arr pathway) may be triggered at concentrations as low as 100 nM.

The crucial balance between As(III) and As(V) is largely controlled by microbes and reactions with iron and sulfur. Thus, an understanding of freshwater Fe and S cycles is central to determining the long term control and variability of arsenic mobilization. The goals of this study were (1) to describe the biogeochemistry that is physically and chemically affected during arsenic cycling across the oxic-anoxic transition in the water column or sediment and (2) determine the source of arsenic fluxes. The content of Chapter 2 has been published as Chapter 16 in the 915th ACS Symposium Series on Advances in Arsenic Research (Chow and Taillefert, 2005).

1.3 Effect of Arsenic Concentration on Microbial Iron Reduction and Speciation in Freshwater Sediments

Although informative, depth profiles by themselves cannot clearly establish the biogeochemical processes regulating the speciation of arsenic in these sediments. From anoxic vertical profiles it is inferred that the microbial community shifts to take advantage of the reduction of a sequence of chemical substrates coupled with organic matter oxidation producing CO_2 resulting in a net decrease in pH. In addition, the effects of low concentrations of arsenic (i.e., $\leq$ 10 μM) on biogeochemical processes in natural aquatic systems are unknown. More specifically, the effect of the accumulation of low levels of arsenic on microbial iron and manganese reduction in freshwater sediments has not been investigated. In addition, most research on the biogeochemical cycling of arsenic is conducted in the laboratory with elevated concentrations of arsenic (Pierce and Moore, 1982; Cullen, 1989; Belzile and Tessier, 1990; Guo et al., 1997; Kneebone et al., 2002; Ryu et al., 2002; Smedley and Kinniburgh, 2002; Mucci et al., 2003). In this chapter, we report the biogeochemical transformation of arsenic in the iron-rich sediments of the Chattahoochee River (GA). Sediments from the same area were incubated to investigate the impact of arsenate concentrations on the biogeochemical cycling of iron, manganese, and arsenic. The objectives were to characterize sediment composition to help identify dominant biogeochemical processes and implement incubations to determine the effect of arsenic concentrations on microbial processes in these natural sediments. A combination of depth profiles and sediment incubations with different but low arsenic concentrations unravels the effect of arsenic on indigenous

metal-reducing bacteria. The findings of Chapter 3 have been submitted to Environmental Science & Technology.

1.4 Consequences of Tidal Forcing on the Distribution of Trace Metals in the Redox Transition Zone of the Chesapeake Bay

The distribution and partitioning of trace metals in estuaries is a central interest to the understanding of the global cycling and transport of metals (Chiffoleau et al., 1994). In general, trace metals are introduced into estuaries by riverine (Matisoff et al., 1975; DeGroot et al., 1976; Knight and Pasternack, 2000; Mason et al., 2004;) and atmospheric inputs (Scudlark et al., 1994; Hussain et al., 1999; Kim et al., 2000; Scudlark et al., 2005). Estuaries are essentially geochemical reactors whose heterogeneous reactions determine the fate and supply of trace metals of continental origin to the oceans. Dissolved metals are transported to the open ocean while most particulate metals are retained on the continental shelf (Caccia and Millero, 2003). When particle-reactive metals enter estuarine waters, many are rapidly adsorbed on (inorganic and organic) suspended matter (Turner et al., 1998; Turner, 1999; Martino et al., 2002; Turner and Millward, 2002; Turner et al., 2004). As pH and salinity increase along estuaries, suspended matter flocculates and trace metals settle to the sediment (DeGroot et al., 1976; Kuwabara and Baker, 1993; Caccia et al., 2003; Turner and Millward, 2002), where they are either buried or released during the oxidative (POM) or reductive (MnO_X and $Fe(OH)_3$) dissolution of their hosts. In marine sediments, sulfate reduction may further affect the distribution of trace metals by either precipitation of metal sulfide phases or adsorption of trace metals onto $FeS_{(s)}$ and pyrite (MacCrehan and Shea, 1995; Luther et al., 1996; Rickard and Luther, 2003; Rickard et al., 2004; Luther and Rickard, 2005b; Rickard and Luther, 2006; Rickard and Luther, 2007). Although Mn(II) is more reactive to water substitution than Fe(II), and should form its own mineral with sulfide,

MnS is highly soluble and difficult to form, so much so that Mn(II) may be incorporated into pyrite if there is a high degree of pyritization (Morse and Luther, 1999) or be maintained in solution. The rate of water exchange as compared to iron dictates the order of trace metal pyritization for divalent cations in the following order beginning with the fastest (cadmium<lead<zinc<manganese<nickel<cobalt). Thus cobalt and nickel should not form discrete MeS phases and will be incorporated into pyrite due to the slower kinetics of cobalt and nickel substitution for water (Morse and Luther, 1999). In contrast to cobalt and nickel, copper, lead, manganese, and chromium are likely unreactive with respect to iron sulfide minerals due to their higher rate of water exchange (Morse and Luther, 1999), and should preferentially be released in to the overlying waters if sulfide concentrations are below the solubility product of MeS species. Meanwhile, arsenic and chromium are both reduced by sulfide, and As(III) may be co-precipitated with pyrite to form arseno-pyrite, while Cr(III) does not undergo substitution reactions with respect to iron sulfide. In addition, metal sulfide clusters (e.g. FeS, PbS, CuS) may form rapidly and become important transporters of trace metals in anoxic environments (Luther and Rickard, 2005a; Luther and Rickard, 2005b; Burton et al., 2006).

Therefore, variations in oxycline and sulfide-onset have important consequences on the distribution of trace metals in the water column. Manganese and iron cycles are directly affected by these temporal and tidal-related variations in the oxygen and dissolved sulfide levels (Lewis et al., 2007). The influence of tidal variations on the cycling of redox-sensitive elements was investigated in the Chesapeake Bay during the peak anoxic/hypoxic season. This study complements research devoted to monitoring real-time changes in redox stratification during the summer peak anoxic/hypoxic season in Northern Chesapeake Bay from 2002 to 2005 (Lewis et al., 2007).

Chapter 4 focuses on the effect of tidal variations on the redox dynamics of dissolved oxygen, dissolved sulfide, and manganese associated with the transformations of trace metals (e.g. chromium, manganese, cobalt, nickel, copper, barium, arsenic, lead,

and uranium) in the Chesapeake Bay during peak anoxic conditions between the summers of 2002 to 2005. The goals of this study were (1) to describe the biogeochemistry that is physically and chemically affected during tidal cycles across the oxic-anoxic transition in the water column, and (2) to investigate the transformation of a suite of redox-sensitive trace metals during the peak anoxic seasons under tidal forcing. A manuscript with the results of Chapter 4 is in preparation.

CHAPTER 2

ARSENIC DIAGENESIS AT THE SEDIMENT-WATER INTERFACE OF A RECENTLY FLOODED FRESHWATER SEDIMENT

2.1 Abstract

In a previous study, elevated dissolved arsenic concentrations were detected in the Chattahoochee River (GA) and decreased in concentration with increasing distance from a suspected point-source, suggesting that arsenic could be scavenged by particles and settle to the sediment-water interface (SWI). In this study, the distribution of arsenic in sediments was determined to assess its biogeochemical cycling close to the SWI following a high deposition event. A combination of analytical techniques - ICP-MS and voltammetry - was used to measure the speciation of dissolved arsenic in two sediment cores. In addition, the porewater distribution of O_2, Fe(II), Mn(II), and ΣH_2S was measured with Au/Hg voltammetric microelectrodes to obtain high resolution profiles of the redox species involved in arsenic cycling. Our data show that dissolved arsenic is in the form of As(V) only and accumulates directly below the SWI. The significant correlation between Fe(II) and As(V) indicates that As(V) is released from iron oxides during their microbial reduction. These results suggests that sedimentation of As(V) occurring after storm events is followed by remobilization of As(V) in porewaters and upward diffusion, thus recycling arsenic into the overlying water.

2.2 Introduction

The adverse human health effects of arsenic have been known for several centuries. The biochemical behavior and toxicity of arsenic depend on its chemical form. In natural environments, arsenite (As(III)) is more mobile and toxic than arsenate (As(V)), or organoarsenic compounds (Ferguson and Gavis, 1972; Ryu et al., 2002). Most environmental arsenic problems are a result of mobilization under natural conditions (Smedley and Kinniburgh, 2002). The mobilization of arsenic in natural waters is mainly controlled primarily by solid-solution interactions with iron oxides (Ferguson and Gavis, 1972; Cullen, 1989; Stumm, 1992; Jain et al., 1999; Kneebone et al., 2002) because their charge, in contrast to manganese and aluminum oxides, is slightly positive at circumneutral pH (Stumm, 1992). Under oxic conditions, As(V) is negatively charged and readily adsorbs onto iron oxides (Pierce and Moore, 1982; Belzile and Tessier, 1990; Jain et al., 1999; Mucci et al., 2003) limiting its mobility and bioavailability. In anoxic conditions, however, it may be released during the reductive dissolution of these oxides (Smedley and Kinniburgh, 2002) and simultaneously reduced (Guo et al., 1997), thus turning arsenic-contaminated sediments into a continuous source of As(III). As(V) may be reduced to As(III) microbially (Ahmann, 1997; Harrington et al., 1998; Oremland et al., 2000) or chemically by dissolved sulfide (Rochette et al., 2000) and Fe(II) (Appelo, 2002; Charlet et al., 2002), though both chemical reactions are usually slow. As(III) is neutral at circumneutral pH and is less susceptible to adsorption onto metal oxides (Pierce and Moore, 1982; Belzile and Tessier, 1990; Jain et al., 1999). In the presence of dissolved sulfide, As(III) may form thioarsenite complexes (Wilkin et al., 2003) and eventually precipitate as arsenosulfide minerals (Sadiq, 1997; Bostick and

Fendorf, 2003) or, alternatively, adsorb onto iron sulfide minerals (Bostick and Fendorf, 2003). Organoarsenic species are formed biochemically as a detoxification mechanism (Cullen, 1989) but are generally in low concentration in aquatic systems (Smedley and Kinniburgh, 2002). Finally, As(III) can be rapidly reoxidized in the presence of dissolved oxygen (Johnson and Pilson, 1975; Scott and Morgan, 1995) or manganese oxides (Scott and Morgan, 1995; Driehaus, 1995; Manning and Martens, 1997; Chiu and Hering, 2000). Thus, desorption and remobilization of arsenic from sediments is influenced by pH, the activity of microorganisms, and the concentrations of dissolved oxygen, sulfide, iron and manganese in interstitial waters (Pierce and Moore, 1982; Xu, 1988; Mok and Wai, 1990; Kneebone et al., 2002; Meng, 2002; Bostick and Fendorf, 2003). In addition, phosphate, bicarbonate, silicate, and organic matter all compete with arsenic for adsorption sites, thus enhancing arsenic mobility (Meng, 2002).

The biogeochemical cycling of arsenic in aquatic systems has been largely derived from laboratory studies in well-defined conditions (e.g., Johnson and Pilson, 1975; Pierce and Moore, 1982; Driehaus, 1995; Jain et al., 1999; Rochette et al., 2000; Scott and Morgan, 1995; Manning and Martens, 1997; Sadiq, 1997; Chiu and Hering, 2000; Appelo, 2002; Charlet et al., 2002; Bostick and Fendorf, 2003; Wilkin et al., 2003) and mainly examined in groundwater aquifers (Smedley and Kinniburgh, 2002). In contrast, the spatial distribution of arsenic in sediments is rarely investigated (Andreae, 1979; Belzile and Tessier, 1990; Mok and Wai, 1990; Yan et al., 2000; Kneebone et al., 2002; Mucci et al., 2003) and its redox speciation almost never determined (Andreae, 1979; Yan et al., 2000). The objective of this study is to examine the likely factors controlling early diagenesis of arsenic in freshwater sediments with a high spatial

resolution. The biogeochemical processes regulating the cycling of arsenic in the sediment of a major river impoundment in Georgia were investigated using a combination of Au/Hg voltammetric microelectrodes (O_2, Fe(II), Mn(II), ΣH_2S), voltammetry with Hanging Mercury Drop Electrode (HMDE) (As(III)), and Inductively Coupled Plasma-Mass Spectrometry (ICP-MS) (total dissolved As). The influence of iron, manganese, and sulfur cycling on the mobilization of arsenic is discussed in this paper.

2.2.1 Study Location

West Point Lake (inset Figure 2.1) is a 25,900-acre mainstream Chattahoochee River impoundment located 90 km southwest of Atlanta (GA). West Point Lake lies on a 50 km stretch of the Chattahoochee River between Franklin and West Point (GA). The lake has a shoreline of more than 800 km and runs along and across the Georgia/Alabama State line. The lake is controlled by the Army Corps of Engineers and was impounded in 1974 to provide drinking water, flood control, hydroelectric power, navigation, wildlife development, and general recreation for Southwest Georgia.

Five freshwater sediment cores (Figure 2.1) were collected from the outfall of the Chattahoochee River north of the drinking water reservoir of West Point Lake in LaGrange (GA) based on elevated total dissolved arsenic concentrations detected in the water column (Lesley, 2002). There are no recorded geothermal or mining activities located in the surrounding area (Huddlestun, 1988), but a suspected anthropogenic source

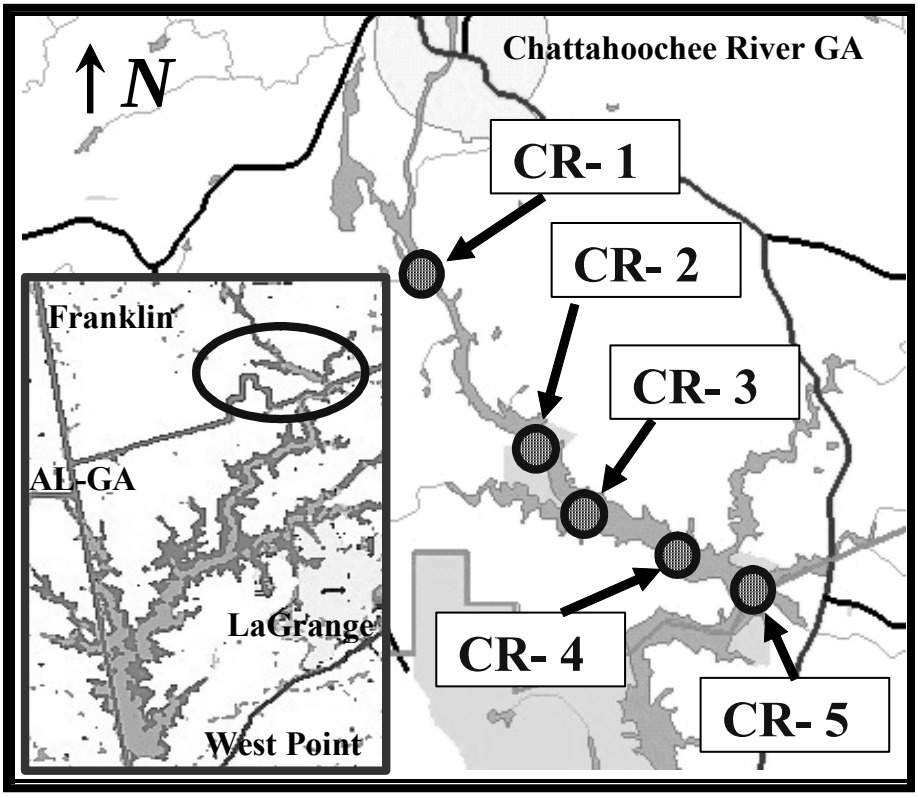

Figure 2.1- Study Location, Chattahoochee River and West Point Lake, GA. Five sediment cores, numbered CR-1 to CR-5, were collected along the Chattahoochee River for this study. Their locations are provided on the map.

has been identified as residual coal ash (Lesley, 2002). The sediment cores were collected in July, 2003 three weeks after the excessive precipitation attributed to Tropical Storm Bill brought approximately 10 foot crests through the study location. In this paper, we present the results from CR-4 and CR-5 only, which are approximately 60 km away from the suspected arsenic source (Lesley, 2002), in an area where dissolved arsenic was depleted from the water column.

2.3 Methods

2.3.1 Sediment Core Collection and Porewater Extraction

Sediment samples were collected with 60 cm long and 10 cm diameter polycarbonate core liners. Approximately 10 cm of overlying water were collected with each core to maintain the integrity of the sediment-water interface and minimize exposure to the atmosphere during transport to the laboratory. High resolution voltammetric and potentiometric profiles of $O_{2(aq)}$, Fe^{2+}, Mn^{2+}, ΣH_2S (H_2S, HS^-, S^0, S_x^{2-}), $FeS_{(aq)}$, and pH were obtained by lowering an Au/Hg voltammetric microelectrode (Brendel and Luther, 1995) and a pH minielectrode (Diamond General Corp.), in millimeter increments, into each sediment core with a micro-manipulator (Analytical Instrument Systems, Inc.).

Voltammetric and pH measurements were conducted with a DLK-100A potentiostat that includes a voltmeter for combined electrode measurements (Analytical Instrument Systems, Inc.). Dissolved oxygen was measured cathodically by linear sweep voltammetry, while Fe^{2+}, Mn^{2+}, ΣH_2S, and $FeS_{(aq)}$ were detected by cathodic square wave voltammetry. Prior to each scan, a conditioning step was applied at -0.1 V for 10 s to clean the microelectrode. Scan rates of 200 mV/s were used for all measurements

(Brendel and Luther, 1995; Taillefert et al., 2002c). The pH was calculated using the Nernst Law after recording the potential and sample temperature at the minielectrode (Taillefert et al., 2002c). By using microelectrodes, a suite of constituents could be measured with a high spatial resolution without sediment handling, thus minimizing contamination while maximizing the volume of porewater for other analyses. Immediately following completion of the electrochemical profiles, the sediments were sectioned and centrifuged under $N_{2(g)}$ atmosphere, and porewaters were filtered (Norm-Ject sterile Teflon syringe and Puradisc 0.2μm Whatman filter) and acidified with Trace Metal Grade HCl or HNO_3 (Fisher) as needed for preservations and analysis. All porewaters were extracted and maintained in a $N_{2(g)}$ atmosphere and kept at 4°C until analysis of As(III), total dissolved arsenic (As_D), chloride, nitrate, sulfate, total dissolved orthophosphate, and total dissolved silica within 24 hours.

2.3.2 Analytical Methods

All solutions were prepared with 18 MΩ-cm Reverse Osmosis (RO) water (Barnstead). All plasticware and glassware used for trace metal analyses were acid-washed in 2% Trace Metal Grade HNO_3 (Fisher) for one week and rinsed thoroughly with RO water. For As(III) analysis, standards were made from an As(III) stock solution prepared daily by dissolving As(III) oxide (Alfa Aesar) in NaOH then acidifying with 12 N HCl (Li and Smart, 1996).

Voltammetric measurements for As(III) were performed with a HMDE using the VA 663 multi-mode mercury drop electrode stand (Metrohm) coupled to the PGSTAT 12 Autolab potentiostat (Ecochemie) The reference electrode was an Ag/AgCl/KCl (3 M)

with a 0.2 M NaCl glass bridge, and a glassy carbon rod acted as the counter electrode. The new electrolyte solutions were thoroughly degassed with ultra high purity $N_{2(g)}$ prior to each As(III) measurement to prevent reoxidation by dissolved oxygen. As(III) concentrations were determined by amending the sample with 0.7 mM Cu(II) ($CuCl_2 \cdot 2H_2O$ Aldrich) and 1 M HCl. A potential was applied at -0.4 V for 10 seconds to form an arseno-copper complex (Equ. 1 - deposition step) (Li and Smart, 1996).

$$yH_3As^{(III)}O_3 + xCu(Hg) + 3yH^+ + 3ye^- \rightarrow Cu_x{}^{(I/II)}As_y{}^{(-III)} + 3yH_2O \qquad \text{(Equ. 1)}$$

The potential was then scanned cathodically (from -0.4 V to -1.2 V) at 300 Hz using square wave voltammetry to reduce $Cu^{(I/II)}$ from the arseno-complex to Cu^0 and allow the indirect measurement of As(III) (Equ. 2 - stripping step).

$$Cu_x{}^{(I/II)}As_y{}^{(-III)} + 3yH^+ + 3ye^- \rightarrow xCu(Hg) + yAs^{(-III)}H_3 \qquad \text{(Equ. 2)}$$

Figure 2.2 shows a triplicate raw data scan of a 1 nM As(III) standard. The detection limit of the method was 0.25 nM As(III) (at 3σ of the blank).

Total dissolved arsenic concentrations (As_d) were determined in triplicate with a Hewlett Packard HP-4500 ICP-MS. Standards were prepared from a 1,000 ppm in 5% HNO_3 As stock solution (Aldrich). An internal standard of 1 ppb yttrium, prepared from 1,000 ppm stock solution (Aldrich) was added to standards and samples to correct for internal drift of the instrument. For quality control, As_d standards were inserted every 10 samples. The detection limit of As_d was found to be 0.25 nM.

Total dissolved phosphate and silica were determined by spectrophotometry (Strickland, 1952; Murphy, 1962). Sulfate, nitrate, and chloride were measured by Ion Chromatography (Dionex Model 300X) with a bicarbonate buffer as eluent. Amorphous iron oxides were extracted in triplicate in selected samples using ascorbate reagent (Kostka and Luther, 1994). Fe(II) produced during the extraction was analyzed with the Ferrozine Method (Stookey, 1970).

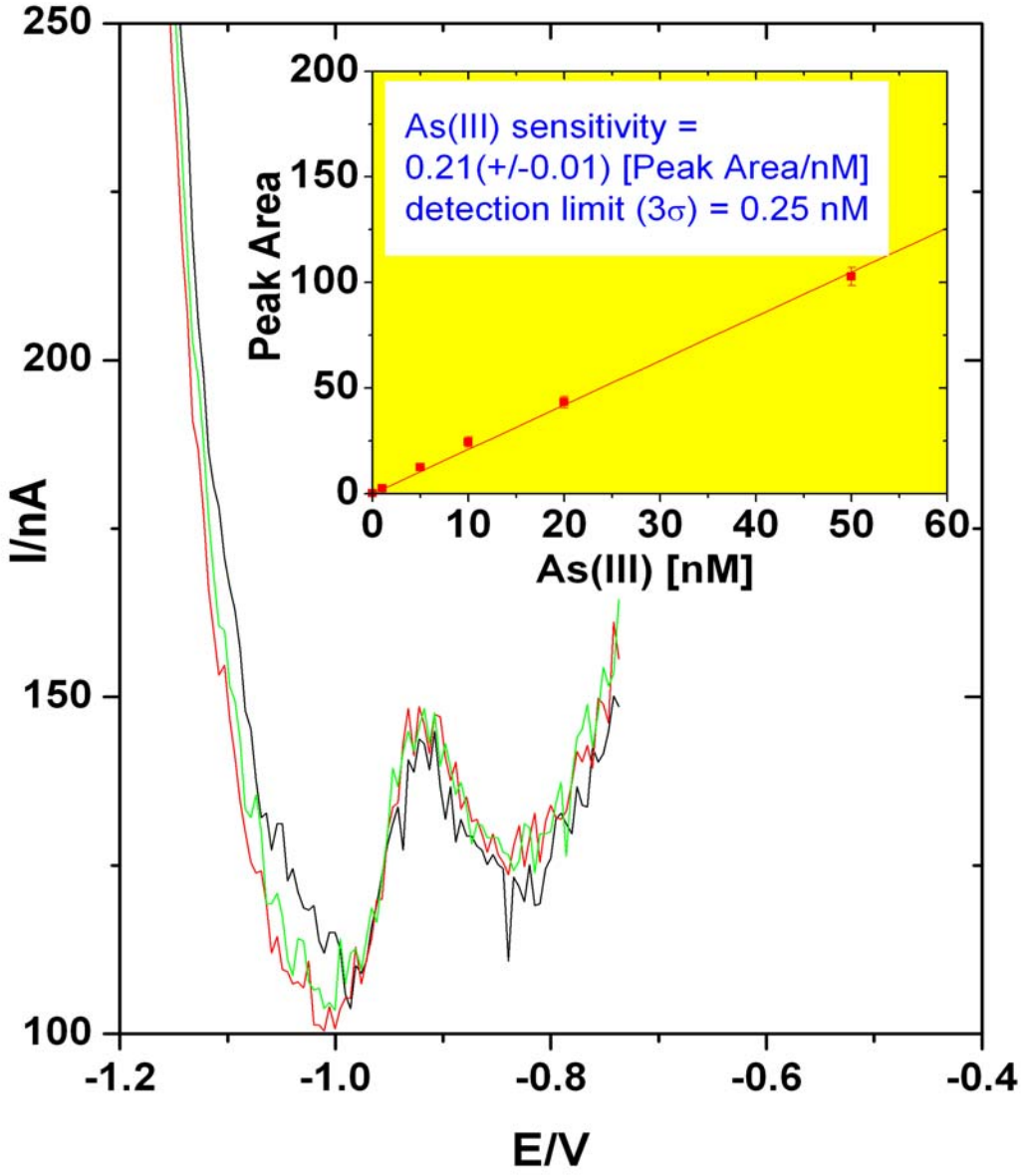

Figure 2.2- Reproducibility of triplicate HMDE voltammetric measurements of a 1 nM As(III) standard. The inset shows a typical calibration curve. The method has a detection limit of 0.25 nM at three standard deviations from the blank.

2.4 Results

Both cores were anoxic, with dissolved oxygen decreasing from approximately 280 μM in the overlying water to undetectable levels just below the sediment-water interface (Figures 2.3a and 2.4a). As illustrated on Figure 2.3b, the pH decreased from 6.4 just below the SWI to 6.1 at 20 mm, then stabilized until 50 mm where it decreased again to reach 5.8 at 80 mm. Fe(II) rose from undetectable levels (< 5 μM) within 10 mm from the SWI to a maximum of 940 μM in CR-4 (Figure 2.3a) and 540 μM in CR-5 (Figure 2.4a). It then stabilized around these values until 40 mm in both CR-4 and CR-5. While Fe(II) abruptly increased in CR-5 to a maximum of 550 μM before decreasing regularly to a minimum of 100 μM at 80 mm, it oscillates between 500 and 900 μM below 40 mm in CR-4. Mn(II) concentrations displayed similar behavior in both CR-4 and CR-5, except that Mn(II) was produced at 5 mm below the SWI in CR-4 and directly at the interface for CR-5. It increased to reach a maximum of 590 μM between 45 and 55 mm in CR-4 (Figure 2.3a) and 470 μM between 20 and 30 mm in CR-5 (Figure 2.4a). Below these depths, Mn(II) decreased in both cores to approximately 100 μM. No ΣH_2S (detection limit < 0.2 μM) was detected in these sediments.

Figure 2.3c illustrates the depth profiles of chloride, nitrate and sulfate. Chloride concentrations were approximately 130 μM in the first 10 cm of the sediment then slightly decreased to 100 μM. Nitrate (Figure 2.3c) was detected in the overlying water only, at a concentration of 27 μM. Sulfate concentrations were highest at 47 μM in the overlying water then diminished regularly to below the detection limit of 2 μM at 43 mm in CR-4 (Figure 2.3c). Total dissolved phosphate and total dissolved silica (data not shown) were below detection limit in both cores.

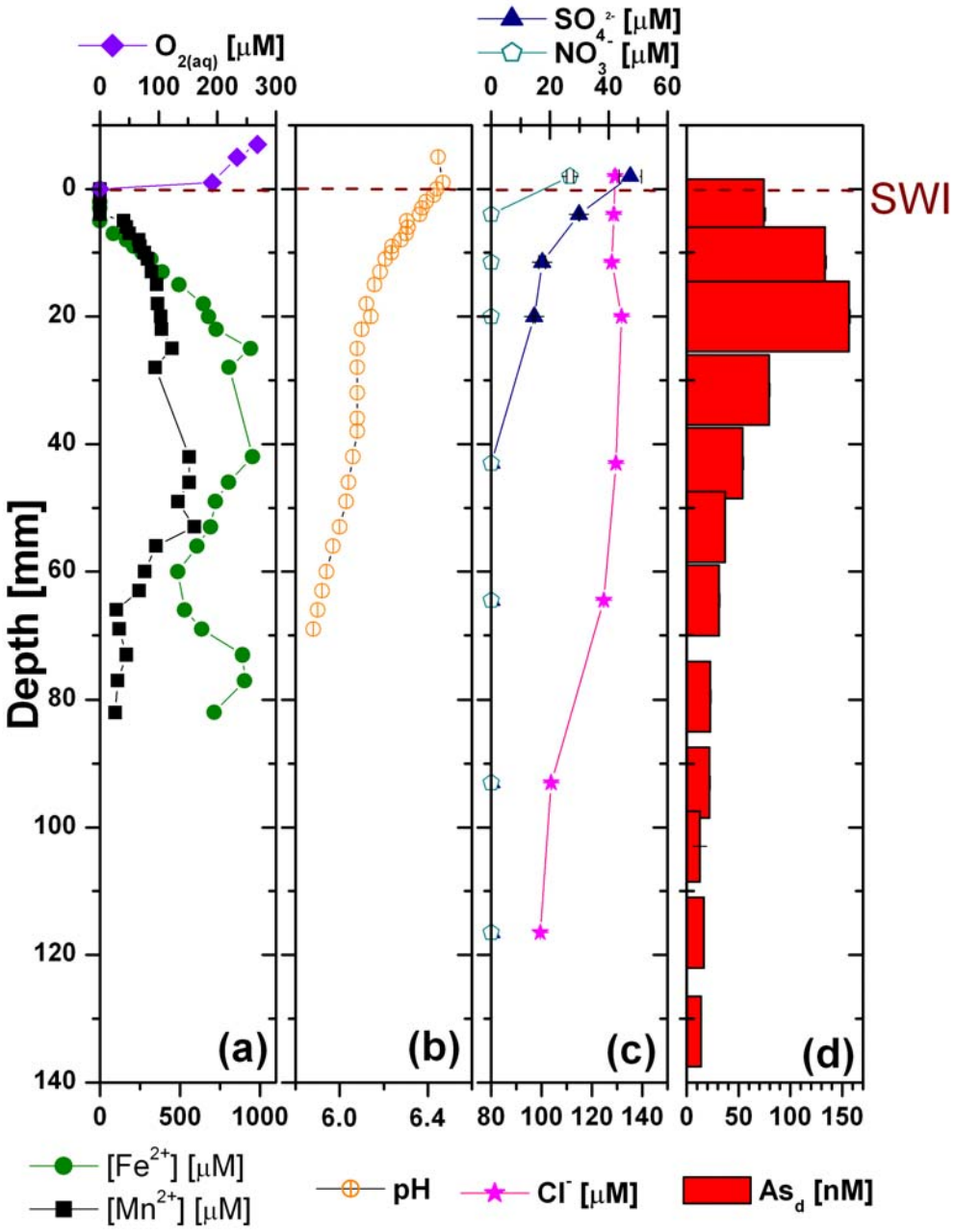

Figure 2.3- Depth Profile of dissolved oxygen, Fe(II), and Mn(II) by voltammetric microelectrode (to 80 mm) (a); pH by minielectrode (to 80 mm) (b); sulfate, nitrate and chloride by ion chromatography (c); and total dissolved arsenic (As_d) by ICP-MS with standard deviation error bars (d) in CR-4 collected in July 2003 in the Chattahoochee River.

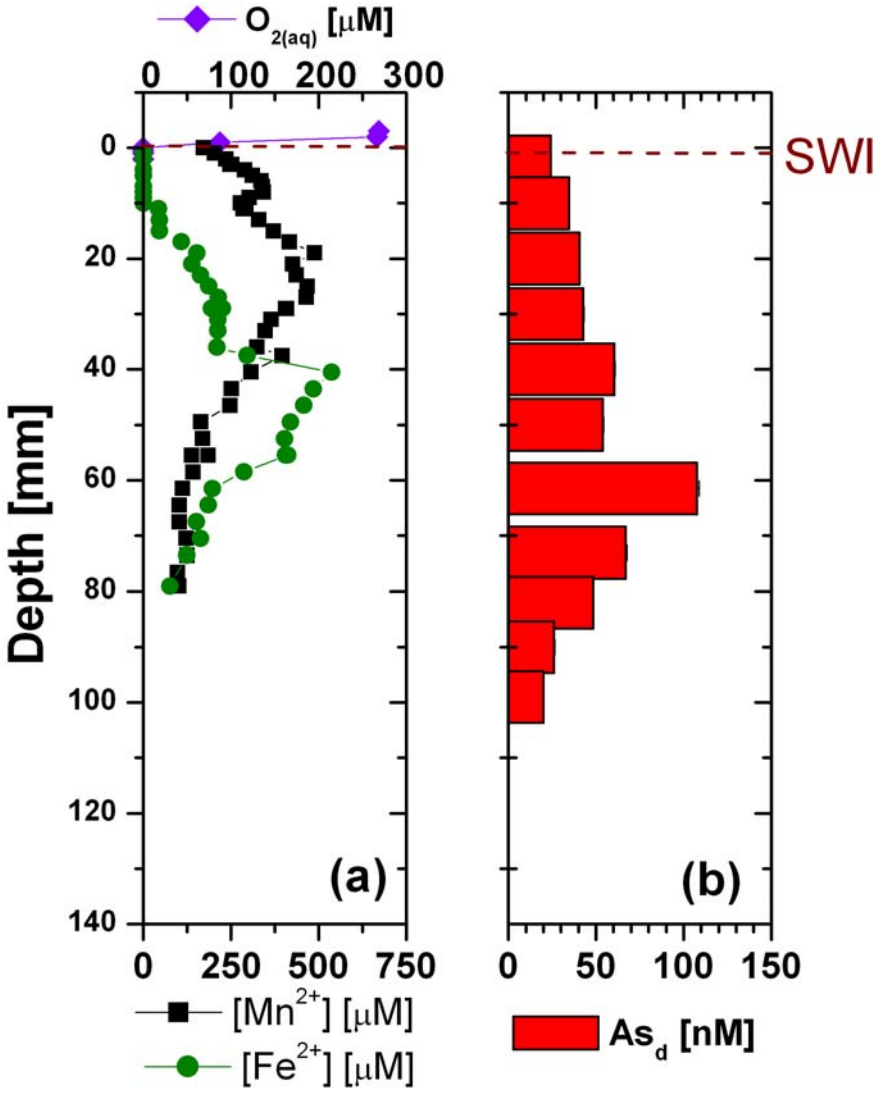

Figure 2.4- Depth Profile of dissolved oxygen, Fe(II), and Mn(II) by voltammetric microelectrode (to 80 mm) (a); and total dissolved arsenic (As_d) by ICP-MS with standard deviation error bars (b) of CR-5 collected in July 2003 in the Chattahoochee River.

The concentration of amorphous iron oxides, as determined by the ascorbate extraction, decreased with depth in CR-4, from 108 ±6 μmol/g in the top 8 mm to 95 ±8 μmol/g between 15 and 25 mm (the depth depicting the highest dissolved As(V) in the porewaters - Figure 2.3d), and to 36 ±2.5 μmol/g between 88 and 98 mm. CR-5 results displayed a more stable profile with concentrations of amorphous iron oxides ranging between 56 ± 2 μmol/g at the surface and 52 ± 4 μmol/g between 58 and 71 mm (depth depicting the highest total dissolved As(V) concentration - Figure 2.4b), and with a slight increase to 71 ± 4 μmol/g between 104 and 114 mm.

As(III) was not detected in the extracted porewaters using HMDE, even after increasing the deposition time from 60 to 600 s to improve the detection limit. We therefore conclude that total dissolved arsenic (As_d) profiles (Figure 2.3d and 2.4b) are indicative of As(V) only. In both cores, the concentration of As(V) was significant at the sediment-water interface, 25 nM in CR-4 and 75 nM in CR-5, and increased deeper to a maximum of 156 nM between 15 and 25 mm in CR-4 and 107 nM between 55 and 68 mm in CR-5. As(V) then decreased to a minimum of 15 nM between 125 and 135 mm in CR-4 and 20 nM between 95 and 105 mm in CR-5. The solid bars represent the length of the sediment section from which porewaters were extracted.

2.5 Discussion

Altogether, these chemical profiles provide a clear picture of the processes regulating the cycling of arsenic near the sediment-water interface. The rapid decrease in dissolved oxygen close to the SWI (Figure 2.3a and Figure 2.4a) indicates that both sediments are anoxic. The low concentration of Fe(II), the absence of NO_3^-, and the

decrease in pH near the SWI suggest that a combination of aerobic respiration (Equ. 3), denitrification (Equ. 4), and possible chemical oxidation of Fe(II) (Equ. 5) occur only within the first centimeter of these sediments:

$$CH_2O + O_2 \rightarrow HCO_3^- + H^+ \qquad \text{(Equ. 3)}$$

$$5CH_2O + 4NO_3^- \rightarrow 5HCO_3^- + 2N_2 + H^+ + 2H_2O \qquad \text{(Equ. 4)}$$

$$4Fe^{2+} + O_2 + 10H_2O \rightarrow 4Fe(OH)_{3(s)} + 8H^+ \qquad \text{(Equ. 5)}$$

Iron oxidation is confirmed by the high concentration of amorphous iron oxides detected in the upper sediment of CR-4 and CR-5. Additionally, manganese and iron oxide reduction is demonstrated with the production of Mn(II) and Fe(II) within the first 3 to 4 cm of these sediments (Figure 2.3a and 2.4a). The occurrence of metal reduction leads to a subsequent stabilization of the pH in the sediment porewaters (Figure 2.3b) because these reactions consume protons (Taillefert et al., 2002c). Chemical reduction of manganese and iron oxides by dissolved sulfide (Equ. 6 and 7) may occur in sediments. However, the maximum concentration of dissolved sulfide available from the sulfate, FeS, and FeS_2 present in these freshwater sediments (i.e. 50 μM) is not high enough to account for all the Mn(II) and Fe(II) produced (compare maximum sulfate to maximum Mn(II) and Fe(II) concentrations in Figure 2.3 and 2.4).

$$MnO_2 + H_2S + 2H^+ \rightarrow Mn^{2+} + S^{(0)} + 2H_2O \qquad \text{(Equ. 6)}$$

$$2Fe(OH)_{3(s)} + H_2S + 4H^+ \rightarrow 2Fe^{2+} + S^{(0)} + 6H_2O \qquad \text{(Equ. 7)}$$

Similarly, the chemical reduction of manganese oxides by Fe(II) is also possible (Equ. 8) but is usually slow above pH 4 (Postma, 1985).

$$MnO_2 + 2Fe^{2+} + 4H_2O \rightarrow Mn^{2+} + 2Fe(OH)_{3(s)} + 2H^+ \qquad \text{(Equ. 8)}$$

It can therefore be concluded that most of the reduction of manganese and iron oxides is microbial in these sediments. Not surprisingly, Mn(II) reaches the sediment-water interface in core CR-5, suggesting that it diffuses out of the sediment at this location. This feature is well known and due to the slow oxidation kinetics of Mn(II) at circumneutral pH in the presence of oxygen (Stumm and Morgan, 1996). The disappearance of sulfate within the first 40 mm of CR-4 (Figure 2.3c) suggests that sulfate reduction proceeds in these sediments. Dissolved sulfide was not detected in the porewaters suggesting that it was removed by precipitation with FeS and FeS_2. The formation of iron sulfide minerals was supported by MINEQL+ calculations using an average pH of 6.1, Fe(II) concentration of 800 μM and assuming 50 μM H_2S (i.e. the maximum sulfate measured) entered as HS^-. Anoxic conditions were established for these calculations by entering concentrations for reduced species only rather than fixing pE values. The results indicate that the solubility products of pyrite, sulfur, FeS, and mackinawite are exceeded as listed in Table 2.1 along with solubility constants, as well as thermodynamic data for acid dissociation reactions of sulfide. These calculations assume equilibrium and can be used cautiously as a predictive tool. At this point, it is not clear if the freshwater system is not at equilibrium. Nevertheless, the sulfate profile suggests that H_2S is produced episodically in these sediments.

Arsenic is thought to enter the Chattahoochee River upstream of the study location and is transported in the oxic river water in the form of As(V) (Lesley, 2002). As As(V) flows downstream, it may adsorb onto colloidal and particulate matter contained in the river and settle to the sediment-water interface. The data indicate that

Table 2.1 MINEQL+ thermodynamic data for sulfur and iron

INPUT:		
$[H^+]$	7.96E-7	pH 6.1
$[Fe^{2+}]$	8.00E-4	
[HS-]	5.00E-5	
OUTPUT:		
Iron:	Fe^{2+}	34.4%
	$Fe(HS)_{2(aq)}$	65.3%
Sulfur:	HS^-	3.3%
	$H_2S_{(aq)}$	26.9%
	$Fe(HS)_{2(aq)}$	69.2%
	log K_{sp}	**SI= log (IAP/K_{sp}) ***
Pyrite	18.5	18.500
Sulfur	2.44	3.957
Wustite	-11.7	-2.916
$Fe(OH)_2$	-13.6	-4.972
FeS (ppt)	2.88	1.130
Mackinawite	3.53	1.780

* The solubility product (SI) is calculated by dividing the ion activity product for the solids (IAP) by the solubility constant for the solid (K_{sp}). The IAP is determined by the activity of input components, and changes with pH.

this sediment is not a natural source of arsenic, since the concentration of dissolved arsenic is high near the SWI and depleted at depth, and support the earlier hypothesis that the anthropogenic input of arsenic is significant in the Chattahoochee River (Lesley, 2002).

The role of manganese and iron on the arsenic cycle has been investigated extensively (Pierce and Moore, 1982; Belzile and Tessier, 1990; Mok and Wai, 1990; Scott and Morgan, 1995; Manning and Martens, 1997; Chiu and Hering, 2000; Rochette et al., 2000; Appelo, 2002; Charlet et al., 2002; Kneebone et al., 2002; Bostick and Fendorf, 2003). In these sediments, adsorption of arsenic should dominate in the upper sediments that contain the highest concentration of amorphous iron oxides. The adsorption of arsenic is also affected by the degree of crystallization of the iron oxides because the density of adsorption sites decreases as the minerals are more crystallized (Dzombak and Morel, 1990). To determine the extent of adsorption of As(V) onto iron oxides in the first centimeters of these sediments, we implemented a double-layer surface adsorption model with MINEQL+ using parameters from the literature (Dzombak and Morel, 1990). The model assumes a specific surface area of 600 m^2/g for amorphous iron oxides and two types of binding sites: high affinity sites with a density of 5 mmol/mol Fe and low affinity sites with a density of 0.2 mol/mol Fe. The input concentrations used in the model are based on the data of Figures 2.3 and 2.4 (pH = 6.4; $[AsO_4^{3-}]$ = 150 nM; $[Cl^-]$ = 130 μM; $[Fe^{2+}]$ = 10 μM; $[SO_4^{2-}]$ = 50 μM) or are estimated from previous work (Lesley, 2002) in the area (i.e. DIC = 300 μM). The model was closed to the atmosphere with respect to carbonate. Assuming a sediment density varying between 0.98 and 0.87 g/cm^3 clayey and silty sediments (Kastler and Wiberg, 1996), the molar concentration of

amorphous iron oxides is ~ 0.05 M. The model calculation predicts that 97% and 2.9% of the arsenate in our system was in the form of $H_2AsO_4^-$ and $HAsO_4^{2-}$, respectively, and is adsorbed onto iron oxides.

As(V) is produced simultaneously with Fe(II) in the first few centimeters of both sediments (Figures 2.3 and 2.4). A positive correlation exists between Fe(II) and As(V) in both cores, though with different slopes (Figure 2.5). From the slopes, a As:Fe(II) ratio of 3:10,000 in the top 25 mm of CR-4 and 6:100,000 in the top 40 mm of CR-5 were found. These data indicate that adsorbed arsenic may be released during the reduction of iron oxides, thus confirming the significant role of iron in the arsenic cycle. These data also indicate that more arsenate is scavenged onto iron oxides in CR-4 than in CR-5. Dissolved silicates and orthophosphate were below the detection limit in both cores, suggesting they probably do not significantly effect arsenic mobilization in this system. Mn(II) depth profiles indicate that the reduction of manganese oxides occurs in these sediments, however their involvement with arsenic is not evident. First, adsorption is not favored because at circumneutral pH, manganese oxides are negatively charged (Stumm, 1992) while As(V) is mainly deprotonated (Postma, 1985; Stumm and Morgan, 1996). It is also known that manganese oxides oxidize arsenite to arsenate (Chiu and Hering, 2000; Driehaus, 1995; Manning and Martens, 1997) according to:

$$MnO_2 + H_3AsO_3 \rightarrow Mn^{2+} + HAsO_4^{2-} + H_2O \quad \text{(Equ. 9)}$$

However, there is an inconsistent correlation between Mn(II) and As(V) in both cores (not shown). The lower adsorption affinity of As(V) onto manganese oxides at circumneutral pH along with the poor correlation between Mn^{2+} and As(V) suggest that manganese oxides play a minor role in the arsenic cycle in these sediments.

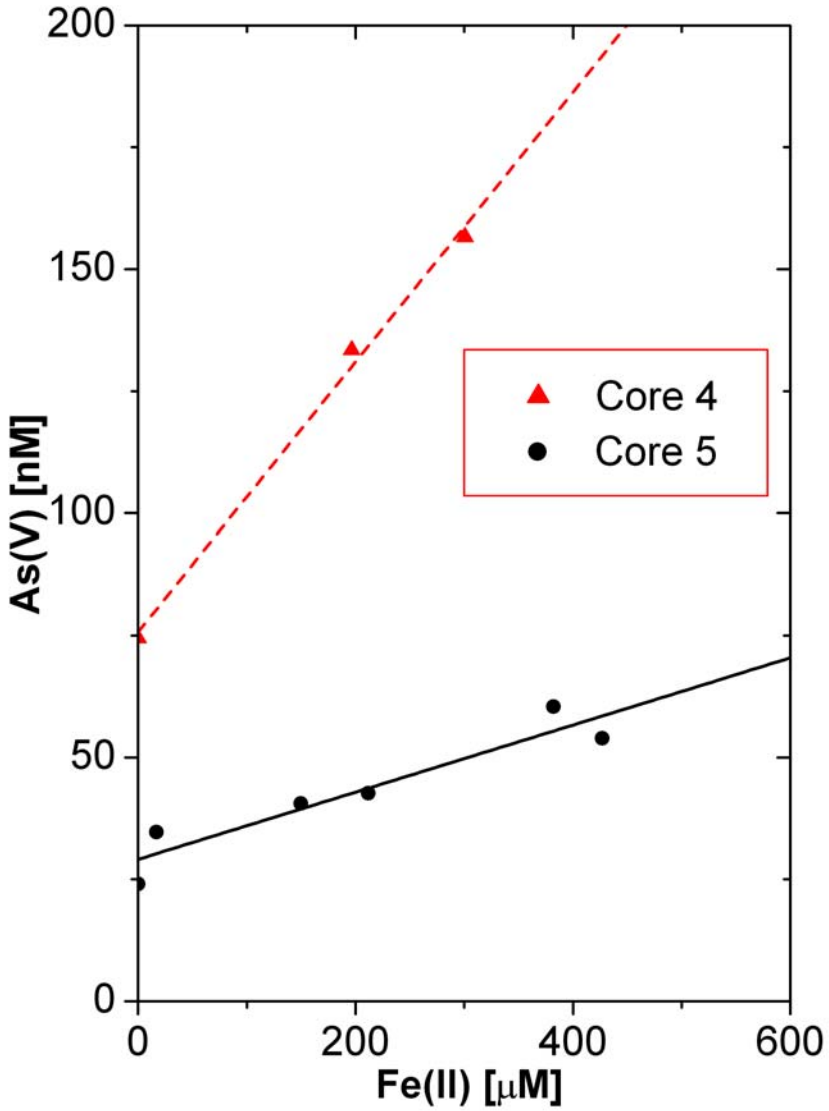

Figure 2.5- Correlation between Fe(II) and As(V) between 0 and 25 mm in CR-4 (triangles) and between 0 and 40 mm in CR-5 (circles).

As previously mentioned, sulfate disappears in these porewaters, suggesting that sulfate reduction may occur in these sediments. It has been shown recently that dissolved sulfide may slowly reduce As(V) and complex As(III) in the form of electrochemically inactive AsO_xS_y (Bostick and Fendorf, 2003; Wilkin et al., 2003) that could then undergo precipitation. Our measurements, however, could not detect any As(III) in solution in these sediments. We ruled out the possible oxidation of our samples after porewater extraction, because the sediment cores were sectioned, centrifuged, filtered, acidified, and stored at 4˚C under a $N_{2(g)}$ atmosphere until As(III) analysis, which was conducted within 24 hours after collection. In addition, the arsenosulfide complexes, if present, should be dissociated in the acidic conditions of the As(III) analysis (pH 1) and detected electrochemically.

The fact that the sediment is reduced but arsenic is oxidized may be due to the dynamic nature of the system studied. The surficial sediments evaluated in this study were most likely deposited after the passage of Tropical Storm Bill, which impacted the site three weeks prior to this investigation. It is possible that the kinetically slow reduction of As(V) had not occurred so soon after deposition, while microbial iron reduction released As(V) in solution. Finally, the presence of As(V) and Fe(II) at deeper locations in CR-5 as compared to CR-4 is probably due to the more turbulent river flow at CR-5 where advective forces may introduce dissolved oxygen deeper into surficial sediments and increase erosion. This process is evidenced by a general decrease in both the Fe(II) and amorphous iron oxide concentrations in the sediment of CR-5 compared to CR-4 (Figures 2.3 and 2.4).

Diffusive fluxes were calculated for each core using Fick's Law with the molecular diffusion coefficient of phosphate as a proxy for that of arsenate (9.1×10^{-5} cm^2/sec for $H_2PO_4^-$). According to these calculations, approximately 60 to 200 nM/cm^2yr of arsenic may be diffusing into the overlying water column from the sediment. Although the arsenic concentrations detected in the porewaters are not considered high compared to contaminated sites, the data suggest that arsenic is remobilized and may impact the drinking water reservoir located downstream.

2.6 Conclusions

This study successfully combined several analytical techniques to determine the profiles of major redox species and the speciation of As(III) and As(V) with a fine spatial resolution (i.e., < 10 mm) in two contaminated freshwater sediments. Results provide evidence of a substantial correlation between the diagenetic processes involving iron and arsenic in these sediments. The sediment profiles suggest that iron oxides scavenge arsenic in the form of arsenate in the water column and settle to the sediment-water interface where they are reduced by iron reducing bacteria. As a result of microbial iron reduction, As(V) is released and accumulates in the porewaters near the sediment-water interface, where it can diffuse back to the overlying waters.

Interestingly, As(III) was never found in the porewaters, suggesting that the reduction of As(V) is a slow process that was not occurring in these recently deposited sediments. Future studies will test the hypothesis that microbial and chemical reduction of As(V) are too slow compared to the hydraulic residence time of arsenic in these sediments.

2.7 Acknowledgements

The authors express their gratitude to Flip Froelich and Stephany Rubin-Mason for their help with the ICP-MS measurements and Judson Partin, Elizabeth Carey, and Gwendolyn Bristow for their assistance in the field and laboratory. This work was funded by the Georgia Water Resources Institute through a grant from the Department of Interior/Geological Survey (Contract # 01HQGR0139).

CHAPTER 3

EFFECT OF ARSENIC CONCENTRATION ON MICROBIAL IRON REDUCTION AND SPECIATION IN FRESHWATER SEDIMENTS

3.1 Abstract

Depth profiles in the sediment porewaters of the Chattahoochee River (Georgia) show that iron oxides scavenge arsenate in the water column and settle to the sediment-water-interface (SWI) where they are reduced by iron reducing bacteria. During their reduction, these particles seem to release arsenic to the porewaters under the form of arsenate only. Sediment slurry incubations were conducted to determine the mechanisms and rates of arsenic biogeochemical transformations in these sediments. Experiments confirm that any arsenate (As(V)) added to these sediments is immediately adsorbed in oxic conditions and released in anoxic conditions during the microbial reduction of authigenic iron oxides. Incubations in the presence of ≤ 1 μM As(V) reveal that arsenate is released but not concomitantly reduced during this process. Curiously, microbial iron reduction is enhanced significantly when As(V) amendments are increased from natural levels to a threshold of approximately 2 to 6 μM, spurring the simultaneous formation of crystalline iron oxides and release of arsenate into porewaters. Above this threshold, however, the microbial reductive dissolution of iron oxides is inhibited by arsenate and arsenite is produced, probably through a detoxification mechanism. These findings suggest that arsenic may block adenosine triphosphate (ATP) formation at concentrations as low as 0.1 μM As(V) and that indigenous iron-reducing bacteria are able to increase

respiration rates to overcome this effect up to a threshold approximately one order of magnitude above natural levels. These incubations show that even low inputs of arsenic to riverine sediments may affect microbial processes, the stability of iron oxides and, indirectly, the cycling of arsenic.

3.2 Introduction

Arsenic is a drinking water contaminant of major concern, and its fate in aquatic systems has recently been the subject of intense research (Oremland and Stolz, 2003; Horneman et al., 2004; O'Day et al., 2004; Oremland and Stolz, 2005). Arsenic toxicity is related to its oxidation state (Slotnick et al., 2006), and its mobility in reduced conditions is controlled by the biogeochemical cycling of iron and sulfide (Smedley and Kinniburgh, 2002; Meng et al., 2003; O'Day et al., 2004). When dissolved sulfide concentrations dominate in anoxic waters, sulfide precipitates arsenic-sulfide minerals (Rochette et al., 2000). However, if iron concentrations are much higher than sulfide concentrations, sequestration of arsenic is controlled by iron (Rochette et al., 2000; Bose and Sharma, 2002), because aqueous sulfide is rapidly depleted during the formation of iron sulfide minerals. In iron-dominated systems, arsenic is removed by adsorption onto iron oxides (Pierce and Moore, 1982) and is generally released in solution during the reductive dissolution of iron oxides (Guo et al., 1997). As a consequence, a strong correlation is evident between the dissolution of iron oxides and the release of arsenic in freshwater sediment (Aggett and O'Brien, 1985). Arsenate is usually not reduced chemically by any other reductant than sulfide (O'Day et al., 2004), and the presence of

arsenite in anoxic, but sulfide-depleted, freshwaters has been attributed to microbial arsenate reduction (Newman et al., 1998; Smedley and Kinniburgh, 2002).

The dissimilatory microbial reduction of arsenate may occur via a respiratory process, typically observed in the presence of high concentrations of arsenate (Stolz and Oremland, 1999). Alternatively, microbial reduction of arsenate may occur through a detoxification process during which organisms do not acquire energy for growth (Saltikov et al., 2005). So far, it has been shown with a pure culture that arsenate reduction as a detoxification process does not occur below a threshold of around 100 μM arsenate (Saltikov et al., 2005). However, most research on the biogeochemical cycling of arsenic has been conducted in laboratory or environmental conditions with elevated concentrations of arsenic (Pierce and Moore, 1982; Cullen, 1989; Belzile and Tessier, 1990; Stumm, 1992; Guo et al., 1997; Jain et al., 1999; Kneebone et al., 2002; Ryu et al., 2002; Smedley and Kinniburgh, 2002; Mucci et al., 2003). More specifically, the effects of low concentrations of arsenic (i.e., $\leq$ 10 μM) on biogeochemical processes in natural aquatic systems are unknown.

In this study, we investigated the chemical and biological processes involved in arsenic diagenesis in the sediment of the Chattahoochee River, an area of relatively low arsenic and sulfide concentrations, but where arsenic accumulates in the water column upstream from the selected sites (Lesley, 2002). Porewater depth profiles illustrated the dominance of iron reduction processes on arsenic cycling. After a severe flood that accumulated fresh particles at the sediment-water interface (SWI), arsenate was released in the porewaters below the SWI and diffused into the overlying waters. Although informative, depth profiles by themselves cannot clearly establish the biogeochemical

processes regulating the speciation of arsenic in these sediments. Thus, sediments from the same area were incubated to investigate the impact of arsenate concentrations on the biogeochemical cycling of iron, manganese, and arsenic.

3.2.1 Study Site

The study site is a section of the Chattahoochee River located in the Middle Chattahoochee-Lake Harding Watershed near LaGrange, GA. The biogeochemical cycling of arsenic in these waters is a major concern since elevated total arsenic concentrations were detected in the water column (Lesley, 2002) and sediment (Chow and Taillefert, 2005) upstream of West Point Lake Reservoir. Although levels are below the drinking water standards of 133 nM (10 ppb), chronic exposure to sub-acute levels (Slotnick et al., 2006) potentially ingested via water supplies, may represent a danger for local residents and consumers of locally grown crops, such as rice (Williams et al., 2007). In addition, this location was subjected to severe flooding that potentially shifted the redox transition zone and temporarily altering biological and chemical processes (Mucci, 2002; Chow and Taillefert, 2005). Two sites were selected for this study. The first site represents an area along the southwest bank of the Chattahoochee River at the mouth of a placid cove (PC). The second site is an area in the river bend (RB) and experiences more turbulent flow.

3.3 Materials and Methods

3.3.1 Porewater Measurements

Sediment cores were collected with a sediment corer from the two sites (PC and RB) in the early summer of 2003 and 2004. *In situ* pH minielectrode (Diamond General) and voltammetric microelectrode depth profiles were collected within five hours after collection. High resolution voltammetric and pH depth profiles were respectively measured with an Au/Hg microelectrode (Brendel and Luther, 1995; Chow and Taillefert, 2005) and a pH minielectrode (Diamond General) connected to a dual potentiostat and voltmeter (DLK-100, Analytical Instrument Systems, Inc. (AIS, Inc.)). To obtain depth profiles, the electrodes were lowered in millimeter increments in the sediment by a micromanipulator (AIS, Inc.) controlled by the computer-operated potentiostat. Square wave voltammetry was applied cathodically (CSWV) from –0.1 V to –1.8 V with a scan rate of 200 mV/s after conditioning steps at -0.9 and -0.1 V for 10 seconds. Concentrations of O_2, ΣH_2S ($H_2S+HS^-+S^0+S_x^{2-}$), Fe(II), and Mn(II) and presence of organic complexes of ferric iron (org-Fe(III)) and aqueous complexes of FeS were measured at least in triplicate. Immediately following completion of voltammetric profiles, sediments were sectioned for porewater analysis.

Immediately following completion of voltammetric profiles, the sediments were sectioned, centrifuged under N_2(g) atmosphere, and porewaters filtered (0.2 μm Whatman Puradisc). Aliquots from each section were frozen until analysis (e.g. anions, silicates, and TOC) or acidified with 1% HNO_3 and maintained under N_2(g) atmosphere at 4˚C until analysis. Porewater sulfate, nitrate, and chloride were measured by ion

chromatography (Dionex Model 300) with anion exchange and guard columns (IonPac AB14A and AG14A). Dissolved orthophosphate and silicate were determined by spectrophotometry (Strickland, 1952; Murphy, 1962). Total organic and inorganic carbon in porewaters was analyzed with a TOC analyzer (Sievers Instruments).

3.3.2 Solid Phase Analyses

Amorphous iron oxides were extracted from wet sediments by the ascorbate method (Kostka and Luther, 1994), while total reactive iron, including amorphous and crystalline iron oxide and iron from the acid volatile sulfide (AVS) fraction, was extracted by the dithionite method (Kostka and Luther, 1994). As the sulfur content of the porewaters is low in these freshwater sediments, iron from the AVS fraction is probably not significant, and the difference between total reactive and amorphous iron concentrations can be attributed to the crystalline iron fraction mainly (i.e. goethite, hematite, and magnetite). Total iron, including crystalline and amorphous iron oxides, iron from the AVS fraction, and iron-containing clays (Kostka et al., 1999), was also extracted with 1 M HCl on wet sediments. The ascorbate extraction was also used to determine concentrations of amorphous manganese oxides and the HCl extraction to quantify crystalline manganese oxides including those associated with carbonate and aluminum silicates (Hyacinthe et al., 2001).

Depth profiles of total solid arsenic in sediment cores were quantified after a hot acid extraction at 80˚C for 6 hours with 1 M Aqua regia. In contrast, arsenic was extracted from incubated sediments using four parallel extractions: 1) 1 M NaH_2PO_4 for 24 hours to obtain poorly to mildly adsorbed arsenic by ligand exchange (Goh and Lim,

2005); 2) 1 M HCl for 1 hour to liberate arsenic co-precipitated with highly amorphous iron oxyhydoxides (Goh and Lim, 2005) and carbonates (Ona-Nguema et al., 2005); 3) 1 M HNO_3 for 1 hour to extract arsenic co-precipitated with pyrite and amorphous As_2S_3 (Ona-Nguema et al., 2005); 4) 1 M Aqua regia for 6 hours at 80˚C to extract total arsenic (Shaw, 2006), including that bound to biogenic magnetite, silicates, and organic matter (Horneman et al., 2004). Just before analysis, sediments were centrifuged for 10 minutes at 3000 rpm and supernatants filtered (0.2 μm Whatman Puradisc). Sediment sections displaying the highest arsenate concentrations in the porewaters were selected for the incubation experiments.

3.3.3 Sediment Incubations

Wet sediment sections were homogenized into slurries and incubated in triplicate Hungate anaerobic culture tubes (Bellco, Inc.) to account for the heterogeneity between solid samples. All reactor parts and solutions were autoclaved at 250°C for 30 minutes. Just before use, 5 g of wet sediment was placed into each reactor with 15 mL of autoclaved Chattahoochee River Water. The reactors were then amended with either 0, 0.1, 1, or 10 μM of As(V) stock under controlled oxic atmosphere and kept in the dark at 25°C for 24 hours to allow adsorption of As(V) onto the natural sediment. After 24 hours, the supernatant was purged with $N_{2(g)}$, and the reactors were sealed with butyl rubber stoppers, crimped with aluminum caps, and kept in the dark at 25°C while rotating at 40 rpm for the duration of the experiment. Aliquots were periodically collected inside an anaerobic chamber for analyses of As(III), dissolved arsenic (As_D), Fe(II), Mn(II), pH, and ΣH_2S as a function of time. Voltammetric measurements of As(III) were performed using a hanging mercury drop electrode (HMDE) stand model 663 VA (Metrohm) and a

DLK 60 potentiostat (AIS, Inc.) with a glassy carbon rod as counter electrode and an Ag/AgCl/KCl (3M) as reference electrode. As(III) was measured indirectly as an arseno-copper complex formed on the mercury drop (Li and Smart, 1996) with a detection limit of 0.2 nM (Ahmann, 1997). Total dissolved arsenic concentrations (As_D) were determined in triplicate with an Agilent 7500a Inductively Coupled Plasma-Mass Spectrometer (ICP-MS) using quality controls and certified reference material solutions to verify accuracy (Ahmann, 1997). As(V) concentrations were determined by difference between As_D and As(III). Mn(II), Fe(II),ΣH_2S, and pH were measured electrochemically as described for the depth profiles. After *in situ* measurements, additional Fe(II) and total dissolved iron concentrations were analyzed using the Ferrozine method (Stookey, 1970). Aliquots were analyzed for the same suite of species measured in porewaters. Each aliquot was analyzed in triplicate, therefore, mean concentrations and standard deviations reported represent an average of nine measurements (triplicate analyses of triplicate reactors) for each treatment.

After 160 days, the speciation of iron, manganese, and arsenic was determined in the solid phases of reactor sediments by the same methods used to determine depth profile fractions. Sediment from each reactor was sectioned in triplicate, thus the concentrations presented represent the average of at least nine replicates: three extractions per method for each of the triplicate sub-section. Concentrations were corrected for water content and are reported in dry weight.

3.4 Results and Discussion

3.4.1 Sedimentary Arsenic Transformation

Both sediments were anoxic (Figures 3.1a and 3.2a), but not sulfidic. The pH decreased within 10 mm in RB and 4 mm in PC, then rebounded and stabilized deeper around a pH of 7.3. These pH profiles indicate that respiration and denitrification were both ongoing in the first 10 mm, as already determined just after a flood event, and that iron and manganese reduction probably dominated diagenetic processes deeper in these sediments. Indeed, Mn(II) concentrations increased to ~ 500 μM around 25 mm in both sediments, then stabilized around this value in RB (Figure 3.2a) or decreased with depth in PC (Figure 3.1a). Fe(II) was produced below the pH minimum at both locations and reached 950 μM at 31 mm in RB and 320 μM at 26 mm in PC. While Fe(II) disappeared at 70 mm in RB, the concentration of Fe(II) progressively increased in PC to a maximum of 545 μM at 73 mm. The production of soluble organic-Fe(III) complexes also coincided with the onset of Fe(II) in each core (Figure 3.1a and b and Figure 3.2a and b). Current intensities of soluble organic-Fe(III) complexes reached 75 nA within a 5 to 8 mm gradient and stabilized between 75 and 100 nA (Figure 3.1b and 3.2b). The good correlation between soluble organic- Fe(III) complexes and Fe(II) in both sediments may indicate the intermediate formation of soluble Fe(III) complexes prior to reduction (Chow and Taillefert, 2005; Taillefert et al., 2002a). A distinct voltammetric signal for ΣH_2S was detected at 17 mm in RB, just below the onset of Fe(II). ΣH_2S reached a concentration of 75 μM at 28 mm and stabilized around that value deeper, though it was removed at discrete locations in the porewaters (Figure 3.2b). As the voltammetric

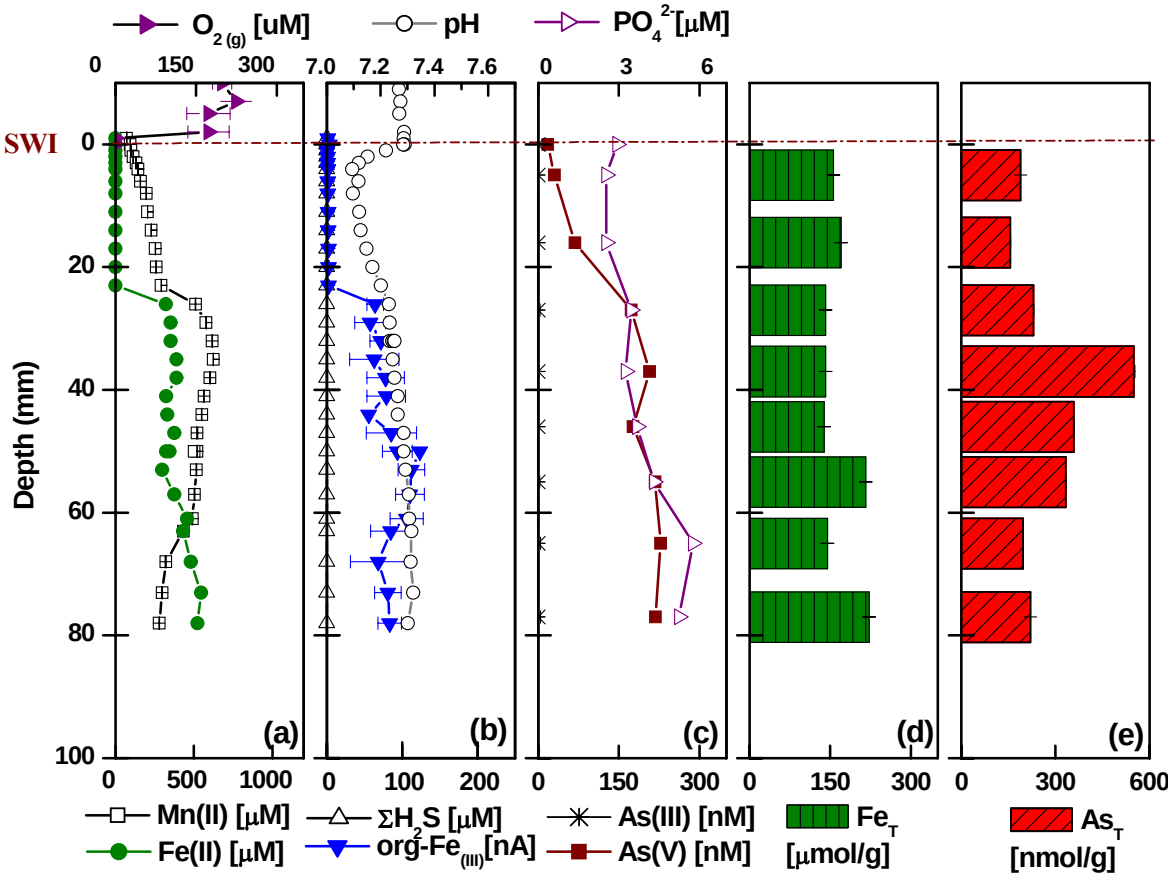

Figure 3.1 – Depth profiles obtained by microelectrodes and porewater extractions in Placid Cove sediment in July 2004: a) $O_{2(aq)}$, Fe(II), and Mn(II); b) ΣH_2S, org-Fe(III), and pH; c) ΣPO_{4D} and ΣAs_D in extracted porewaters; d) solid phase Fe-oxides; and e) solid phase As_T, sediment-water interface (SWI) indicated by the dashed line.

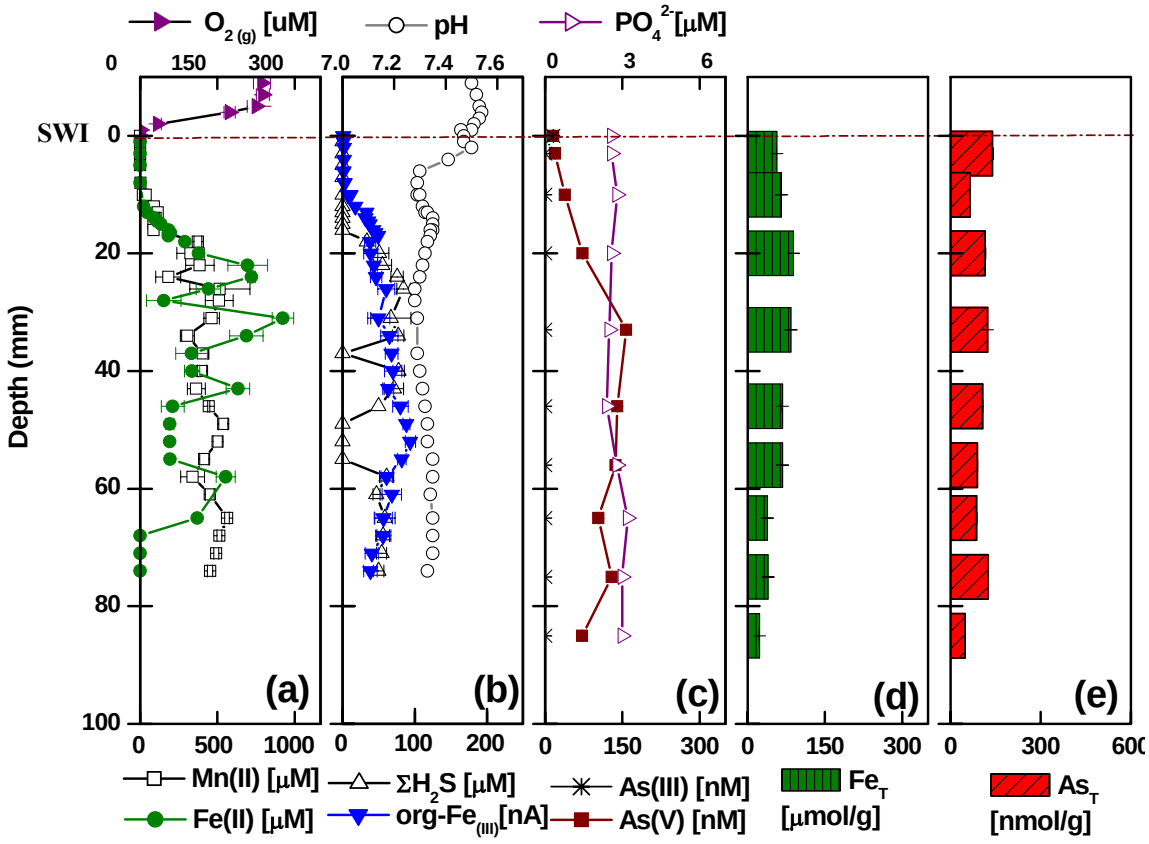

Figure 3.2– Depth profiles obtained by microelectrodes and porewater extractions in River Bend sediment in July 2004: a) $O_{2(aq)}$, Fe(II), and Mn(II); b) ΣH_2S, org-Fe(III), and pH; c) ΣPO_{4D} and ΣAs_D in extracted porewaters; d) solid phase Fe-oxides; and e) solid phase As_T, sediment-water interface (SWI) indicated by the dashed line.

technique used for these measurements cannot separate sulfide species from elemental sulfur, it is not clear what the oxidation state of sulfur is in this sediment. Nonetheless, interstitial ΣH_2S concentrations were always minimal in RB cores and never detected in any cores from the PC site. Interstitial ΣH_2S was never detected during the incubation experiments, suggesting that reduction of iron and/or arsenate by ΣH_2S did not occur.

Total dissolved orthophosphate ranged between 2.5 and 3 μM in the overlying water and porewaters in RB, while it increased to 6 μM below 60 mm in PC (Figure 3.1c and 3.2c). The concentration of total organic carbon varied between 500 μM in CRW and 330 and 400 μM in RB and PC porewaters, typical of freshwater concentrations. It is worth noting that the ratio of total organic carbon compared to other redox-active solutes is high in this system. Average concentrations of 130 μM Cl^- and 28 μM NO_3^- were found throughout the porewaters and the overlying water. In contrast, SO_4^{2-} decreased from 45 μM at the SWI to below detection limits within 10 mm in both sediments. The concentrations supplied to incubations for biotic and abiotic processes were limited to these initial levels. The dissolved silica was below detection limit in the water column and approximately 2 μM in the porewaters (not shown).

The primary objectives of this study were to identify the major redox processes controlling arsenic speciation in these iron–rich sediments and investigate how they are affected by increasing concentrations of arsenate that could be supplied by the Chattahoochee River. Depth profiles of total dissolved arsenic (As_D) in both cores (Figures 3.1c and 3.2c) displayed similar trends: As_D increased below the SWI, reached a maximum of 156 nM between 20 and 33 mm for RB and 227 nM between 55 and 65 mm for PC, and stabilized at these concentrations deeper. As(III) concentrations were below

detection limit in all porewaters collected in 2003 and 2004, indicating that dissolved arsenic was mainly under the form of arsenate in these sediments. More specifically, sediment depth profiles demonstrate arsenate accumulates in the porewaters near the SWI and diffuses back to the overlying waters at both sites (Figures 3.1 and 3.2). The flux of As(V) to the overlying water decreases from 135 and 267 nmol cm^{-2} y^{-1} in flood-impacted RB and PC cores (Chow and Taillefert, 2005), down to 54 and 80 nmol cm^{-2} y^{-1} in base flow conditions. The accumulation of As(V) in the porewaters coincides with the production of both Fe(II) and Mn(II) (Figures 3.1 and 3.2) revealing that arsenate was released during the reductive dissolution of iron and manganese oxides. The concentration of dissolved sulfide was either insignificant or much smaller than that of Fe(II) at both sites suggesting that the reduction of iron oxides was mainly microbial in these sediments (Figures 3.1 and 3.2).

RB sediment contained 56 (± 0.17) μmol/g amorphous iron oxides just below the SWI and displayed a maximum of 89 (± 0.23) μmol/g at 20 mm before decreasing regularly to 23 (± 0.28) μmol/g at 85 mm (Figure 3.2d). In contrast, amorphous iron oxide concentrations, ranging from 140 to 222 μmol/g, were much higher and uniform in PC (Figure 3.1d). The solid phase arsenic profile matched that of amorphous iron oxide and was constant around 140 (± 20) nmol/g in RB (Figure 3.2e). In turn, solid phase arsenic was generally higher around 189 (± 20) nmol/g over the first 30 mm in PC and formed a peak with a maximum of 550 (± 3) nmol/g As(V) at 40 mm. Solid phase iron and arsenic depth profiles show that in base flow conditions, the distribution of iron and arsenic is more uniform than just after flooding events (Chow and Taillefert, 2005), suggesting that arsenic-bearing iron oxides accumulate at the SWI during the flooding

events. Deposition of fresh particles is not uncommon after flooding events and may have significant effects on processes establishing redox zonation (Mucci, 2002).

It is widely accepted that As(III) is the dominant arsenic species under reducing conditions (Smedley and Kinniburgh, 2002). Therefore, the absence of As(III) in anoxic porewaters at both locations and in different flow conditions was unexpected. Initially, the absence of As(III) in reducing conditions was attributed to the disruption of regular redox zonation by recent particulate deposition after a flooding event (Chow and Taillefert, 2005). However, the same behavior was observed in sediments from the same sites under base flow conditions (Figures 3.1 and 3.2), indicating that these processes are independent of the flow conditions in the Chattahoochee River. These findings imply that the reduction of As(V) is either a slow process in these sediments or that another process, such as adsorption onto metal oxides (Pierce and Moore, 1982; Belzile and Tessier, 1990), anaerobic oxidation by nitrate-reducing bacteria (Oremland et al., 2002), or chemical oxidation by chelated Fe(III) (Hoeft et al., 2002) or manganese oxides (Chiu and Hering, 2000) removes As(III) rapidly.

3.4.2 Effect of Arsenate Concentration on Microbial Iron Reduction

The extent of reductive dissolution of authigenic iron oxides and its effect on arsenic speciation at increasing arsenate amendments were investigated in sediment slurry incubations. Approximately 200 nM As(V) from the original sediment was present in all sediment slurries at the beginning of the incubations. Incubations established that arsenate added to the sediment is initially removed from porewaters (Figures 3.3 and 3.4), probably by adsorption onto authigenic iron oxides only. Depending on the treatment,

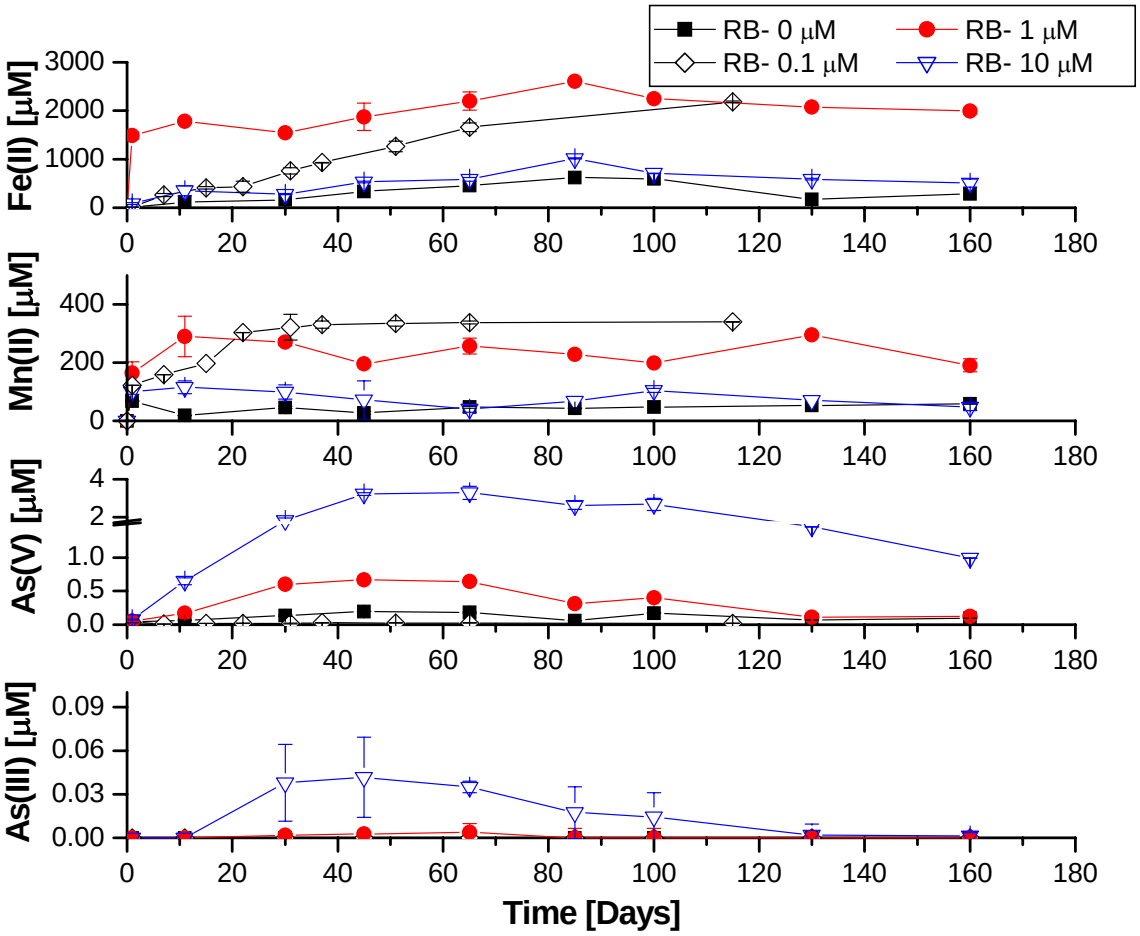

Figure 3.3- Time evolution of Fe(II), Mn(II), As(V), and As(III) concentrations during incubations of River Bend (RB) sediments at different initial arsenate amendments: 0 μM (squares), 0.1 μM (open diamonds), 1μM (circles), and 10 μM (open triangles).

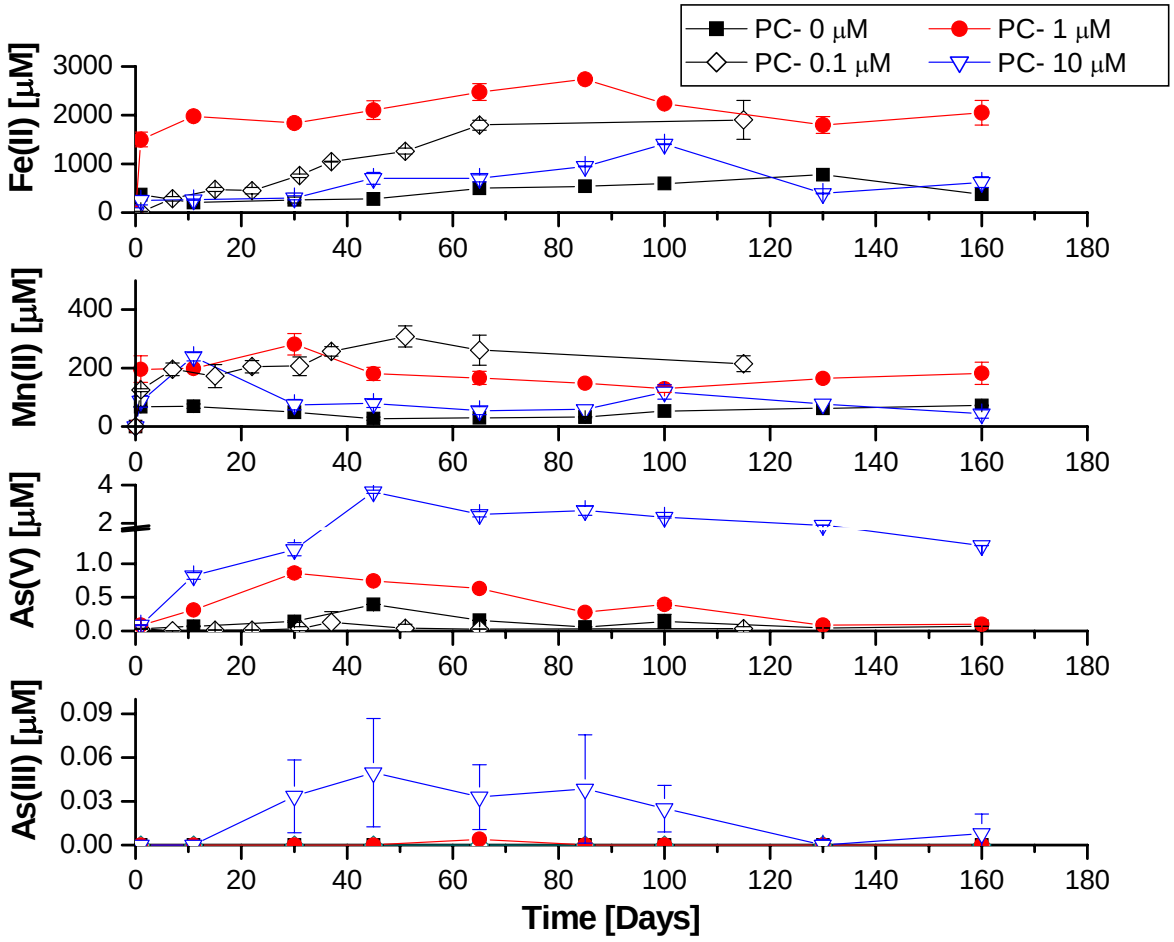

Figure 3.4- Time evolution of Fe(II), Mn(II), As(V), and As(III) concentrations during incubations of Placid Cove (PC) sediments at different initial arsenate amendments: 0 μM (squares), 0.1 μM (open diamonds), 1μM (circles), and 10 μM (open triangles).

the pH of sediment slurries decreased from 6.95 in the beginning of the experiments to a range between 6.20 and 6.59 after 160 days (not shown). Natural manganese oxides generally carry negative surface charges at the initial pH of both natural and incubated sediments and should, therefore, not scavenge arsenate significantly (Ouvrard et al., 2005).

All arsenate treatments in both PC and RB sediments displayed a progressive release in As(V) until 45 to 65 days, followed by a gradual removal of As(V) from porewaters for the duration of the incubations (Figures 3.3 and 3.4). More importantly, these incubations showed that As(V) loading impacted the reductive dissolution of both iron and manganese oxides, as well as the reduction of As(V) in these sediments. Mn(II) and Fe(II) were produced over time in each incubation, reached maximum concentrations around day 45, then manganese stabilized as iron was slowly removed from the porewaters (Figures 3.3 and 3.4). Low but slightly above background concentrations of As(V) (0.1 to 1 μM) accelerated an increase in the production of both Mn(II) and Fe(II) at both sites though in greater concentration for Fe(II) than Mn(II) (Figures 3.3 and 3.4). As(III) production was below the detection limit for all of the reactors with initial arsenate amendments lower than 1 μM (Figures 3.3 and 3.4). In turn, an average of 3 (± 1) nM of As(III) was detected between 35 and 65 days in both RB and PC sediments amended with 1 μM As(V). More importantly, As(III) was produced after 10 days in the 10 μM As(V)-amended reactors of both sites and steadily increased to maxima of 49.4 nM in PC and 41.4 nM in RB at day 45, before decreasing gradually to below detection limit by day 160. In contrast, a decline in iron reduction accompanying the production of As(III) was observed in the highest arsenic amendments.

The effect of arsenic on microbial processes is a function of its oxidation state (Oremland and Stolz, 2005). As(III) reversibly combines with thiol groups, via cellular proteins such as aqua-glycerolporin, and affects cellular processes (Oremland and Stolz, 2005). In turn, As(V) substitutes for phosphorus and inhibits oxidative phosphorylation in the formation of adenosine triphosphate (ATP) necessary to generate energy (Stolz and Oremland, 1999). Therefore, the increase in reductive dissolution of iron oxides in these incubations may have risen from efficient substitution of As(V) for PO_4^{3-} during ATP formation in indigenous iron reducing bacteria. This substitution would limit ATP production and promote an increase in anaerobic respiration of iron oxides to achieve a similar output of metabolic activity. Incubations revealed an apparent increase in the rate order of iron reduction with increasing arsenic concentrations (Figures 3.3 and 3.4). Fe(II) production in the non-amended reactors was indicative of a zero-order rate law (Appendix Figure B.1), while its production followed an apparent first-order rate law when arsenic concentrations increased up to 1 μM (Appendix Figure B.2). The rate law for iron respiration is proportional to the cell concentration, the concentration of electron donors and acceptors, and the thermodynamic driving force (Jin and Bethke, 2005). As these incubations were subject to the exact same terminal electron acceptor and donor concentrations, and as the number of cells, at least initially, can be assumed constant between reactors, the only parameter that could change between incubations was the thermodynamic driving force. The thermodynamic driving force, F_T, depends on the energy gained during the redox reaction and energy cost during ATP synthesis according to:

$$F_T = 1 - \exp\left(\frac{\Delta G_{redox} + \frac{\chi}{m}\Delta G_p}{\chi RT}\right) \qquad \text{(Equ. 1)}$$

where ΔG_{redox} is the Gibbs free energy change of the redox reaction between terminal electron acceptor and donor, ΔG_p is the Gibbs free energy change of ATP synthesis and is related to the proton motive force (Equ 2.), m is the number of ATP molecules synthesized, χ is an estimated average stoichiometric number of ATPs synthesized per reaction turnover, R is the gas constant, and T is the absolute temperature (Jin and Bethke, 2005).

$$\Delta G_p = \Delta G_p^0 + mRT \ln \frac{[ATP]}{[ADP]\ [PO_4^{2-}]} \qquad \text{(Equ. 2)}$$

Initially, it can be assumed that the ΔG_{redox} remained constant between incubations. Therefore, if arsenate blocked ATP formation, ΔG_p decreased and the thermodynamic driving force increased. An increase in thermodynamic driving force has a non-linear effect on the rate law and can account for the enhanced rate of iron respiration observed in reactors with 0.1 and 1 μM As(V) amendments. These results also imply that indigenous microorganisms were not respiring on iron oxides at maximum rate in unamended incubations.

At high concentrations of arsenate (>1 μM), the rate of iron reduction decreased. This decrease most likely reflected an inhibition process due to the presence of high arsenic concentrations. The effect of inhibition on rates of reaction can be examined using Michaelis-Menten kinetics (Bailey and Ollis, 1986). The rate law for microbial iron reduction may be written as:

$$R = \frac{d[Fe(II)]}{dt} = \frac{R_{\max}[Fe(OH)_3]}{K_{app} + [Fe(OH)_3]} \qquad \text{(Equ. 3)}$$

where R_{max} is the maximum rate of iron reduction, $[Fe(OH)_{3(s)}]$ is the concentration of iron oxides substrate calculated as the difference between the initial total reactive iron ($[Fe(OH)_{3(s)}{}^0]$) and the concentration of dissolved ferrous iron produced ([Fe(II)]) over time, and K_{app} is the apparent Michaelis-Menten rate constant modified to include arsenic inhibition. Equation 3 was integrated using a fourth order Runge-Kutta numerical procedure, and R_{max} and K_{app} values were optimized to fit experimental data (Fe(II) produced) from each reactor using a least-square non-linear fitting procedure written in Matlab™ (Appendix B). While K_{app} increased linearly as a function of the arsenic added, the optimized R_{max} in both RB and PC sediments was estimated to be 100 μM/d for iron oxides in all incubations, except in 1 μM As(V) amendments. The higher R_{max} estimated from 1 μM As(V) amendments suggests supplemental reduction activity, possibly a result of enhanced respiration caused by the arsenate stress described above. An increase in K_{app} but constant R_{max} associated with incubations conducted at high arsenic levels (10 μM) compared to low levels (≤ 1μM) indicates that arsenic inhibition was fully competitive. Thus, K_{app} can be calculated as (Bailey and Ollis, 1986):

$$K_{app} = K_m\left(1 + \frac{[HAsO_4^{2-}]}{K_{As}}\right) \qquad \text{(Equ. 4)}$$

where K_m is the Michaelis–Menten constant for iron respiration, $[HAsO_4^{2-}]$ is the total concentration of inhibitor, and K_{As} is the inhibitor constant. The Michaelis-Menten constants for iron reduction (K_m) and arsenic inhibition (K_{As}) were calculated for the sediment of each site based on the linear relationship between optimized K_{app} and the As(V) concentration of each incubation (Appendix Table C.1 and Figure C.3).

Ominously, calculated toxicity thresholds (K_{As}) ranged between 2 ± 0.65 μM for RB and 4 ± 1.5 μM for PC sediments. The K_m estimates for iron reduction (1 ± 0.58 for RB and 3 ± 0.32 for PC) are 1 to 4 orders of magnitude lower than those from synthetic iron oxide and pure culture experiments of iron reducing bacteria in the absence of inhibitor (Bonneville et al., 2004). Fundamentally, the lower K_m suggests more efficient enzyme-substrate complexation by indigenous iron-reducing bacteria (Bailey and Ollis, 1986). Our findings indicate that these bacteria are able to overcome the inhibition of ATP formation when concentrations of arsenate are in the range of 0.1 to 1 μM (i.e. below toxicity threshold) by increasing anaerobic respiration of iron oxides. When the concentration of arsenate reaches the toxicity threshold (K_{As}), however, the ATPase is probably completely complexed by arsenate, and iron respiration is inhibited. As rates of iron reduction never completely decrease to zero in the highest As(V) amendments, these experiments demonstrate that microbial iron reduction will not be completely impaired in these sediments.

Alternatively, the addition of As(V) to reactor sediments could hypothetically stimulated ATP production and Fe respiration by liberating phosphate bound to metal oxides. However, the preferential adsorption of $HAsO_4^{2-}$ needed to liberate HPO_4^{2-} by ion exchange (Manning and Goldberg, 1996) is less likely in the circum-neutral pH range of the incubation slurries. In addition, microorganisms store excess phosphate in their cell tissues for ATP production, therefore if some phosphate is displaced by the low arsenate additions, it should not affect microbial iron respiration. Our data can not fully dispute this alternative hypothesis, therefore competitive adsorption of phosphate and arsenate on natural sediments should be investigated in greater detail with respect to iron

respiration. Regardless, iron respiration was enhanced by the addition of low levels of As(V) whether directly or indirectly through phosphate liberation.

3.4.3 Effects of Arsenate Concentrations on Sediment Transformation

Figures 3.5 and 3.6 illustrate the similarities between the solid phase composition of both RB and PC sediments. Initially, both sediments contained 73 (±10) μmol/g of amorphous and crystalline iron oxides (Figure 3.5). At the end of the incubations, all sediments demonstrated a decrease in amorphous iron oxide concentrations. In contrast, the concentration of crystalline iron oxide increased significantly in both PC and RB sediments that demonstrated enhanced microbial reductive dissolution (0.1 and 1 μM), but only slightly in the 10 μM As(V) amendment (Figure 3.5a). These data suggest that Ostwald ripening of amorphous iron oxides to more thermodynamically stable phases occurred during the incubations, probably accelerated by high concentrations of Fe(II) (Hansel et al., 2005). Indeed, sulfate, pH, and Fe(II) ranges in all our reactors were conducive of secondary solid-phase transformation to goethite (Hansel et al., 2005). The increase in crystalline iron oxides correlated with the rate of iron reduction and indicates that the increase in As(V) loading impacted both iron reduction rates and the mineralogy of iron oxides. In contrast, the concentration of amorphous and crystalline manganese oxides did not change considerably over the course of the incubations (Figure 3.5b), implying that manganese reduction was not significantly affected by the increase in arsenic concentrations.

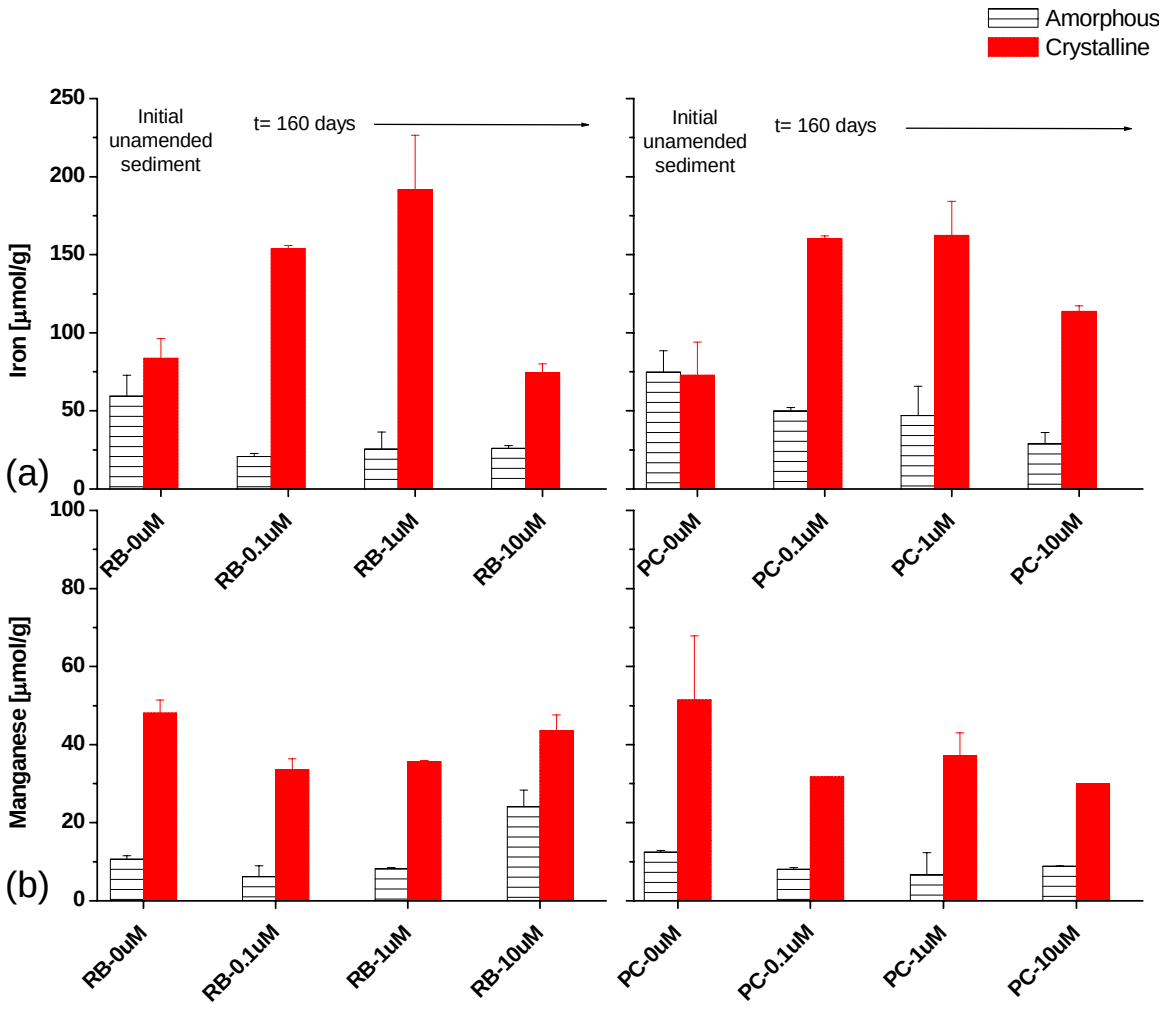

Figure 3.5- a) Amorphous and crystalline iron oxides; and b) amorphous and crystalline manganese oxides at the end of the incubations in the Placid Cove (PC) and River Bend (RB) sediments exposed to different As(V) concentrations. The unamended samples were quantified at time 0 only.

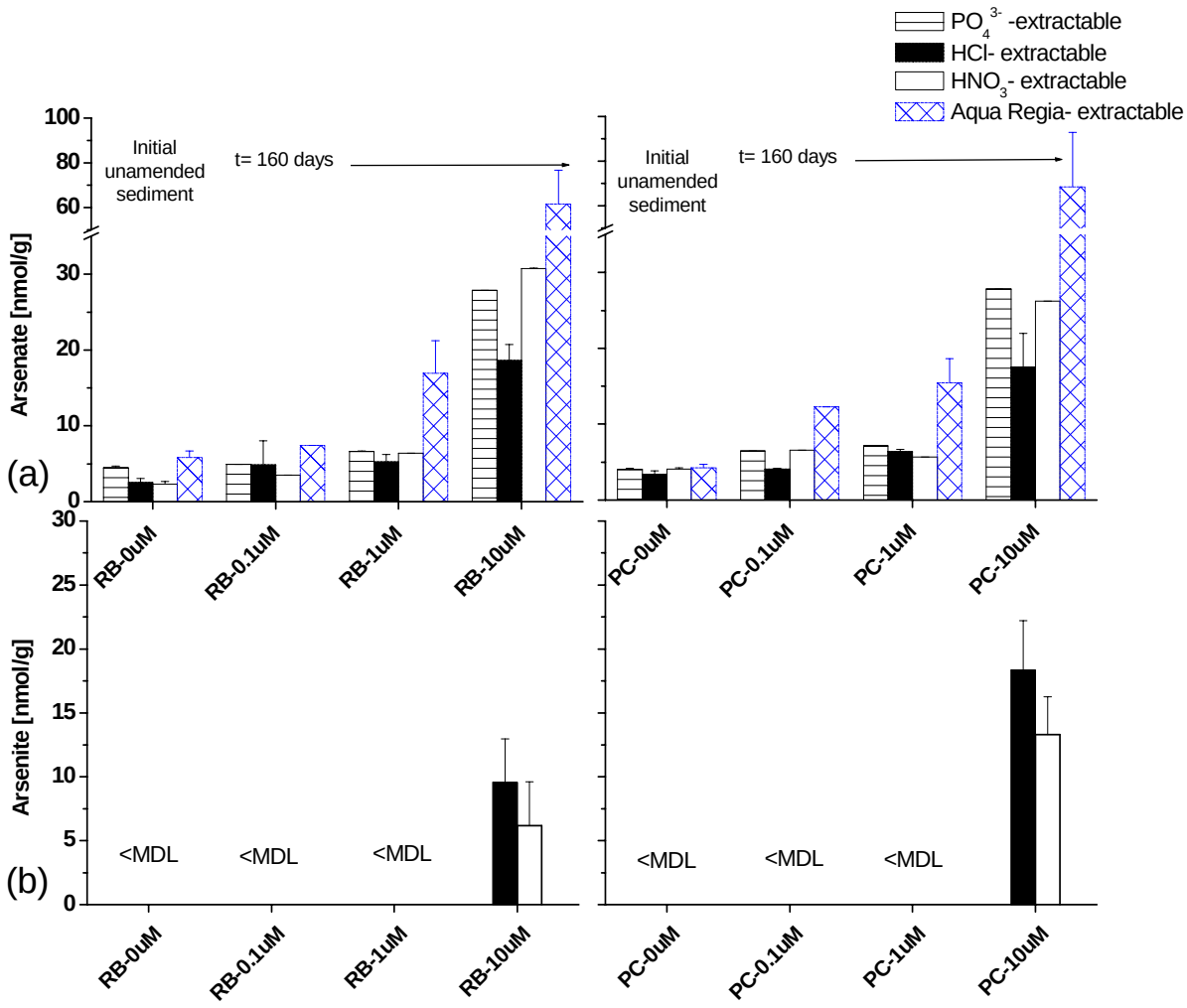

Figure 3.6- Solid Phase Extractions of: a) arsenate; and b) arsenite after incubations in the Placid Cove (PC) and River Bend (RB) sediments in the case of the 0.1, 1 and 10 μM As(V) amendments. The unamended samples were quantified at time 0 only.

Comparison of the different solid phase extractions of As(V) (Figure 3.6a) demonstrates that most of the As(V) was in fact adsorbed and not incorporated into the iron oxide lattice during re-crystallization, regardless of the As(V) load. In addition, arsenite formed in these incubations was partly adsorbed onto iron oxides and dissolved in the porewaters (Figure 3.6b). The secondary mineralization of amorphous iron oxides to more crystalline phases (Hansel et al., 2005) is accompanied by a decrease in specific surface area, and thus site densities, which decreases sorption of both arsenate and arsenite (Dixit and Hering, 2003; Ona-Nguema et al., 2005). Thus, maturation of the iron oxides spurred by the presence of arsenate probably decreased the ability of authigenic sediments to retain arsenic. To illustrate this effect, the release of arsenate into the porewaters was correlated to the production of Fe(II) as a function of time. To compare the different incubations, As(V) levels were also normalized to the total As(V) concentration, including the initial solid phase and porewater amendments. In general, the ratio of As(V) to Fe(II) for both PC and RB sites were similar and showed that the fraction of As(V) released initially increased proportionally to the concentration of Fe(II) produced in all the As(V) amendments (Appendix Table C.1). Once iron reduction reached steady- state (i.e. ~45 to 85 days), however, adsorbed As(V) was released in excess compared to Fe(II) in the 0.1 and 1 μM As(V) amendments, resulting in a slight decrease in the correlation coefficients. Simultaneously, the concentration of total arsenic extracted by Aqua regia was between 46 and 63 % higher in the 1 and 10 μM reactors than in the low amendment incubations (Figure 3.6a). These data indicate that As(V) was partly released during the recrystallization of iron oxides in the 0.1 and 1 μM As(V) incubations and partly associated with silicates, magnetite, or organic matter when

As(V) loading was ≥ 1 μM. Indeed, biogenic magnetite formation is promoted by surface loads greater than 0.3 mM Fe(II) (Hansel et al., 2005), well within the range of Fe(II) levels in these sediments, suggesting that As(V) may also be sequestered during recrystallization of amorphous iron oxides into biogenic magnetite.

The absence of As(III) in the porewaters of incubations with initial As(V) ≤ 1μM was likely not due to its removal by oxidation nor its incorporation in the solid phase. These incubations were conducted in anaerobic conditions, and chemical oxidation of As(III) by MnO_2 (Chiu and Hering, 2000) probably did not dominate in this sediment, because Mn(II) and As(III) were produced simultaneously in the 1 and 10 μM As(V) amendments (Figures 3.3 and 3.4). In addition, phosphate-exchangeable As(III), As(III) bound to iron oxides, and As(III) precipitated with pyrite and arsenopyrite were below detection limit in both sediments amended with ≤ 1μM As(V) (Figure 3.6b). At higher As(V) loads (>1 μM), As(III) was probably produced by microbial reduction of As(V), as dissolved sulfide (abiotic reductant) was not detected during the incubations. Assuming a first order rate law of arsenate reduction (modified Michaelis-Menten equation), the rate of arsenite production is:

$$\frac{d[As(III)]}{dt} = k[HAsO_4^{2-}] \qquad \textit{(Equ.5)}$$

where k is the rate constant (d^{-1}) and [$HAsO_4^{2-}$] is the initial concentration of As(V) adsorbed onto iron oxides (nmol/g) in these sediments. The latter was calculated from the maximum amount available for desorption prior to reduction (i.e. sediment content plus amendment) and the maximum concentration of As(III) measured (Figures 3.3, 3.4, and 3.6b). Rate constants of 0.029 ± 0.006 and 0.0279 ± 0.008 (d^{-1}) were calculated from As(V) reduction in the 10 μM As(V) amendments for PC and RB, respectively. Rate

constants from pure culture studies tend to be 5 to 10 orders of magnitude lower for As(V) detoxification compared to As(V) respiration (Newman et al., 1998; Jones et al., 2000). The rate constants calculated from our incubations are two orders of magnitude lower than detoxification rate constants determined with microorganisms isolated from soils (Jones et al., 2000), suggesting that As(III) production in these incubations was a result of detoxification. In similar fashion to As(V), As(III) was slowly removed by adsorption at the end of both sets of 10 μM amended incubations (Figures 3.3 and 3.4). Equivalent concentrations of arsenite were detected in both HNO_3 and HCl extractions of the 10 μM As(V)-amended sediments but, as expected, not in the PO_4^{3-} exchangeable extractions (Figure 3.6b). The solid phase analysis confirmed that the majority of As(III) produced was immobilized in the sediments. These findings demonstrate that Chattahoochee River sediments can retain As(III) produced by iron-reducing bacteria.

3.4.4 Environmental Implications

Our incubations show that the indigenous iron-reducing bacteria may accelerate iron respiration to overcome an up to 1 μM increase in arsenic loading to sediments. However, if As(V) input to sediments rise by one order of magnitude above the current porewater content (i.e. 200 nM), iron respiration will be inhibited and As(III) produced in significant quantities. The present river waters contain in average about 40 nM of As(V) in the dissolved phase (Lesley, 2002) that can be delivered to the sediments, especially during flood events (Chow and Taillefert, 2005). If the loading of As(V) to these sediments persists or increases, the currently abundant amorphous iron oxides will be transformed into more stable iron oxides with lower adsorption capacity for As(V).

Compounded with the production of As(III), if the toxicity threshold is exceeded, these sediments may be a non-point source of both As(V) and As(III) to the overlying waters, including the drinking water reservoir of West Point Lake which currently complies to State and Federal standards. These incubations show that to prevent hazardous conditions, it is necessary to maintain the concentration of arsenate in the porewaters below the estimated threshold of 2 to 6 μM.

3.5 Acknowledgements

This research was supported in part by the Georgia Water Resource Institute and by the National Science Foundation (EAR-0216368). We would like to offer our sincere gratitude to J. Partin for his help in the field, and to E. Carey, G. Bristow, J. Newton, J.-F. Koprivnjak, F. Yasmin, D. Putrasahan, and J. Elsenbeck for their contribution to the extractions and analyses of the original sediment cores.

3.6 Supporting Information Available (Appendices B and C)

Figures are provided in Appendix B to demonstrate non-amended reactors followed a zero-order rate law (Figure B.1) while reactors with up to 10 μM As(V) added followed first-order rate laws (Figure B.2) represented by the data from the 1 μM triplicate reactors of Placid Cove sediments. Figure B.3 represents the composite of the correlation between Fe(II) and As(V) concentrations released over time in triplicate reactors. These slopes were used to calculate the potential binding sites occupied on Fe-oxides. A descripition of the kinetic model, model output figures (C.1 to C.3), and tabulated input and output kinetic data (Table C.1) are provided in Appendix C.

CHAPTER 4

CONSEQUENCES OF TIDAL FORCING ON THE DISTRIBUTION OF TRACE METALS IN THE REDOX TRANSITION ZONE OF THE CHESAPEAKE BAY

4.1 Abstract

A combination of *in situ* measurements with discrete water sampling was utilized to determine the influence of tidal variations on the cycling of trace metals during two consecutive tidal cycles in the Chesapeake Bay (MD) during the peak anoxic/hypoxic season. *In situ* profiles show as the tides progress from high to low, both buoyant oxic freshwater and saline suboxic waters flowing seaward result in the vertical mixing of oxic and anoxic waters that shifts the oxycline up in the water column. At the next flood tide, the oxycline is lowered in the water column when oxygenated dense seawater flowing landward sinks in water column. The expansion of the anoxic zone as tides ebb and compression caused by destratification during flood tide shifts the distribution of both sulfide and manganese. As tides oscillate, dissolved Mn and sulfide accumulate in the suboxic zone. The increase of dissolved manganese and sulfides below the oxycline seems to be accompanied by an enrichment of dissolved trace metals, especially during the 2nd tidal cycle. The distribution of uranium and barium, two natural conservative tracers, during both tidal cycles indicates mixing of buoyant freshwater and denser oceanic water in the Chesapeake Bay, and sediment-water interactions result in an input of dissolved constituents, with no significant sediment resuspension, to the overlying

waters during the 2nd tidal cycle. More specifically, the bottom water enrichment is much higher for dissolved lead, chromium, and maybe copper during the 2nd tidal cycle, while no perceptible change is observed for dissolved cobalt and nickel, and a decrease in dissolved arsenic is evident. This research suggests that suboxic dissolved sulfides, chromium, manganese, cobalt, copper, arsenic, barium, lead, and uranium concentrations are enriched from tidally-driven horizontal advective flushing of chemical reserves stored in Chesapeake Bay sediments, regardless of resuspension. More importantly, the magnitude of fluxes of trace metals from the sediment is regulated by the chemical reactivity of trace metals with sulfide in the sediment. While Co and Ni are preferentially retained onto pyrite due to their low rate of water exchange compared to Fe, Cu, Pb, and Cr are likely unreactive with respect to iron sulfide minerals due to their high rate of water exchange. Therefore, Pb, Cu, and Cr may preferentially form MeS or be released in the overlying waters if dissolved sulfide levels are not significantly enough to induce precipitation of discrete sulfide phases. In turn, the removal of arsenic during the 2nd tidal cycle may be due to its co-precipitation with pyrite in the sulfidic bottom waters. Overall, trace metal cycling at the redox transition in the Chesapeake Bay is influenced by transformation of sulfide and tidal advection across the sediment-water interface.

4.2 Introduction

The water column of the Chesapeake Bay is subject to three modes of circulation: river-forced, wind-forced, and gravitational (Goodrich and Blumberg, 1991) that play important roles in the seasonal variability of biogeochemical processes (Schubel, 1968; Schubel and Pritchard, 1985; Boicourt, 1992; Roman et al., 2005). The confluence of

riverine and denser marine waters results in the suppression of vertical exchange and establishes longitudinal and lateral density gradients throughout the Bay. This stratification of the water column, characterized by a more saline lower-layer that is influenced by tides, drives estuarine circulation (Pritchard, 1952). Local wind and weather patterns may also affect tides by moving water away from coastlines (offshore winds), exaggerating low tide exposures, or virtually eliminating low tide exposures with onshore winds (Goodrich and Blumberg, 1991; Guo and Valle-Levinson, 2007). Wind-driven mixing associated with strong storm events may cause surface waters to flow landward, resulting in episodic periods of water column destratification that are rapidly reestablished by density gradients (Goodrich et al. 1987). The combined effect of wind-forcing and longitudinal density gradient is responsible for the two-layered estuarine flow pattern dominating circulation in the Chesapeake Bay (Goodrich and Blumberg, 1991). As a result of its shallow sill, high freshwater inflow, and relatively mild tidal mixing, the residence time of freshwater is long (90 to 180 d) in the estuary. On short-term tidal time scales (2 to 4 hours), baroclinic (density-driven) pressure gradients are influenced by tidal asymmetry such that, at ebb tide, stratification and shear stress along-channel is enhanced while stratification is reduced during flood tides (Jay and Smith, 1990; Boicourt, 1992). A schematic of the general estuarine circulation pattern is presented on Figure 4.1. As oxygen rich ocean water flows landward during flood tide, oxygen is consumed during processes oxidizing organic matter in the sediment such that inland bottom waters are depleted of oxygen that is not replenished by buoyant freshwater flowing seaward above the pycnocline (Figure 4.1a). At ebb tide, this oxygen-depleted water flows seaward and is partially mixed with oxygenated seawater during the next flood tide (Figure 4.1b). The

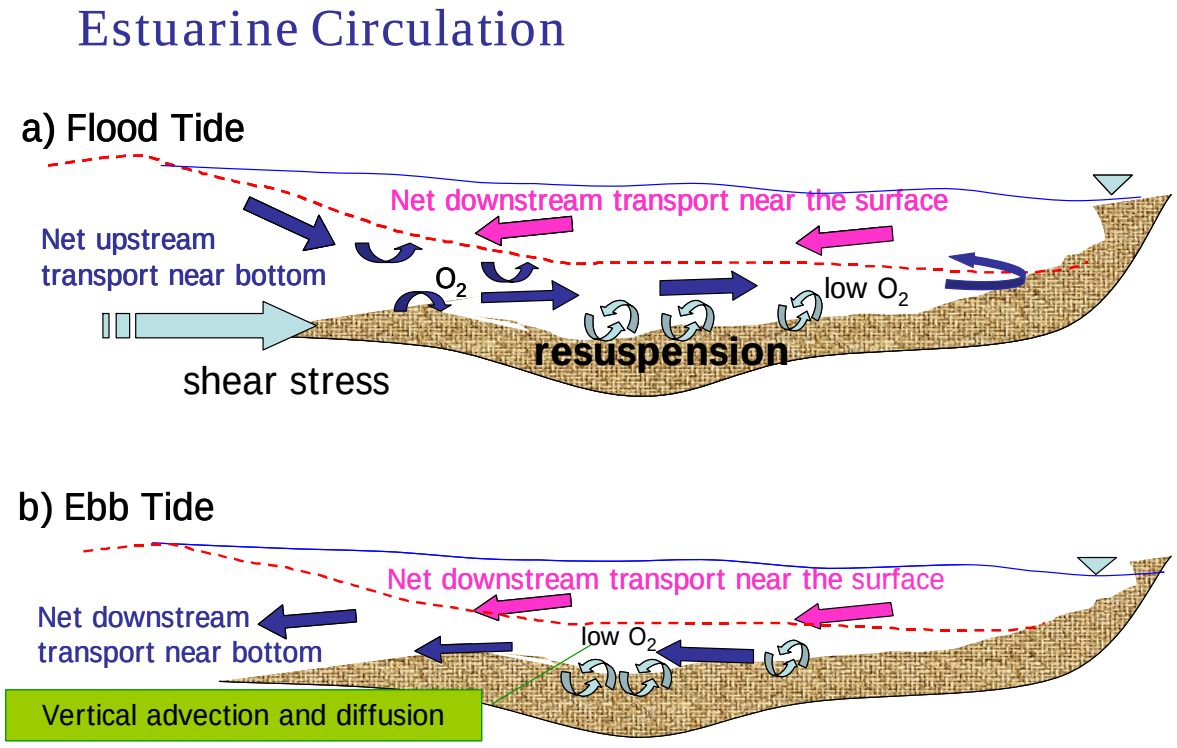

Figure 4.1- Schematic of the general estuarine circulation pattern during flood and ebb tides. As oxygen rich oceanic water flows landward during flood tide, oxygen diffuses across the pycnocline or is consumed in the sediment such that inland bottom waters are depleted of oxygen. Meanwhile, buoyant freshwater above the pycnocline continuously flows seaward. At ebb tide, this oxygen-depleted water flows seaward and is partially mixed with oxygenated seawater during the next flood tide. This estuarine circulation keeps the dense waters deaerated and promotes sulfate reduction in the sediments. In addition, as tides flow, their force may cause shear stress along-channel sediments resulting in the advection of dissolved species from surficial sediments.

density gradient and circulation pattern promote oxygen depletion in bottom waters by restricting supply below the pycnocline. Seasonal anoxia (from late spring to early fall) arises as oxygen demand increases in those same bottom waters as a response to enhanced primary production due to elevated nutrient (P and N) inputs from tributaries (Boicourt, 1992; Jonas, 1997; Kemp et al., 2005; Li et al., 2005). Consequently, sulfate reduction dominates organic matter remineralization in Chesapeake Bay sediments, and high sulfide concentrations are found in porewaters and even in the water column (Burdige, 1991; Roden and Tuttle, 1992; Roden and Tuttle, 1993; MacCrehan and Shea, 1995; Roden et al., 1995; Marvin-DiPasquale and Capone, 1998; Marvin-DiPasquale et al., 2003; Lewis et al., 2007).

The mixing of freshwater and marine waters during tidal oscillations vertically transports dissolved oxygen into suboxic and anoxic bottom waters resulting in the oxidation of sulfide and other abundant reduced species such as Mn(II) and Fe(II) (Boicourt, 1992). Manganese and iron cycles are directly affected by these tidal-related variations in oxygen and dissolved sulfide levels (Lewis et al., 2007). In the presence of oxygen, Mn-and Fe-oxides settle to the anoxic water column and sediment where they are reduced microbially or chemically by sulfide. Chemical reduction by sulfide may also occur in the water column if sulfide is transported across the sediment-water interface (SWI). In turn, evidence for microbial reduction of Fe- and Mn-oxides in the water column is lacking. These temporal variations in oxygen and sulfide concentrations have important consequences on the distribution of trace metals in the water column.

In general, trace metals are introduced into estuaries by riverine (Matisoff et al., 1975; DeGroot et al., 1976; Knight and Pasternack, 2000; Mason et al., 2004) and atmospheric inputs (Hussain et al., 1999; Kim et al., 2000; Scudlark et al., 2005). The

transformation of trace metals in estuaries does not follow a universal pattern (Van den berg, 1993; Caccia and Millero, 2003) because their physico-chemical properties are different. As particle-reactive metals enter estuarine waters, they are rapidly adsorbed on inorganic and organic suspended matter that sinks toward sediments (Burdige, 1991; Burdige and Homstead, 1994; Roden and Tuttle, 1996; Roden et al., 1995; Jonas, 1997; Fisher et al., 1998; Canuel, 2001; Zimmerman and Canuel, 2001). In addition, flocculation of metal oxides as a consequence of increasing pH and salinity can remove trace metals from the water column and result in a decrease of trace metal fluxes to the oceans (DeGroot et al., 1976; Caccia et al., 2003). Conversely, trace metals may be released from particles when they cross salinity gradients as a result of ion exchange processes (Millero and Hawke, 1992; Millero, 2000; Caccia and Millero, 2003). In anoxic conditions, sulfide is available to precipitate or complex with dissolved metals released from the reduction and dissolution of iron and manganese oxides (Luther et al., 1991; Luther et al., 1994; Luther et al., 1995; Luther et al., 1996; Morse and Luther, 1999; Luther et al., 2001; Luther et al., 2002; Herszage and Afonso, 2003; Poulton, 2003; Poulton et al., 2004; Rickard and Luther, 2003; Luther and Rickard, 2005a; Luther and Rickard, 2005b; Rickard and Luther, 2006; Rickard and Luther, 2007). Therefore, the vertical distribution of trace metals in estuaries may be a function of salinity and the chemical or microbially-mediated reductive dissolution of their geochemical hosts (Martino et al., 2002).

Simultaneously, the processes regulating the sediment-water exchange of dissolved trace metals are also important in controlling their distribution in the water column. The enrichment of bottom water Mn and H_2S by tidally-driven advection may be

accompanied by the release of trace metals stored in sediments. The sediment of the Chesapeake Bay contributes Hg (Lawson et al., 2001), Mo (Adelson et al., 2001), Mn (Holdren et al., 1975), As, Cu, Cd (Riedel et al., 1999), and U (Sarin and Church, 1994) to its overlying waters. In other estuaries, sediment bound Co has also been found to enrich surrounding waters (Martino et al., 2002; Preda and Cox, 2002; Tovar-Sanchez et al., 2004). Forebodingly, trace metal concentrations in sediments are typically orders of magnitude higher than interstitial and water column levels, such that the flux of potential pollutants into a more mobile phase is a concern in the Chesapeake Bay and to its inhabitants (Hartwell and Hameedi, 2007).

The objective of this research was to determine the effect of estuarine circulation on redox processes and the transformation of trace metals in the Chesapeake Bay during peak anoxic conditions between the summers of 2002 and 2005. For this study, a combination of CTD casts, discrete bottle sampling, and *in situ* voltammetric profiling was used to examine changing redox conditions and redox-sensitive chemical species in the water column. These parameters were observed to vary in response to tidal fluctuations, episodic mixing events, and interannual changes. The goals of this study were (1) to describe the biogeochemistry that is physically and chemically affected during tidal cycles across the oxic-anoxic transition in the water column, and (2) to investigate the effect of tidal forcing on the distribution of a suite of trace metals during the peak anoxic seasons.

4.2.1 Study Site

The study site is in the Northern Chesapeake Bay (Figure 4.2) which undergoes seasonal stratification controlled by the rates of benthic organic carbon deposition (Kemp et al., 2005) and mixing of surface waters with saline bottom waters moving along-channel during tidal cycles (Lewis et al., 2007). Based on redox stratification, trace metal transformations were determined in the water column at a single sampling location. Station 858, is an ~25 m deep, 4 km long and 0.8 km wide hole located at 38˚58.8'N; 76˚22'E. This area is influenced by a moderate tidal range <1 m (Li et al., 2005) and is located just south of the Bay Bridge, west of Kent Island and east of the main shipping channel. The study site is subject to advective-mixing processes which may include strong tidally-driven semi-diurnal oscillations, lateral standing waves motion, and/or episodic wind-forced pycnocline disruptions during storm events (Guo and Valle-Levinson, 2007; Lewis et al., 2007). Based on wind and tidal fluctuations, storm activity made a minor impact relative to the baseline 2004 and 2005 levels. Sediment deposition is estimated based on sediment accumulation models in the Chesapeake Bay on the order of 1 cm/yr (Schubel, 1968) while the sediment density is around 1.35 g cm^{-3} (Hartwell and Hameedi, 2007). The sediments in Northern Chesapeake Bay are typically fine grained organic-rich and sulfidic sediments with occasional interbedded sand layers (Sholkovitz et al., 1992; Shaw et al., 1994; Burdige, 2001). The bottom topography of this location is representative of the upper and mid-bay, with an average depth ranging from 18 to 30 m (Schubel, 1968; Schubel and Kana, 1972; Fugate et al., 2007).

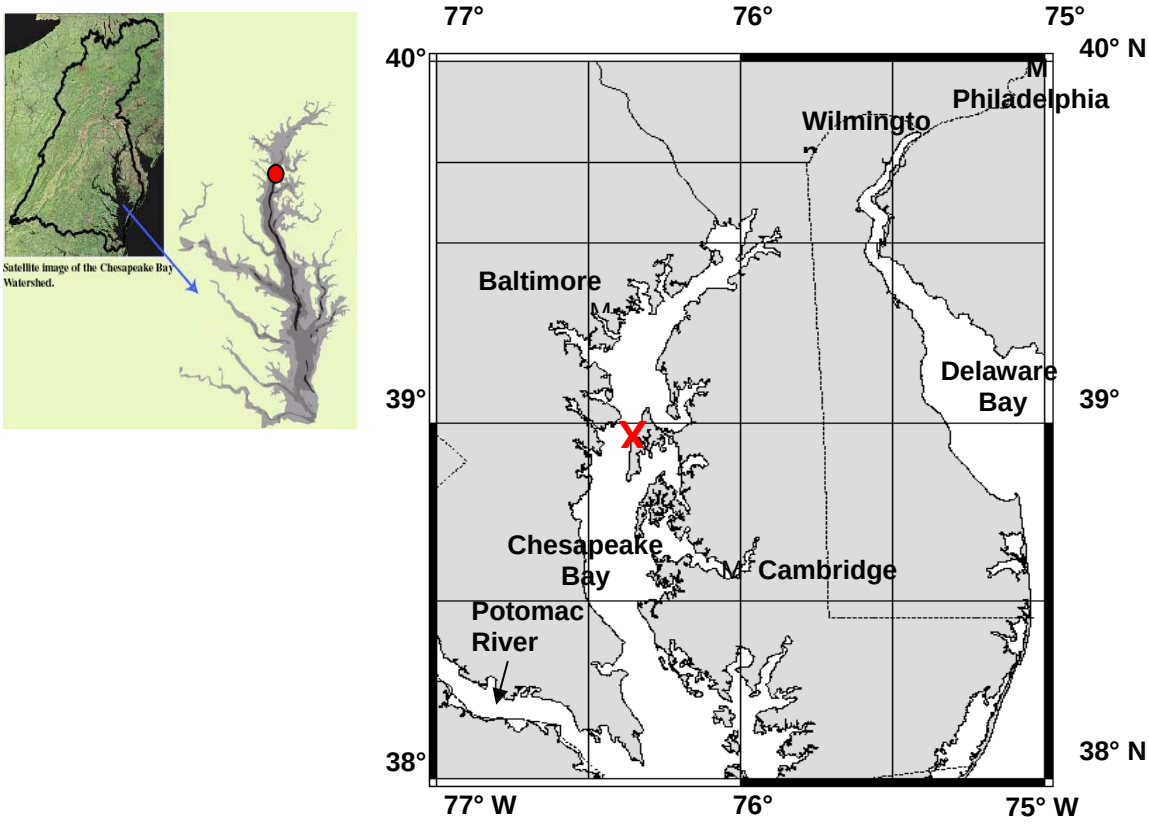

Figure 4.2- Study Site- Chesapeake Bay Monitoring Station 858-8 located at 38˚58.8'N; 76˚22'E. Inset of the Chesapeake Bay Watershed (Image from USGS)

Near surface mean flow was 5 cm s^{-1} seaward while bottom flow was landward at about 15 cm s^{-1}, with a maximum along-channel and across-channel velocity of 75 cm s^{-1} and 15 cm s^{-1} (Lewis et al., 2007). Redox potentials are very negative in the upper 10 cm of these sediments (Eh ~ -120 mV) (Burdige, 2001).

4.3 Sampling and Analyses

Cruises departed annually during peak anoxic/hypoxic summer season. The most pronounced oxygen depletion is noted in late July and August (Kemp et al., 2005), therefore water column samples were collected for analysis in conjunction with *in situ* measurements on August 22 (Tidal Cycle 1) and 23 (Tidal Cycle 2), 2005. Preliminary field investigations were conducted on July 24 to 29, 2002, August 2 to 8, 2003, and August 16 to 19, 2004, whose results are also discussed in this study and presented in Appendix D as Figures D.1 through D.11. Ship-board and *in situ* measurements of chemical and physical parameters were collected from aboard the R/V Cape Henlopen maintained at the site using two-point anchorage.

4.3.1 *In Situ* Measurements

Salinity, temperature, density, and chlorophyll a were measured *in situ* using a rosette-mounted Seabird CTD and two fluorometers (Sea Tech Fluorometer and WetLabs ECO-AFL/FL). *In situ* measurements of $O_{2(aq)}$, Fe(II), Mn(II), ΣH_2S (= H_2S + HS^- + S^{2-} + S^0 + S_x^{2-}) were obtained using Hg/Au microelectrodes (Brendel and Luther, 1995) interfaced to an ISEA-I^{TM} *in situ* electrochemical analyzer (Analytical Instrument Systems, Inc.) mounted on the CTD rosette. Steep gradients and thin interfaces that are

difficult to detect by traditional methods are easily identified by *in situ* voltammetric techniques (Brendel and Luther, 1995; Glazer et al., 2006a; Glazer et al., 2006b).

The *in situ* ISEA-I^{TM} system was linked to a Seabird Microcat to provide temperature, salinity, density, and depth for each voltammetric scan. The Microcat-ISEA-I^{TM} package (Luther et al., 2007) allowed for continuous real-time detection of specific redox zones to guide water sampling. The voltammetric system consisted of three electrodes including a working, reference, and counter electrode (Luther et al., 2007). The working electrodes were solid-state 100 μm diameter gold-amalgam (Au/Hg) fabricated in polyethyletherketone (PEEK^{TM}) tubing (Luther et al., 2007). The Ag/AgCl solid-state reference electrode was made of a 0.5 mm diameter Ag wire oxidized in 3 M KCl to produce the AgCl coating. The counter electrode was made of a 0.5 mm platinum wire.

For linear sweep voltammetric measurements (LSV), the voltage was scanned from -0.1 V to –1.9 V at a scan rate of 1000 mVs^{-1}. For cyclic voltammetry (CV), the same potential range was used, but anodic current was also obtained during the return to the initial potential. Electrochemical conditioning was performed for five seconds at -0.9 V, where none of the chemical species are electroactive, to restore the electrode surface between measurements (Brendel and Luther, 1995). Prior to field trips and aboard ship, standard curves were produced for O_2, Mn(II), and sulfur species (Brendel and Luther, 1995). The voltammetric operating conditions provided detection limits of ~3 μM for O_2, ~ 10 μM for Mn(II), ~ 30 μM for Fe(II), and ~30 nM for H_2S with a high spatial resolution (mm). Voltammetric scans were integrated using VOLTINT, a new Matlab ™ software developed for these applications (Bristow and Taillefert, 2007, *in press*).

Dissolved oxygen concentrations measured with the CTD agreed with *in situ* voltammetric measurements.

4.3.2 Trace Metal Sampling

In addition to dissolved nitrite, Mn(II), and Fe(II) analyses (Lewis et al., 2007), samples for trace metal analysis (Cr, Mn, Co, Ni, Cu, As, Cd, Pb, Ba, and U) were collected using acid-cleaned 5-liter Go-Flo or 10-liter Niskin bottles (General Oceanics) on the R/V Cape Henlopen CTD-rosette system at intervals of 0.5 to 1 m. Samples were collected based on O_2 and H_2S profiles determined by Au/Hg microelectrodes. Normally a total of 8 to 10 depths were selected and collected per cast (i.e. ~40 samples per tidal cycle). To avoid oxidation artifacts, the bottles were sub-sampled by drawing aliquots directly into acid-cleaned polyethylene syringes. Processing of subsamples was carried out in a shipboard clean van using "trace-metal-clean" protocols. Four types of subsamples were collected: (1) unfiltered unacidified, (2) unfiltered acidified, (3) filtered unacidified, and (4) filtered acidified. Subsamples were immediately filtered through acid-cleaned 0.2 μm filters (Millipore) directly into trace-metal clean 15 and 50 mL Falcon tubes or 250 mL Nalgene bottles. Particulate material was also collected from 0.2 μm Millipore filters (pre-cleaned in 10% HNO_3) for particulate trace metal analysis. Particulate material was recovered by soaking filters for 35 days in 2% HNO_3 (Fisher TM Grade) and triplicate samples were diluted in 2% HNO_3 (Fisher TM Grade) for analysis. Particulate concentrations were normalized to the initial volume filtered, as well as, the volume of leaching solution. With 0.2 μm filters, 96% of colloidal and particulate fractions can be separated as permeate (Doucet et al., 2004). All subsamples were kept

frozen until prepared for laboratory analysis. Unacidified samples were analyzed for macronutrients (Lewis et al., 2007), while unfiltered acidified (total) samples were analyzed for comparison to particulate and filtered fractions. One surface sample was compromised by damage to the filter, therefore making dissolved and particulate results unavailable.

Trace metal concentrations were determined in triplicate with an Agilent 7500a Inductively Coupled Plasma-Mass Spectrometer (ICP-MS). Experimental results obtained on triplicate samples presented standard deviations better than 5%. Quality control blanks, standards, and certified reference material solutions NASS-5 and SLRS-4 (National Research Council Canada) were used in conjunction with internal standards to verify accuracy and reproducibility. The mean detection limit and standard deviations (3σ of the blanks) were calculated from the average of 12 quality control standards analyzed every 20 samples and at the start and completion of each sequence to account for instrument drift.

Matlab™ scripts were written to determine the statistical significance of temporal and spatial correlations between salinity, dissolved oxygen, temperature, dissolved sulfide, and dissolved and particulate trace metal concentrations. Finally, species abundance and solid phase saturation states were calculated with MINEQL+ version 4.5, across a range of redox conditions, with sulfate concentrations held constant in a range between 20 mM (calculated from salinity) down to the average water column concentrations of 4 mM for Upper Chesapeake Bay (Marvin-DiPasquale and Capone, 1998), and at a constant pH of 7.45. The model is set to anoxic conditions by entering concentrations of reduced trace metal species, rather than inputting fixed pE values.

Therefore, sulfate will not affect the solubility of trace metal species. Representative concentrations for major constituents not directly measured in this study were obtained from average water quality data (waterdata.usgs.gov./nwis) in the Northern Chesapeake Bay near our study site. These concentrations change as a function of salinity and therefore were multiplied by a dilution factor calculated as [Salinity Measured]/[Average Seawater Salinity]. The affect of K, Mg, and Ca concentrations are likely limited to the carbonate system and should not compete with trace metals during sulfide precipitation. The dissolved concentration for each dissolved metal including sulfide was provided to calculate the speciation. The data input into the equilibrium model for each tidal stage separated by vertical depth in the suboxic zone was summarized and included in Appendix D (Table D.1 and D.2).

4.4 Results

Tidal stages (high, ebb, low, and flood) were assigned based on tidal charts available for NOAA Station 8572770 at Matapeake, MD Kent Island 38° 57.4' N; 76° 21.3' W. Vertical profiles of data obtained by CTD casts (e.g. temperature, salinity, dissolved oxygen, and chl a), and *in situ* voltammetric microelectrode profiling ($O_{2(aq)}$, Fe(II), Mn(II), ΣH_2S, and $FeS_{(aq)}$) are displayed for two consecutive tidal cycles in Figure 4.3 (Tidal Cycle 1) and Figure 4.4 (Tidal Cycle 2). Temperature decreased with depth from ~27.5 to 26 ˚C with little variation between tides, except in the thermocline. The average salinity was ~11 in the surface waters and increased with depth to ~ 20 in bottom waters during both tidal cycles. The depth of the pycnocline varied slightly (~2-5 m) during tidal cycles causing changes in the position of the oxycline. At the surface, dissolved

oxygen ranged between 200 μM in the morning up to 300 μM in afternoon tides (low and flood) and coincided with high chl a maxima. In general, dissolved oxygen decreased with depth in the thermocline. Oxygen penetration depths ranged between 12 to 19 m depending on the state of the tide: oxygen was below detection limit at shallower depths as tides progressed from high to low (Figures 4.3 and 4.4); during flood tide, however, oxygen penetrated deeper into the water column and returned to shallower depths in the following high tide. A larger variation in depth of the pycnocline during Tidal Cycle 1 was accompanied by greater variations in oxygen concentrations and penetration depths than in Tidal Cycle 2.

During low tide, dissolved oxygen occasionally overlapped with dissolved sulfide, therefore, minimizing the width of the suboxic zone, as already observed in 2002 during ebb tide (Lewis et al., 2007). In 2005, dissolved sulfide maxima measured in anoxic bottom waters ranged between 25 and 190 μM, with higher concentrations during Tidal Cycle 2 (Figures 4.3 and 4.4). During Tidal Cycle 1, dissolved sulfide concentrations were generally low, reaching a maximum ~ 35 μM just above the SWI at ebb tide. In general, $\sum H_2S$ decreased in the water column from high to ebb tide during Tidal Cycle 1. Sulfide onset depths were deeper for Tidal Cycle 1 ranging between 17 to 20 m (Figures 4.3). Meanwhile, sulfide concentrations during Tidal Cycle 2 were much higher than Tidal Cycle 1 and the onset of sulfide was located at shallower depths ranging between 11.5 to 16 m (Figure 4.4). In addition, a pronounced drop in sulfide concentrations occurred just above the sediment water interface (SWI) during ebb and

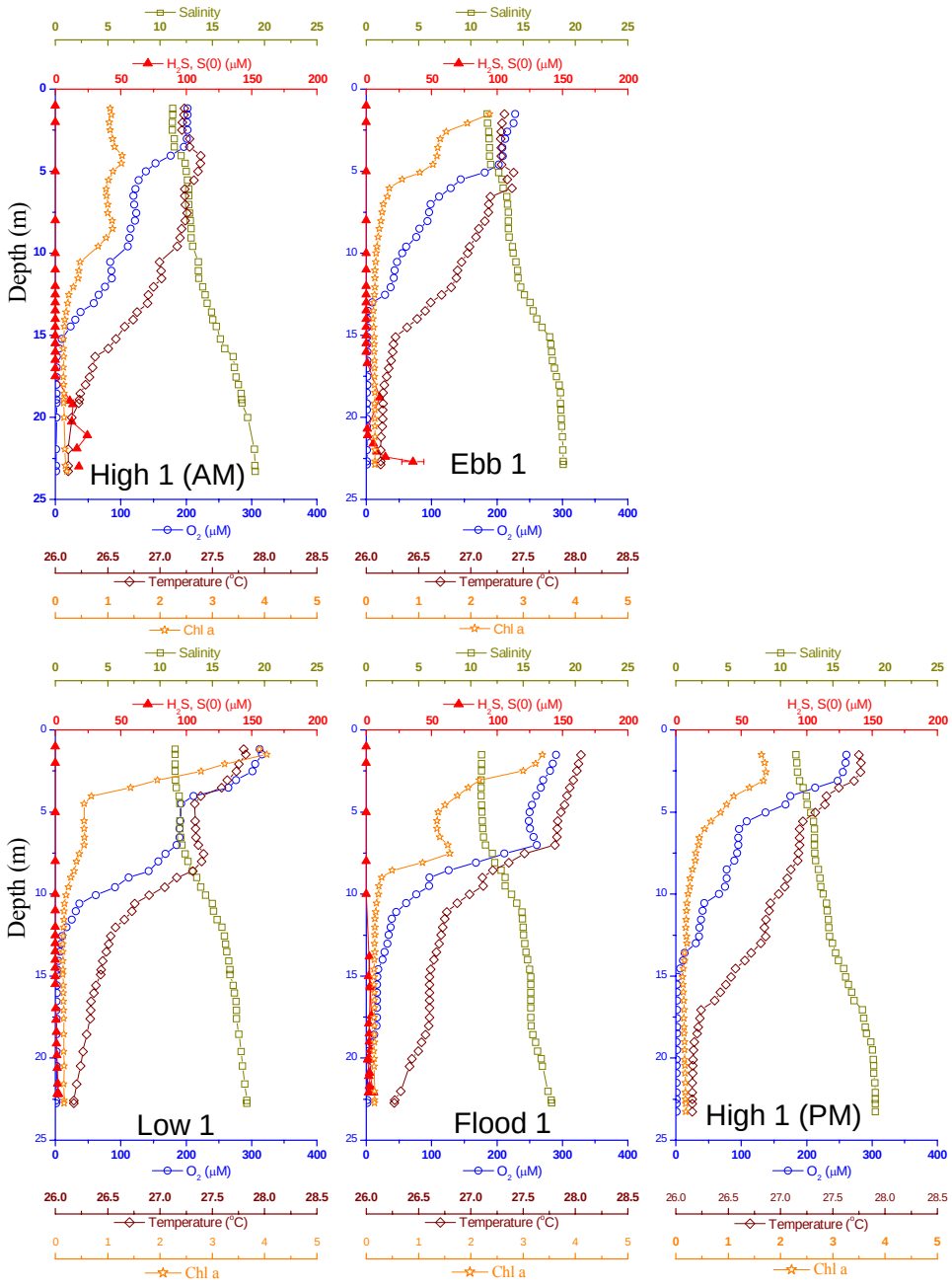

Figure 4.3- Vertical profiles of tidally separated redox sensitive parameters for Tidal Cycle 1: 1) voltammetric *in situ* $\Sigma[H_2S]$ in red triangles; 2) obtained with CTD: Dissolved oxygen in open blue circles, Temperature in open brown diamonds, salinity in open dark yellow squares, and chl a proxy in orange stars. $\Sigma[H_2S]$ data during High (PM) was not available. Times (EST) associated with tidal stage: High (7:07AM), Ebb (10:44AM), Low (1:41PM), Flood (5:05PM), High PM (7:35PM).

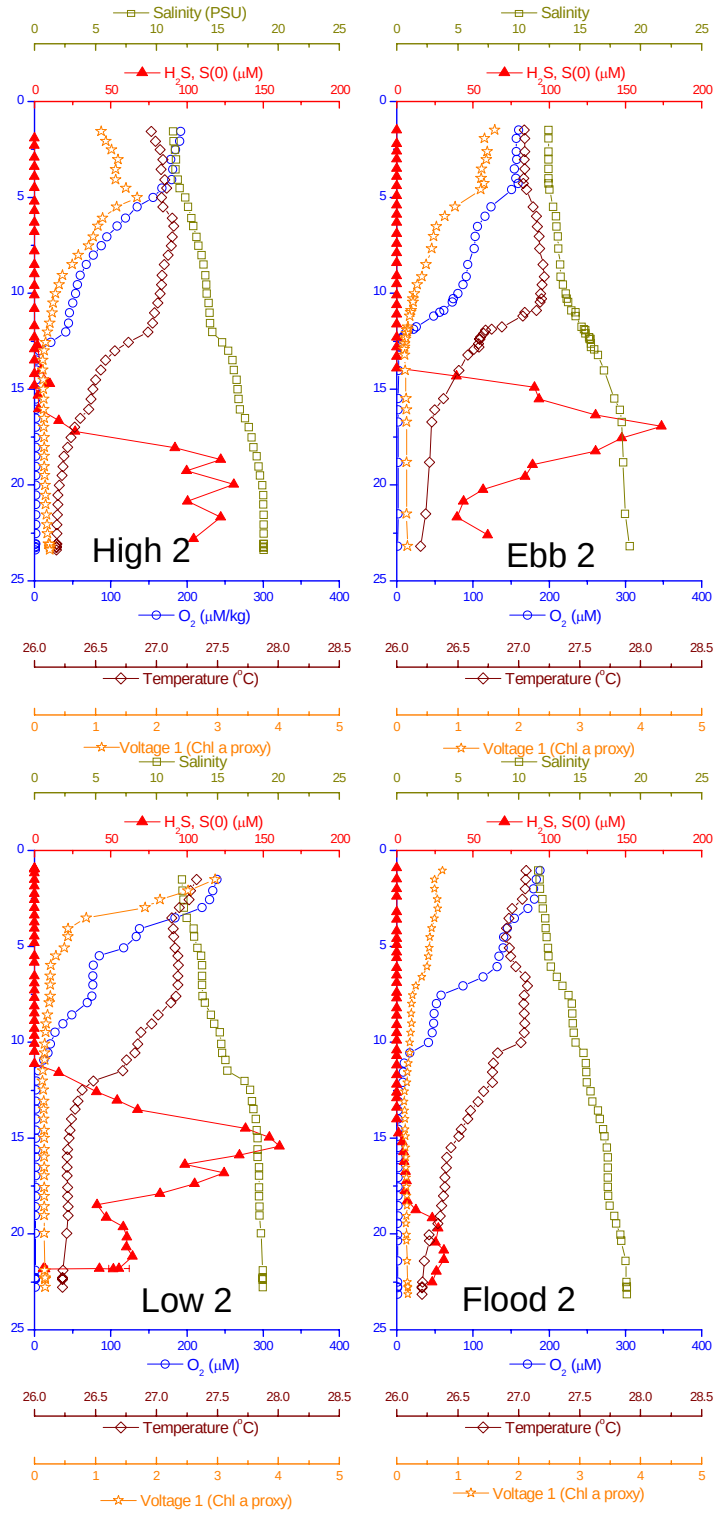

Figure 4.4- Vertical profiles of tidally separated redox -sensitive parameters for Tidal Cycle 2: 1) voltammetric *in situ* $\Sigma[H_2S]$ in red triangles; 2) obtained with CTD: Dissolved oxygen in open blue circles, Temperature in open brown diamonds, salinity in open dark yellow squares, and chl a proxy in orange stars. Times (EST) associated with tidal stage: High (7:38AM), Ebb (10:35AM), Low (2:01PM), and Flood (4:36PM).

low tide, such that at the next flood tide dissolved sulfide only rose to 30 μM and produced similar depth profiles as during Tidal Cycle 1.

Figure 4.5 illustrates the distribution of Ba_D, Mn_D, U_D, and As_D as a function of depth over two consecutive semi-diurnal tidal cycles. Dissolved manganese was approximately 500 ± 100 nM in oxic waters, accompanied by large increases in and below the oxycline during both tidal cycles. Once oxygen was depleted, dissolved Mn accumulated and formed a peak in the lower end of the oxycline with maximum concentrations around 9 μM during the Tidal Cycle 1 and 14 μM during Tidal Cycle 2 (Figure 4.5). The Mn_D gradients associated with Tidal Cycle 2 were much more uniform corresponding to greater concentrations than Tidal Cycle 1, similar to ΣH_2S profiles.

Conversely, Mn_D during Tidal Cycle 2 increased across the oxycline and remained elevated around the same concentration deeper, except during the 2nd flood stage which displayed a small decrease in concentration just above the SWI. The concentrations of U_D and As_D were low in oxic waters and increased with depth below the oxycline from ~4.5 to 10 nM and 4 to 16 nM, respectively (Figures 4.5). In contrast, the distribution of Ba_D (Figure 4.5) gradually decreased in concentration from 450 nM just below the surface to 200 nM near the bottom, respectively. On the other hand, Cr_D and Pb_D (Figure 4.6) increased slightly with depth from an average of 35 to 60 nM and 20 to 40 nM, respectively. Although depth profiles do not vary greatly with depth, Cr and Cu showed less sensitivity to tidal fluxes and more variation with depth across the pycnocline. In 2004 (Appendix Figure D.1), Cr concentrations increased from ~10 to 25 nM with occasional concentration spikes in samples collected from depths between 5 to

a)

b)

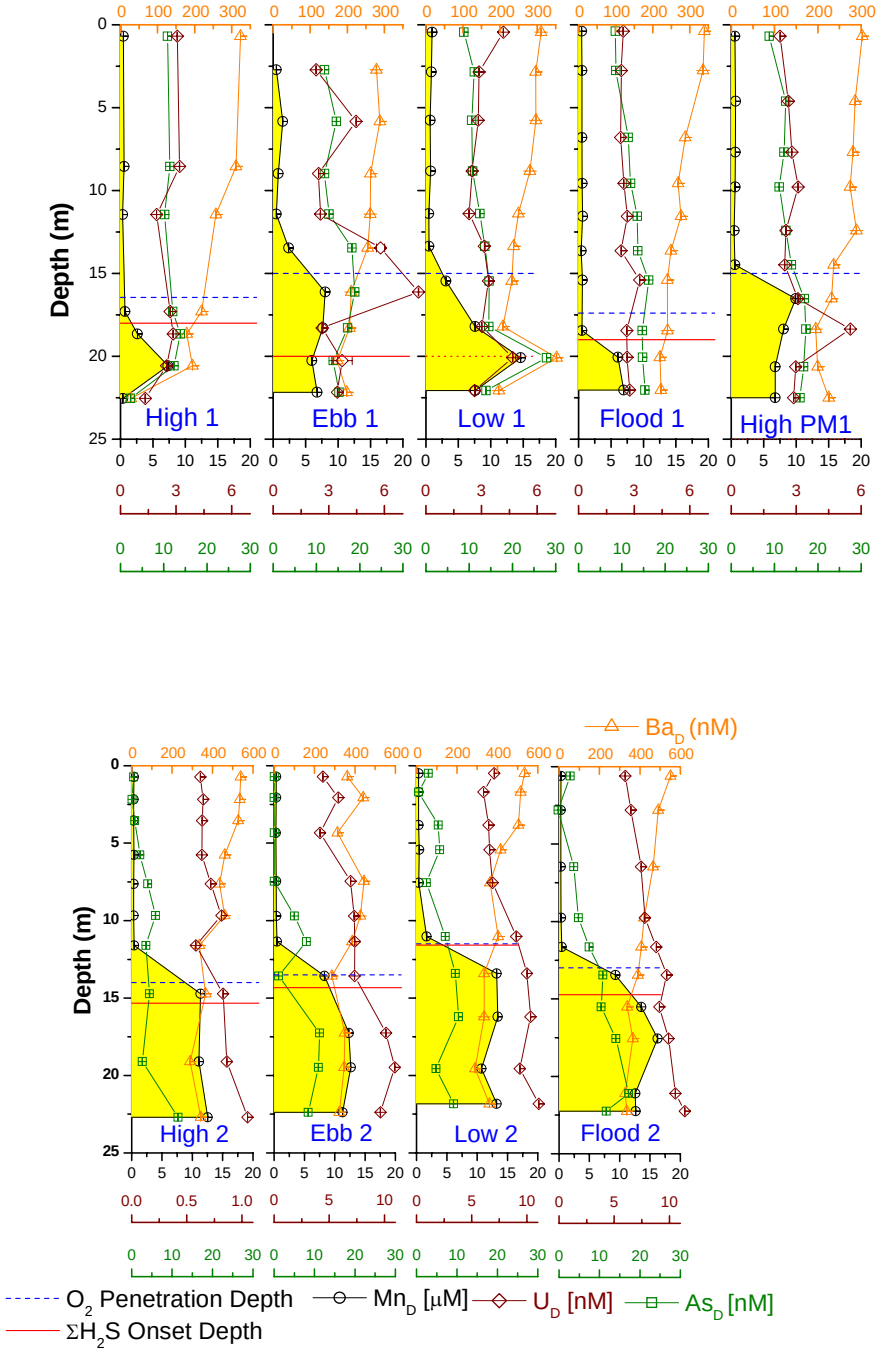

Figure 4.5- Vertical profile of dissolved Ba, Mn, U, and As over two solar tidal cycles. Dissolved concentrations for a) Tidal 1 and b) Tidal 2 are depicted as Ba_D [nM] in open orange triangles, Mn_D [µM] in open black circles with area under the curve highlighted with yellow, U_D [nM] in open brown diamonds, and As_D [nM] in open green squares. Oxygen penetration depth was determined from CTD data and is marked with a blue dashed line. ΣH_2S–onset depth was determined voltammetrically and is marked with a solid red line. $\Sigma[H_2S]$ data was not available for High (PM1) cast of Tidal Cycle 1. Scales changed in Tidal Cycle 2 to fit increase in Ba.

a)

b)

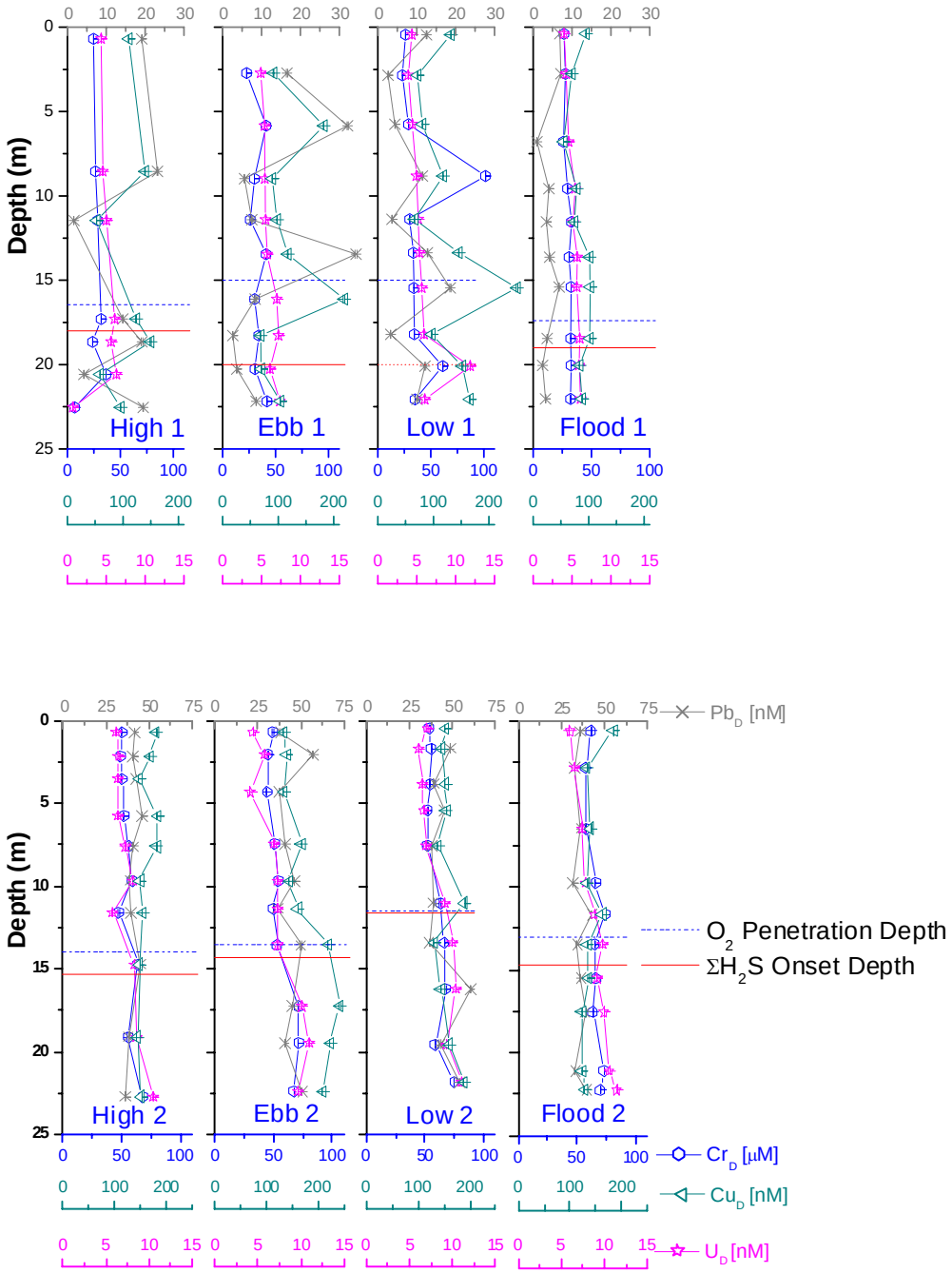

Figure 4.6- Vertical profile of dissolved Pb, Cr, Cu and U over two solar tidal cycles. Dissolved concentrations for a) Tidal 1 and b) Tidal 2 are depicted as Pb_D [nM] in gray Xs, Cr_D [μM] in open blue hexagon, Cu_D [nM] in open light green triangles, and U_D [nM] in open magenta stars. Oxygen penetration depth was determined from CTD data and is marked with a blue dashed line. ΣH_2S–onset depth was determined voltammetrically and is marked with a solid red line. Scales changed in Tidal Cycle 2 to fit increase of Pb.

15 m. Following a similar trend Cu_D, concentrations slightly increased with depth averaging between 4 to 6 nM in 2004 and 10 to 20 nM in 2005. Interestingly, concentrations of Cr_D, Mn_D, U_D, Ba_D, Cu_D, as well as Pb_D change with depth and are generally higher during Tidal Cycle 2 concurrent with sulfide enrichment in anoxic bottom waters (Figures 4.3 to 4.6). Meanwhile, Ni_D varied consistently between 15 to 30 nM in both 2004 and 2005 with little fluctuation with depth (data not shown). Similarly, concentrations of Cd_D were consistently below the detection limit of 0.02 nM over tidal cycles and interannually (Figure D.11). Trace metal concentrations were generally reproducible interannually (Appendix Figure D.1 through D.11).

Mn_D and Mn_P profiles from 2004 illustrate that particulate concentrations are lower and corresponding dissolved levels are elevated in bottom waters. Conversely, dissolved and particulate profiles for Co, As, and Ba are similar in both oxic and suboxic zones, except at flood tide when particles disappeared in the anoxic layer as dissolved levels increased. Particulate trace metal profiles for Tidal Cycle 1 and Tidal Cycle 2 in 2005 were uniform with depth, except during Flood 1 (Figure 4.7 and 4.8). Although profiles were mainly straight at low concentrations (< 2 nM), particulate Mn, Co, As and Ba concentrations were highest at low tides, and during the 1st of the semidiurnal cycles. During Tidal Cycle 1 Mn_P average levels were 10 ± 3 μM, and levels increased to 14 ± 2 μM throughout the water column during Low 1 and below 13 m at Flood 1. Meanwhile, during Tidal Cycle 2 average Mn_P levels dropped to 6 ± 1.5 μM, and maximum concentrations reached only up to 9 μM during low tide. Small increases in As_P , Ba_P, Pb_P, and U_P near the SWI coincided with a rise in Mn_P, most notably during flood and

a)

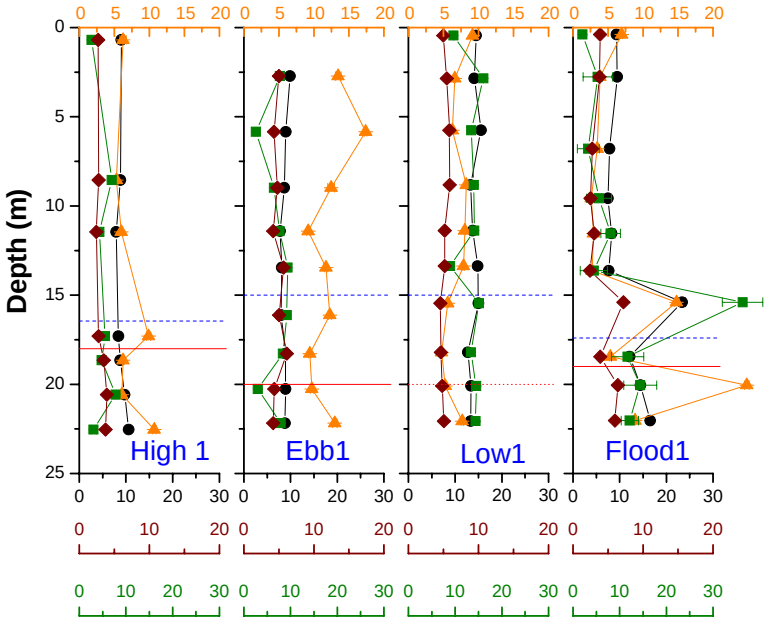

b)

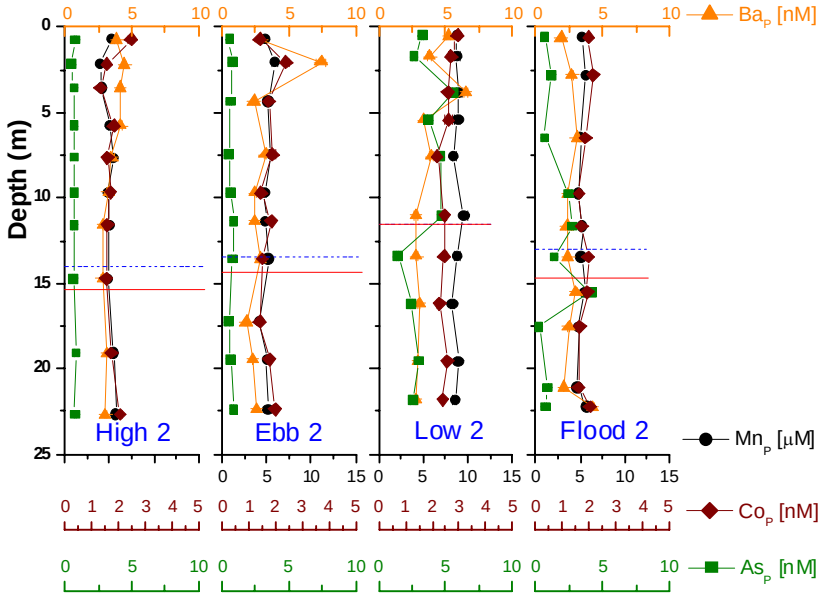

Figure 4.7- Vertical profile of particulate Ba, Mn, Co, and As over two solar tidal cycles. Dissolved concentrations for a) Tidal 1 and b) Tidal 2 are depicted as Ba_P [nM] in solid orange triangles, Mn_P [µM] in solid black circles, Co_P [nM] in solid brown diamonds, and As_P [nM] in solid green squares. Oxygen penetration depth was determined from CTD data and is marked with a blue dashed line. ΣH_2S–onset depth was determined voltammetrically and is marked with a solid red line. Scales changed in Tidal Cycle 2 to fit decrease in concentrations.

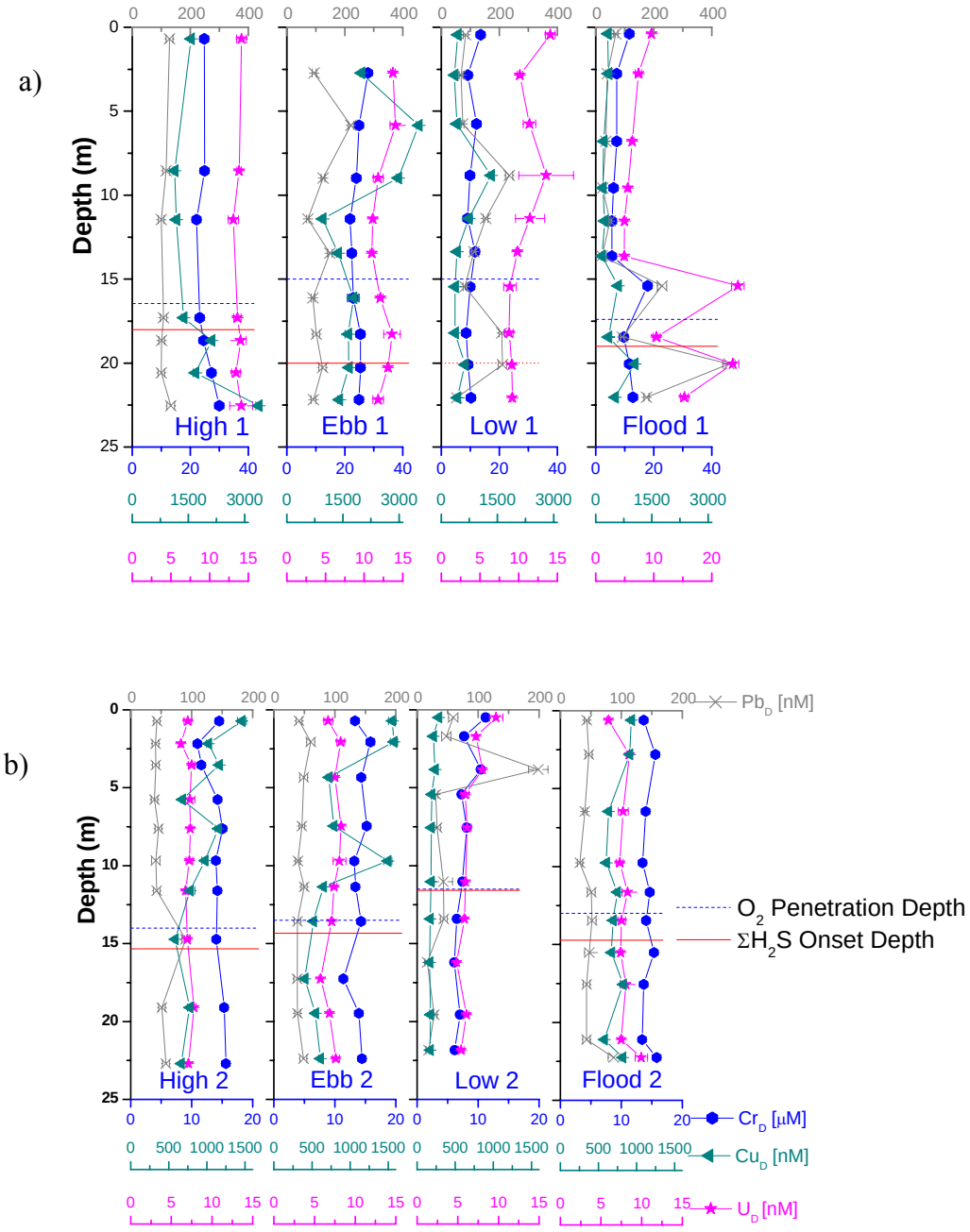

Figure 4.8- Vertical profile of particulate Pb, Cr, Cu and U over two solar tidal cycles. Dissolved concentrations for a) Tidal 1 and b) Tidal 2 are depicted as Pb_P [nM] in gray Xs, Cr_P [µM] in solid blue hexagon, Cu_P [nM] in solid light green triangles, and U_P [nM] in solid magenta stars. Oxygen penetration depth was determined from CTD data and is marked with a blue dashed line. ΣH_2S–onset depth was determined voltammetrically and is marked with a solid red line. Scales changed in Tidal Cycle 2 to fit decrease in concentrations.

ebb tides (Figure 4.7 and 4.8). On average, Co_P concentrations ranged between 4 ± 1.4 nM during Tidal 1 and dropped to 2 ± 0.4 nM for Tidal 2. Whereas, Cr_P concentrations were the highest of the suite of trace metals analyzed, with an average of 20 ± 8 μM during Tidal 1 and 12.5 ± 3 μM during Tidal 2 (Figure 4.8). Concentrations of Ni_P, Cu_P, and As_P were similar for the two tidal cycles analyzed. Ni_P profiles (data not shown) matched closest to Cu_P trends with spatial and temporal concentration averages of 300 ± 173 nM and 83 ± 78 nM, respectively. During the two tidal cycles, As_P concentrations averaged 0.7 nM with a maximum of 5.5 nM reached during Flood 1 in the 20 m depth sample. Incidentally, this discrete sample depth also registered maximum concentrations of Cd_P (1.1 nM), Ba_P (24 nM), as well as Pb_P (380 nM). Maximum particulate concentrations are associated with 15 and 22 m depths during the 1st flood tide, with 24 μM of Mn_P and 5nM of As_P.

Although informative, it was very difficult to decipher concurrent trends on the depth profiles even when relationships are known (e.g. Mn and Co). Therefore, Mn_D, Mn_P, DO, ΣH_2S, and salinity gradients were compared to dissolved and particulate trace metal profiles to investigate the significance of co-variances and assess salinity and redox dependence on sorption and precipitation mechanisms (Morris et al., 1982). Respecting their spatial and temporal distributions, statistical analyses of covariances were calculated using a two-tailed T-test and are presented in Table 4.1 and 4.2. Particulate material would be expected in oxygenated waters, yet correlations between particulate trace metals and dissolved oxygen did not exhibit statistical significance. In contrast, there is a strong positive correlation between DO and Ba_D, while DO, not surprisingly, is negatively correlated with Mn_D, Co_D, As_D, and U_D over all tides. Salinity had a

significant positive relationship with most dissolved trace metals, except Ba_D with an inverse covariance. Moreover, significantly larger correlation coefficients were calculated for Tidal Cycle 2. Similar to covariance with salinity, correlations were stronger between Mn_D, As_D, Co_D, and U_D, and $\Sigma[H_2S]$ during Tidal Cycle 2 when there was a much higher $\Sigma[H_2S]$ concentration detected in bottom waters most likely from sulfate reduction occurring in underlying sediments. Similarly to dissolved phase relationships, Cr_P and Co_P correlated strongly with Mn_P over several tides, while U_P covariances were limited to ebb and flood tides, and As_P and Ba_P displayed poor correlations with Mn_P.

Table 4.1- Correlation coefficients (R^2) from a statistical between dissolved trace metal concentrations and: dissolved manganese; salinity; dissolved oxygen; and dissolved sulfide at different tidal stages. (-) depicts negative correlations.

	Cr_D	Mn_D	Co_D	As_D	Ba_D	U_D
vs Mn_D						
High 1	0.26	**1.000**	0.007	0.140	- 0.018	0.232
Ebb 1	0.13	**1.000**	0.070	**0.493**	- **0.546**	**0.777**
Low 1	0.03	**1.000**	- 0.006	**0.782**	0.016	**0.811**
Flood 1	0.15	**1.000**	0.056	0.183	- 0.331	0.279
High PM	0.40	**1.000**	0.323	**0.757**	- **0.666**	**0.714**
High 2	**0.60**	**1.000**	**0.660**	0.341	- **0.527**	**0.702**
Ebb 2	**0.84**	**1.000**	**0.884**	**0.525**	- 0.329	**0.735**
Low 2	**0.72**	**1.000**	**0.716**	**0.594**	- **0.569**	**0.844**
Flood 2	0.12	**1.000**	**0.685**	**0.795**	- **0.672**	**0.671**
vs Salinity						
High 1	- 0.02	0.256	- 0.303	- 0.049	- **0.721**	- 0.004
Ebb 1	0.24	**0.827**	0.204	**0.541**	- **0.456**	**0.826**
Low 1	0.01	**0.469**	- 0.031	**0.414**	- 0.259	0.381
Flood 1	**0.75**	0.389	0.291	**0.880**	- **0.959**	**0.970**
High PM	**0.45**	**0.708**	0.264	**0.886**	- **0.844**	**0.957**
High 2	**0.55**	**0.844**	**0.423**	**0.506**	- **0.818**	**0.711**
Ebb 2	**0.81**	**0.895**	**0.905**	**0.684**	- 0.291	**0.823**
Low 2	**0.68**	**0.817**	**0.592**	**0.589**	- **0.814**	**0.906**
Flood 2	**0.48**	**0.739**	**0.832**	**0.871**	- **0.936**	**0.967**
vs DO						
High 1	0.00	- 0.154	0.275	0.011	0.546	- 0.005
Ebb 1	- 0.32	- **0.500**	- 0.145	- 0.625	0.143	- **0.737**
Low 1	- 0.06	- 0.228	0.002	- 0.295	0.271	- 0.257
Flood 1	- **0.72**	- 0.164	- 0.249	- **0.911**	**0.935**	- **0.919**
High PM	- **0.42**	- 0.273	- 0.147	- **0.664**	**0.501**	- **0.626**
High 2	- 0.35	- 0.300	- 0.073	- **0.471**	**0.734**	- 0.334
Ebb 2	- **0.60**	- **0.662**	- **0.717**	- **0.624**	0.196	- **0.758**
Low 2	- **0.44**	- **0.503**	- 0.313	- **0.606**	**0.837**	- **0.650**
Flood 2	- **0.53**	- **0.491**	- **0.705**	- **0.668**	**0.871**	- **0.794**
vs $\sum H_2S$						
High 1	- 0.08	0.220	0.449	- 0.192	- **0.824**	- 0.078
Ebb 1	0.12	0.255	0.254	0.004	- **0.410**	0.238
Low 1	0.04	0.298	0.007	0.204	- 0.205	0.215
Flood 1	**0.51**	**0.607**	0.261	**0.674**	- **0.750**	**0.745**
High PM	Sulfide Not Available					
High 2	0.26	**0.613**	0.330	0.313	- **0.442**	**0.614**
Ebb 2	**0.74**	**0.657**	**0.753**	**0.654**	- 0.083	**0.647**
Low 2	**0.53**	**0.842**	**0.484**	**0.593**	- **0.549**	**0.686**
Flood 2	0.35	0.346	0.313	**0.539**	- **0.418**	**0.528**

Statistical Significance: p values **>95% and** <95%

Table 4.2- Correlation coefficients (R^2) from a statistical between particulate trace metal concentrations and: particulate manganese and dissolved sulfide at different tidal stages. (-) depicts negative correlations.

	Cr_P	Mn_P	Co_P	As_P	Ba_P	U_P
vs Mn_P						
High 1	**0.99**	**1.000**	**0.651**	- 0.063	- 0.023	0.327
Ebb 1	**0.97**	**1.000**	0.001	0.311	0.249	**0.619**
Low 1	- 0.07	**1.000**	- **0.473**	- 0.002	- 0.137	- 0.045
Flood 1	**0.87**	**1.000**	**0.882**	0.031	0.182	**0.416**
High PM	**0.65**	**1.000**	**0.871**	0.042	0.050	0.069
High 2	**0.98**	**1.000**	0.350	**0.613**	- 0.026	0.039
Ebb 2	**0.98**	**1.000**	**0.697**	0.235	0.071	**0.560**
Low 2	0.06	**1.000**	0.154	0.174	0.002	0.085
Flood 2	**0.90**	**1.000**	**0.740**	0.108	- 0.006	**0.442**
vs $\sum H_2S$						
High 1	0.48	0.435	**0.699**	- 0.469	0.010	- 0.009
Ebb 1	0.04	0.031	- 0.207	0.000	0.016	- 0.002
Low 1	- 0.15	0.010	- 0.023	- 0.000	0.005	0.067
Flood 1	0.15	0.316	0.309	0.114	0.125	0.241
High PM	Sulfide Not Available					
High 2	0.28	0.348	0.069	0.297	- 0.211	0.036
Ebb 2	- **0.47**	- **0.452**	- 0.111	- 0.085	- 0.188	- 0.244
Low 2	- **0.46**	- 0.196	- 0.276	- **0.710**	- 0.194	- 0.168
Flood 2	0.00	- 0.006	- 0.049	0.000	0.217	0.242

Statistical Significance: p values **>95% and** <95%

4.5 Discussion

In this study *in situ* measurements were combined with discrete water sampling to determine the effects of tidal cycling on the distribution of trace metals during two consecutive tidal cycles at Station 858 in the Chesapeake Bay. *In situ* profiles show that the physico-chemical conditions of the water column are affected over tidal cycles. For example, it is interesting to observe that a <1m tidal range (Shaw et al., 1994) results in a ~ 5 m shift in O_2-penetration depth (Figures 4.3 and 4.4), as was already observed in 2002-2003 (Lewis et al., 2007). It has been shown that a combination of physical events (e.g. river flow, tidal fluxes, and rain storms) and biogeochemical processes cause dissolved oxygen to fluctuate in partially-mixed estuaries (Boicourt, 1992; Lin et al., 2006). Based on concurrent increases in dissolved oxygen and chlorophyll a, additional oxygen is produced in surface waters during afternoon tides (low and flood). However, as the tides progress from high to low, both buoyant oxic freshwater and saline suboxic waters flowing seaward result in the vertical mixing of oxic and anoxic waters that shifts the oxycline up in the water column. At the next flood tide, the oxycline is lowered in the water column when oxygenated dense seawater flowing landward sinks in the water column. Thus, tidal variations affect the stratification of dissolved oxygen, but cannot explain the episodic occurrence of dissolved sulfide. The landward flow of seawater above the sediment may cause shear stress forces that advect dissolved species upward into the bottom waters (Huettel et al., 1998; Huettel et al., 2003; Precht and Huettel, 2003). Therefore, dissolved sulfide found in the water column is likely from microbial sulfate reduction in the sediment (Boicourt, 1992; Roden and Tuttle, 1992; Roden and Tuttle, 1993; MacCrehan and Shea, 1995; Roden et al., 1995; Marvin-DiPasquale and

Capone, 1998; Marvin-DiPasquale et al., 2003) that has been entrained in the water column by shear interaction of bottom waters with the upper sediment and is transported by horizontal advection in the along-channel direction (Luther et al., 1988; Lewis et al., 2007). Tidal flushing of sediments during flood tide is evidenced by the order of magnitude changes in sulfide concentrations within a time-span as short as 3 hours (Figure 4.4).

The vertical movement of the oxycline and the tidal-related fluctuations in dissolved sulfide must also affect the cycling of Mn- and Fe-oxides. In anoxic conditions, Fe is usually removed rapidly by precipitation as FeS (Luther and Ferdelman, 1993; Kostka and Luther, 1994; MacCrehan and Shea, 1995; Luther et al., 2002; Luther and Rickard, 2005; Ma et al., 2006; Rickard and Luther, 2007), which could explain its low concentrations across the water column. In contrast, MnS is highly soluble (Holdren et al., 1975; Morris et al., 1982; Burdige et al., 1992; Luther et al., 1994; Lienemann et al., 1997; Ouvrard et al., 2005), and Mn_D should be maintained in solution. During Flood 1, dissolved oxygen penetrated deeper into the water column and may have favored precipitation of manganese oxides that generated spikes in particulate manganese concentrations just above the sediment (Figure 4.7). *In situ* measurements (Figures 4.3 and 4.4) indicate that oxygen sometimes overlaps and possibly oxidizes Mn (II), while dissolved sulfide diffuses to the oxycline at flooding tide to reduce Mn-oxides. The vertical distribution of trace metals in estuaries may be a function of salinity and microbially mediated reductive dissolution of their geochemical hosts (Martino et al., 2002). The consistency of Mn_D enrichment in suboxic waters (Figure 4.5 and 4.9), regardless of sulfide and the tidal stage, in concert with minimal Fe(II) concentrations (<4

μM) (Lewis et al., 2007) suggest that Mn-oxides, and not Fe-oxides, are the major geochemical hosts of trace metals.

The simplest distribution pattern that might be expected in an estuary would be one established by conservative mixing or simple dilution. A conservative component varies linearly with salinity in both the horizontal and the vertical directions. The reactivity of an element in the estuarine mixing zone (i.e. conservative or non-conservative behavior) is typically illustrated by comparing the dissolved constituent versus salinity (Boyle et al, 1974). Characteristically more conservative with respect to salinity, uranium and its decay series daughters are used as tracers of oceanic processes (Borole et al., 1982). Therefore it is useful to depict the fluvial –ocean water mixing line (Figure 4.10a) based on U_D ranges between 0.42 ± 0.02 nM/kg for freshwater up to 13.6 to 14.5 nM/kg in average ocean water (Sarin and Church, 1994; Shaw et al., 1994). Uranium is soluble under the form of uranyl-carbonate complexes in oxic conditions in oceans and estuaries (Borole et al., 1977; Borole et al., 1982; Shaw et al., 1994). Scavenging of uranium in surface waters produces particle bound uranium, which is delivered to the sediment by deposition of metal oxides and biodetritus (Anderson et al., 1989; Shaw et al., 1994). However, in hydrogen sulfide-rich waters, dissolved U(VI) is neither reduced to the thermodynamically favored U(IV) nor scavenged by particles (Anderson et al., 1989). The U_D enrichment of bottom waters during Tidal Cycle 2 should therefore be a result of the release of bioassociated uranium during decomposition of uranium enriched detritus in surface sediments, as previously found in the Northern

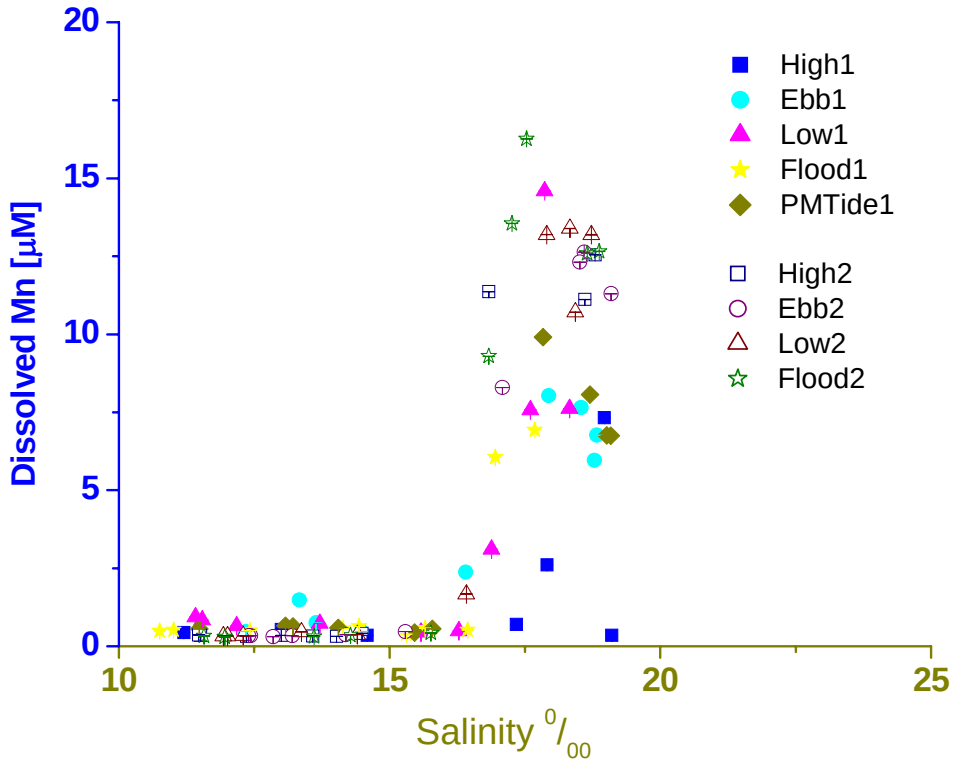

Figure 4.9- Dissolved manganese (µM) and salinity during both tidal cycles. Salinities of 17-20 correspond to the anoxic layers.

a)

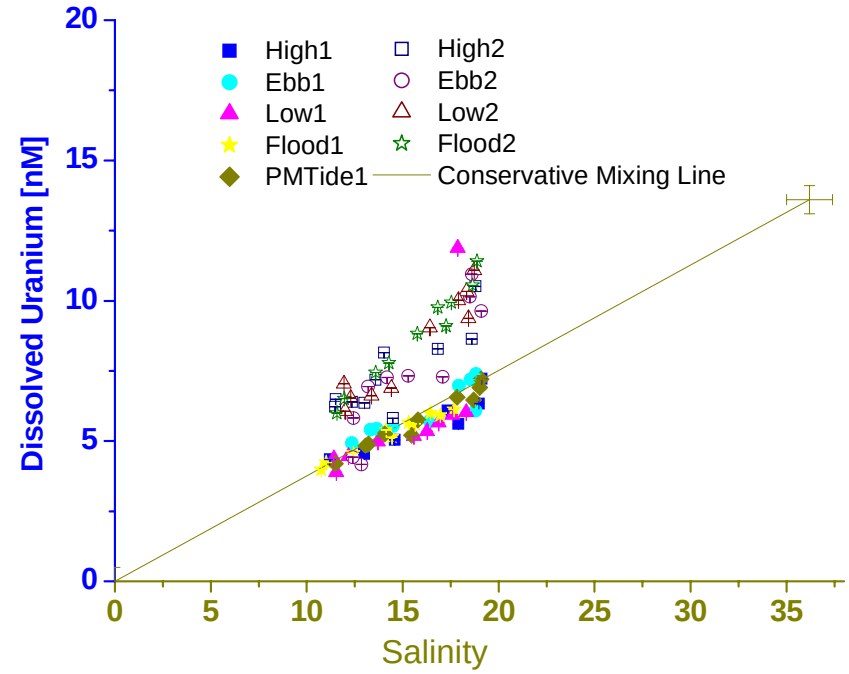

b)

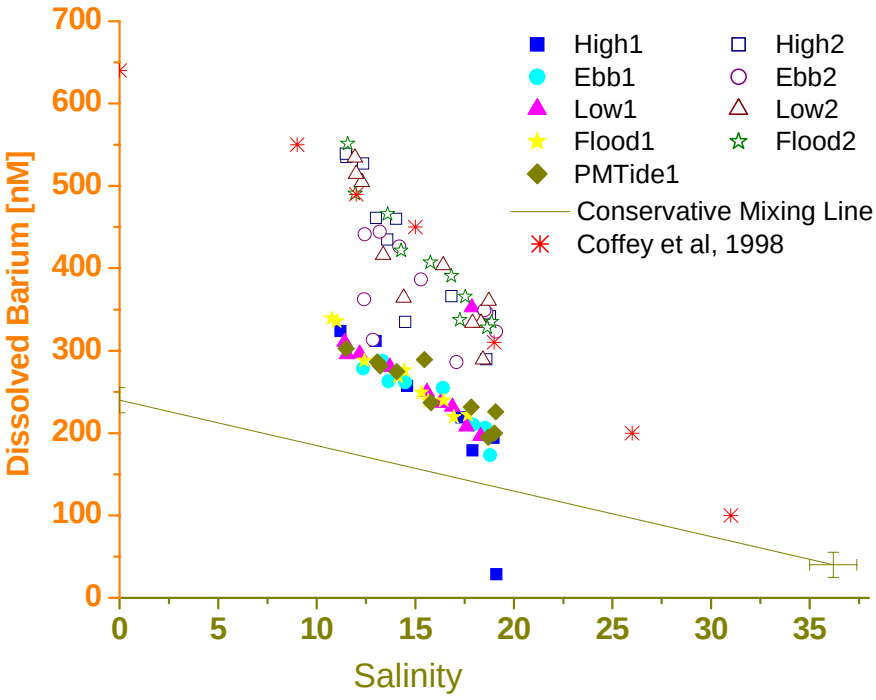

Figure 4.10- Seawater-fluvial mixing line determined by comparison of salinity with a) dissolved uranium (nM) and b) dissolved barium (nM). Conservative mixing lines respects U_D ranges between 0.42± 0.02 nM/kg for freshwater up to 13.6 to 14.5 nM/kg in ocean water, and Ba_D ranges between 240 ± 15 nM for freshwater and 40 nM on average in ocean water.

Chesapeake Bay (Shaw et al., 1994). From Figure 4.10a, it is clear that U_D behaves conservatively during Tidal Cycle 1, while additional uranium, evident in Tidal Cycle 2, coincides with the enhanced maximum sulfide concentrations. These results confirm that sediment-water exchanges of dissolved constituents exist during Tidal Cycle 2, but not during Tidal Cycle 1.

Ba_D enrichment in coastal groundwater has been attributed to desorption from barium rich freshwater solids as they encounter saline tidal waters, and via diagenetic release from barium-bearing metal oxide phases, the dissolution of authigenic barite, and/or the decomposition of barium-rich organic particles (Coffey et al., 1997; Shaw et al., 1998). In a similar fashion, Ba can be used as a tracer of freshwater inputs, since freshwater levels far exceed average ocean concentrations (Coffey et al., 1997; Shaw et al., 1998). Figure 4.10b shows the relationship between Ba_D and salinity during both tidal cycles. To determine conservative mixing of dissolved barium, endmembers were set to 240 ± 15 nM for freshwater and 40 nM in average ocean water (Coffey et al., 1997; Shaw et al., 1998). In general, under low salinity (< 0.5) uranium and barium are scavenged by particles, but are gradually released if salinity increases above the 1-10 range, consistent with their sorption/desorption from suspended particulate matter (Coffey et al., 1997; Shaw et al., 1998). Our salinity range (10 to 22) is at the cusp of the ideal conditions for the dissolution of particulate barium. Dissolved barium behaves conservatively: it decreases when salinity increases but falls above the mixing line during both tidal cycles, which can be interpreted as a large addition of barium relative to conservative mixing of freshwater and seawater (Figure 4.10b). Previous Ba enrichments found in the Chesapeake Bay have been attributed to particulate material deposited in salt

marshes during high flow (i.e. winter season or storm events) that subsequently release barium as salinities rise under low flow conditions (Coffey et al., 1997; Shaw et al., 1998). Similar to uranium, dissolved Ba concentrations from Tidal Cycle 2 (Figures 4.5 and 4.10) exhibit a steeper slope along the conservative mixing line. Incidentally, Ba concentrations as a function of salinity during Tidal Cycle 2 match data obtained from a nearby site, whose source was suggested to be freshwater solids (Coffey et al., 1997).

Overall, the distribution of dissolved uranium and barium during both tidal cycles indicates that freshwater and oceanic water masses are mixing in the Chesapeake Bay, and sediment-water interactions result in an input of dissolved constituents to the overlying waters during the 2nd tidal cycle. The increase of Mn_D and $\sum H_2S$ below the oxycline seems to be accompanied by the enrichment of dissolved trace metals, especially during Tidal Cycle 2. The tidally induced increase in dissolved trace metals may be due to 1) an accumulation of particles from freshwater inputs at the surface resulting in redissolution in the anoxic zone, 2) the resuspension of sediment with fast dissolution of particulate species, or 3) bottom diffusion/advection during tidal flushing.

Particulate concentrations are much higher during Tidal Cycle 1 across the water column, suggesting that particles settled to sediments by Tidal Cycle 2 (Figure 4.7 and 4.8). Initially, this high particulate metals load might have been attributed to precipitation with organic matter and metal oxides, however, there is no clear depletion of dissolved trace metals in the water column during Tidal Cycle 1 compared to Tidal Cycle 2 (Figures 4.5 and 4.6). In fact, particulate trace metals form surprisingly uniform profiles, except at Flood 1 when they are enriched in anoxic waters. To determine whether trace metals were remobilized in the anoxic zone and to help identify a

mechanism responsible for this remobilization, trace metal concentrations were represented versus salinity during both tidal cycles (Figures 4.10, 4.11, and 4.12). All trace metals investigated display an increase in concentration in the anoxic waters, during both tidal cycles. More specifically, this increase is much higher for Pb_D, Cr_D, and maybe Cu_D during Tidal Cycle 2, while no perceptible change is observed for Co_D and Ni_D, and a decrease in As_D is evident during Tidal Cycle 2. The release of Pb_D and Cr_D, and possibly Cu_D during Tidal Cycle 2 could be a result of the reduction of excess Mn- and Fe-oxides in the water column by hydrogen sulfide introduced in bottom waters during ebb tide. However, the entire water column is enriched with dissolved phase metals (e.g. Cu, Cr, Ba, and Pb) and not only restricted to sulfidic depths. Therefore, the observed increase is not solely from the reduction of hosts by hydrogen sulfide.

The elevated dissolved trace metals throughout Tidal Cycle 2 might be a result of the pulse of resuspended solids from Flood 1. Resuspension of particles (e.g. organic and Mn-oxides) in conjunction with dissolved sulfide could reductively dissolve scavenged species. However, our data suggests that increases in dissolved concentrations in bottom waters during flood tides are not entirely due to the dissolution of resuspended solids. Although an increase in particulate concentrations at depth associated with Flood 1 provides evidence of resuspension, the particulate profiles of Tidal Cycle 2 were almost linear with depth, demonstrating that resuspension is not essential for bottom water enrichment. Therefore, another process must be intensifying trace metal inputs between Tidal Cycle 1 and 2. It has been shown that when overlying waters flow above sediments, topographic features (e.g. mounds and ripples) increase hydrostatic pressure

a)

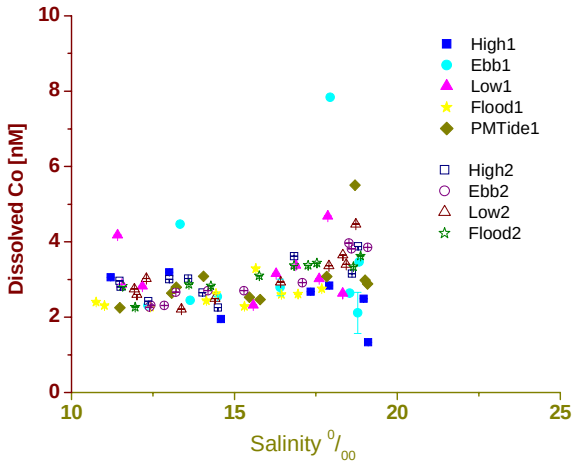

b)

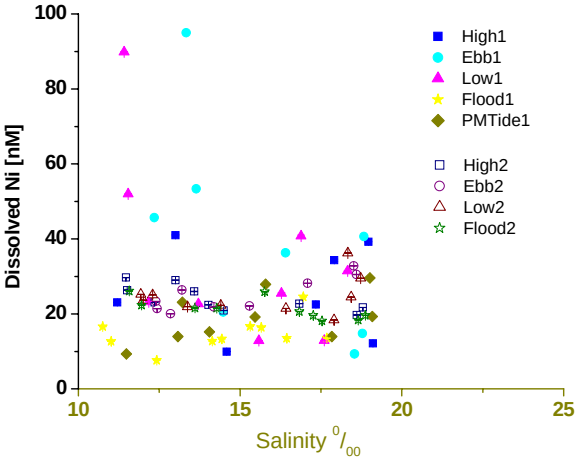

c)

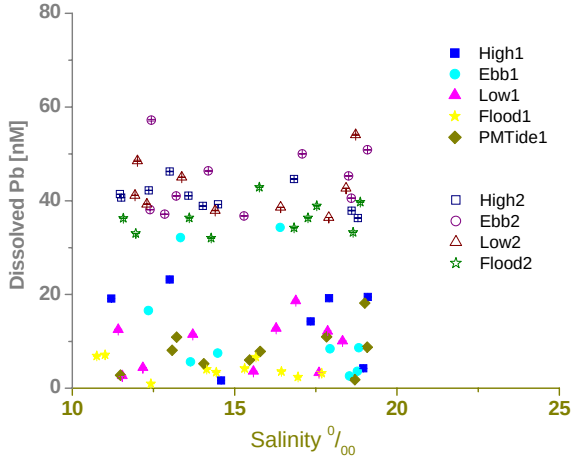

Figure 4.11- Mixing line determined by comparison of salinity with a) dissolved cobalt (nM), b) dissolved nickel (nM), c) dissolved lead (nM).

a)

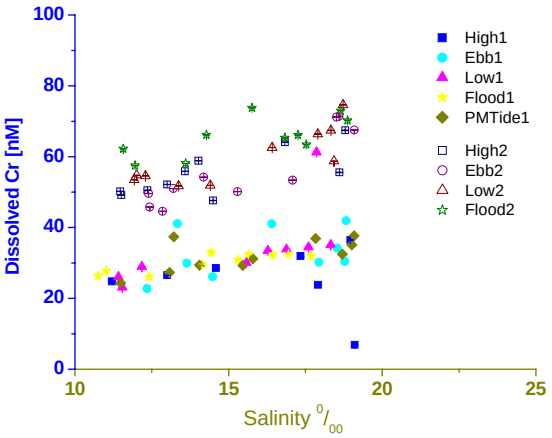

b)

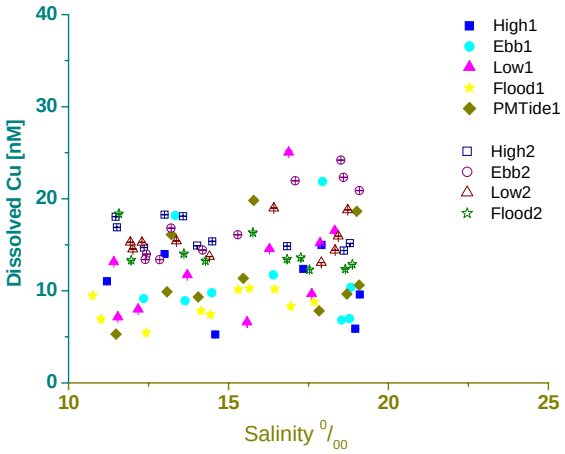

c)

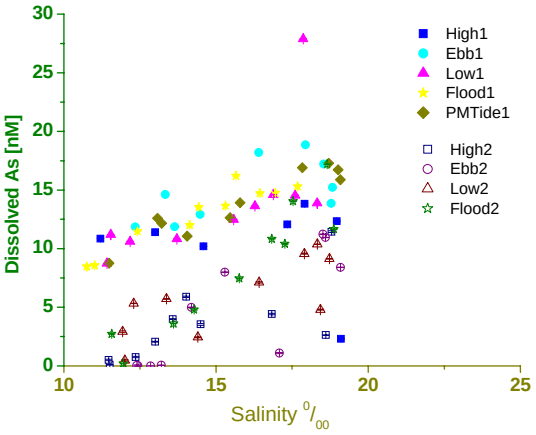

Figure 4.12- Mixing line for redox- sensitive metals determined by comparison of salinity with a) dissolved chromium (nM), b) dissolved copper (nM), c) dissolved arsenic (nM).

causing an unidirectional boundary flow of porewaters to the overlying waters (Huettel et al., 1998; Precht et al., 2004; Precht et al., 2006). In parallel, similar transport may beoccurring in the Chesapeake Bay causing the enhancement of trace metal exchanges at the SWI, resulting in the distribution observed during Tidal Cycle 2.

The mean bottom flow landward during flood tide is about 15 cm s^{-1}, with maximum along-channel flow up to 75 cm s^{-1} (Lewis et al., 2007). The vertical distribution of the mean current is controlled by the ebb-flood asymmetry in the time-dependent flow, vertical mixing processes, baroclinic pressure gradients, and interaction of the flow with topography (Jay and Smith, 1990). Gravitational forces such as spring-neap tidal cycles affect ebb-flood tidal velocity and magnitude. The spring/neap transition in the subtidal flow accompanies changing stratification throughout the water column (Chant, 2002). Spring tides result in water levels that are higher than average, low waters that are lower than average, slack water (apex of High and Low) time that is shorter than average, and stronger tidal currents than average. Conversely, neap tides result in less extreme tidal conditions resulting in less separation between the two-layer circulation pattern (Chant, 2002). Water column sampling in 2004 started on August 16th with the new moon accompanying peak spring tidal effects to churn up sediments and destratifying redox zones. In 2005, with the full moon on August 19th, the strength of the spring tide should have dissipated gradually and transitioned to neap tide during Tidal Cycle 2 collected on August 23rd. The absence of excess particulate matter in the deep waters during Tidal Cycle 2 may be attributed to the weakening of gravitational forces approaching neap tide (Precht et al., 2004; Janssen et al., 2005), when resuspension is not produced and advective fluxes are sole source of deep water species. The increased

resuspension of SPM and chlorophyll α in the Ariake Sea during flood-ebb current was attributed to the strengthened energy of spring tide (Koh et al., 2006). Although theoretically plausible, this is the first time spring-neap tides have been associated with anoxic overlying waters enriched in dissolved sulfide and trace metal from estuarine sediments.

Alternatively, the enrichment of dissolved trace metals observed during Tidal Cycle 2 may be related to their physico-chemical characteristics. Elevated Co_D is usually attributed to inputs from low-salinity regimes (Martino et al., 2002); however, results show increased levels in more saline bottom water (Figure 4.11). In freshwater systems, the geochemical cycling of Co typically involves sorption to Mn particles (Balistrieri et al., 1992; Lee and Fisher, 1993) and the microbially mediated redox-driven partitioning between dissolved Mn and particulate Mn-oxides species (Lienemann et al., 1997). The release of Co_D coinciding with the reductive dissolution of its host carrier, Mn oxide, in the oxic-anoxic transition zone is not novel and has been observed in a well stratified lake (Lienemann et al., 1997; Taillefert et al., 2002b). Despite the fact that Co is an essential micronutrient for the growth of marine phytoplankton, there is limited information on the cycling of this trace metal in the marine environment (Lee and Fisher, 1993), and even less in estuaries (Martino et al., 2002; Tovar-Sanchez et al., 2004). Ni_D is particle reactive and has a strong affinity for dissolved organic matter in oceanic and estuarine systems (Bruland, 1980; Price and Morel, 1991; Turner et al., 1998), which may explain its presence in anoxic waters (Figure 4.11).

Dissolved copper is typically scavenged from surface waters either by particulate organic matter or Mn- and Fe- oxides and released during organic matter remineralization

(Bruland, 1980; Skrabal et al., 2000). For instance, uppermost porewater concentrations and bottom waters just above the sediment may supply 10-50% of Cu-complexing ligands in the Chesapeake Bay water column (Skrabal et al., 2000). In addition, microbial reductive dissolution of Mn- and Fe- oxides has been linked to the release of Cu (Skrabal et al., 2000). On the contrary, correlations between $\Sigma[H_2S]$ with particulate trace metals were mainly insignificant and not reciprocal (Table 4.2) as would be expected if reductive dissolution were evident. Therefore, during flood and high tides Cu_D in the bottom waters is most likely from sediments and predominantly complexed with large organic ligands (Skrabal et al., 2000) or H_2S in porewaters.

Pb distribution has shown strong correlations with Cr and Cu in Chesapeake Bay sediments (Owens and Cornwell, 1995; Mason et al., 2004). The source of Pb is mainly industrial (Long et al., 1995) and should mimic Ba_D, if levels in low salinity surface samples were higher due to riverine inputs. However, the inverse correlation between Ba_D (Figure 4.10b) and Pb_D (Figure 4.11c) makes it apparent that Pb_D is most likely from sediments, especially during Tidal Cycle 2. Anoxic sediments may act as a sink for Cr, whereby chromate is reduced to particle–reactive Cr(III), which can then be scavenged by metal oxides and organic particles and removed to the sediments (Rue et al., 1997). Similarly, arsenic mobility is strongly influenced by redox conditions and metal oxide partitioning. Release of As_D mainly as As(V) into overlying waters has been attributed to the reductive dissolution of Fe-oxides (Moore et al., 1988; Smedley and Kinniburgh, 2002; Chow and Taillefert, 2005). Both the adsorption of Cr and As are strongly influenced by the pH and the complex redox reactions pathways involving these metals. In particular, the pH_{pzc} of MnO_2 is low (~2 for birnessite and 4 for α–MnO_2) (Stumm,

1992) and, therefore, manganese oxides should be negatively charged in the Chesapeake Bay such that adsorption of negatively charged oxyanions (e.g. $H_2AsO_4^{-1}$, $HAsO_4^{2-}$, CrO_4^{2-}, etc.) is not favorable at pH of 7.45. Both must be reduced to As(III) and Cr(III) prior to incorporation into sulfide minerals to form arseno-pyrite and Cr_3FeS_4, respectively. However, due to its high ligand field stabilization energy caused by its electron configuration, Cr(III) has a slow rate of water exchange (~10^{-6} s^{-1}) and does not undergo substitution reactions to form solids (Morse and Luther, 1999). Therefore, chromium flushed from the sediments in bottom waters is likely enriched in Cr(III).

Here, Co_D and Ni_D do not appear to change much between tidal cycles compared to other metals, even though they are under the same physical conditions. The absence of bottom water enrichment may be due to the fact that the sediment is not elevated in Co_D (Hartwell and Hameedi, 2007) as observed in other estuaries (Tovar-Sanchez et al., 2004). However, the sediment is heavily contaminated with Ni (Hartwell and Hameedi, 2007), suggesting that another process is regulating the release of Ni and Co across the SWI. The lower enrichment of Co and Ni during Tidal Cycle 2 may be due to their reactivity with sulfide. Measured using radiolabelled water, the rate of water exchange for metals (Table 4.3) can be used to demonstrate the relative reactivity of a metal compared to Fe(II) (Morse and Luther, 1999). Prior to forming sulfide minerals (MeS), water or hydroxide is displaced by sulfide to form $Me(H_2O)_5(HS)^+$. Strong sulfide constants suggest that sulfide should out compete hydroxide for the metal ions (Morse and Luther, 1999). Pb, Cu, Zn, and Mn have faster rates of water exchange than Fe, and should form their own sulfide mineral faster than FeS and FeS_2 can form. On the other hand, both Co and Ni have slower rates of water exchange than Fe(II) (Morse and Luther,

Table 4.3 Tabulation of the rate of water exchange of divalent trace metals (Burgess, 1988)

Metal Ion	Z (atomic number)	Rate of H_2O exchange (s^{-1})
Pb^{2+}	82	~2 E+9
Cu^{2+}	29	8 E+8
Zn^{2+}	30	3 E+7
Mn^{2+}	25	3 E+7
Fe^{2+}	26	3 E+6
Co^{2+}	27	1 E+6
Ni^{2+}	28	3 E+4
Cr^{3+}	24	~1 E-6

1999) and would be expected to co-precipitate by adsorption onto FeS and FeS_2 rather than forming discrete metal sulfide phases.

More than 50% of annual benthic reduced sulfur in the upper Chesapeake Bay is buried as FeS (3.5 – 5.5 mmol cm^{2-}) or pyrite-S (7.5 -10 mmol cm^{2-}) during the anoxic/hypoxic season (Cooper and Morse, 1998). Thus, the sediment may represent a significant sink for Co and Ni even during tidal flushing of the porewaters. Thermodynamic calculations (MINEQL+) indeed predict supersaturation of several solid phases including metal sulfide phases, such as NiS, CoS, and pyrite, over both tidal cycles (Table 4.4 and 4.5). The saturation indices calculated for orpiment were three times greater at slightly shallower depths near the oxycline compared to indices calculated for anoxic waters closer to the sediment. These calculations also indicate that the water column becomes undersaturated with respect to Fe mineral phases at these shallower depths during each of the tidal stages. The dominant species do not change much over the tidal cycles (Table 4.6 and 4.7), except for Pb that shifts from 99.9% $Pb(HS)_{2(aq)}$ in most anoxic samples to 95.2% $Pb(HS)_3^{-1}$ and 4.8% $Pb(HS)_{2(aq)}$ near the oxycline (Table 4.6). In general, samples with low sulfide concentrations resulted in higher Fe(II) (above 70%), while samples with higher sulfide concentrations distinguished 50% of iron in the form of $Fe(HS)_{2(aq)}$ as the percent abundance of $H_2S_{(aq)}$ also increased up to 25% of sulfur species.

Table 4.4 Results of MINEQL+ Solids Saturation Index Calculations for Tidal Cycle 1 Suboxic Zone

Tidal Cycle 1	High 1				Ebb 1				Low 1					Flood 1			
Depth	22.546	20.576	18.656	17.305	22.173	20.264	18.284	16.125	22.07	20.086	18.202	15.458	13.366	22.042	20.054	18.446	15.405
Cast	c3-1	c3-2	c3-3	c3-4	c4-1	c4-2	c4-3	c4-4	c5-1	c5-2	c5-3	c5-4	c5-5	c6-1	c6-2	c6-3	c6-4
U308	0.689	1.249	1.269	1.185	1.480	1.203	1.422	1.479	1.478	2.083	1.186	1.123	1.474	1.228	1.226	1.200	1.116
U409	3.777	7.545	7.545	7.460	7.776	7.485	7.777	7.778	7.781	8.602	7.408	7.327	7.778	7.461	7.458	7.430	7.299
Pyrite	18.073	17.596	17.586	18.010	18.364	17.985	17.327	15.341	16.138	15.858	15.202	4.486	17.304	16.837	16.654	16.366	17.311
Sulfur	5.030	5.030	5.030	5.030	5.296	5.030	4.756	3.760	4.153	5.030	3.626	3.265	9.737	4.447	4.283	4.205	9.741
Orpiment	6.977	8.434	8.434	22.434	9.265	8.538	7.754	4.864	5.789	5.795	4.238	3.161	22.564	6.772	6.234	6.023	22.706
Fe(OH)2	4.099	4.089	4.078	-6.065	3.912	4.089	4.091	3.954	4.061	4.062	4.060	4.059	-6.065	4.060	4.034	4.059	-6.065
$CoFe_2O_4$	15.993	16.167	16.169	-4.092	15.777	16.629	15.864	15.878	15.901	16.354	16.181	16.236	-4.092	16.120	16.184	16.148	-4.092
Magnetite	12.518	12.517	12.485	-17.896	11.979	12.482	12.109	12.124	12.142	12.446	12.457	12.469	-17.896	12.443	12.452	12.467	-17.896
Lepidocrocite	2.117	2.017	2.103	-8.014	1.945	2.096	1.988	1.993	1.999	2.099	2.102	2.106	-8.014	2.098	2.093	2.105	-8.014
Geothite	2.997	2.936	2.976	-7.134	2.825	2.975	2.868	2.873	2.879	2.979	2.982	2.986	-7.134	2.978	2.980	2.985	-7.134
Hematite	8.394	8.386	8.392	-11.870	8.050	8.387	8.136	8.147	8.158	8.358	8.364	8.371	-11.870	8.355	8.353	8.370	-11.870
Ferrihydrite	0.297	0.297	0.297	-9.834	0.125	0.296	0.168	0.173	0.179	0.279	0.282	0.286	-9.834	0.278	0.272	0.285	-9.834
Maghemitite	0.590	0.590	0.590	-19.674	0.246	0.587	0.332	0.343	0.354	0.554	0.560	0.567	-19.674	0.551	0.533	0.566	-19.674
Magnesioferrite	1.137	1.128	1.122	-17.499	2.458	1.072	2.539	2.536	2.511	1.033	1.043	1.054	-17.499	1.030	1.032	1.053	-17.499
Uraninite	1.071	2.013	2.009	1.992	2.059	1.998	2.059	2.060	2.061	2.268	1.971	1.951	2.065	1.983	1.978	1.977	1.941
CoS (alpha)	0.565	0.837	0.837	0.854	1.011	1.299	0.473	-0.519	-0.111	1.243	1.031	1.021	5.496	0.213	0.213	0.642	5.573
CoS (beta)	4.195	4.467	4.467	4.484	4.641	4.929	4.103	3.111	3.519	3.585	3.076	2.765	9.126	3.843	3.843	3.617	9.203
Chalcopyrite	14.988	14.769	15.152	15.096	14.568	14.849	14.996	16.495	15.941	16.237	16.377	17.157	0.343	15.514	15.541	15.852	0.207
Covellite	5.338	5.120	5.502	5.446	4.893	5.199	5.818	8.307	7.349	7.729	8.194	9.329	-3.831	6.518	6.513	7.085	-3.835
Greigite	11.896	11.898	11.900	0.201	12.236	12.259	10.206	6.240	7.845	7.396	6.091	4.665	0.173	9.352	9.354	8.425	0.188
Mackinawite	0.280	0.282	0.284	-5.129	0.305	0.328	-0.071	-1.182	-0.778	-0.781	-0.770	-0.634	-5.197	-0.374	-0.208	-0.271	-5.193
MnS	-2.207	-2.463	-2.533	-4.326	-3.189	-3.674	-3.237	-4.645	-5.458	-5.851	-5.831	-4.487	0.150	-3.928	-2.524	-4.361	0.270
NiS (alpha)	-1.108	0.211	0.209	-1.364	0.322	-0.875	-0.864	-1.317	-1.017	-1.291	-1.223	-1.341	4.590	-0.909	-1.016	-1.216	4.461
NiS (beta)	6.905	7.411	7.409	7.172	7.522	6.987	6.325	5.883	6.183	6.572	5.424	5.596	11.790	6.291	6.289	6.064	11.661
NiS (gamma)	5.205	5.711	5.709	5.472	5.822	5.287	4.625	4.183	4.483	4.872	3.724	3.896	10.090	4.591	4.587	4.364	9.961
Galena	3.255	2.588	3.244	3.119	2.699	2.523	2.762	4.172	3.996	4.147	3.861	4.948	-3.481	3.089	3.076	3.202	-3.485
Barite	-0.136	0.270	0.268	0.298	0.270	0.269	0.289	0.292	0.352	0.323	0.342	0.328	0.332	0.327	0.315	0.342	0.345

Table 4.5 Results of MINEQL+ Solids Saturation Index Calculations for Tidal Cycle 2 Suboxic Zone

Tidal Cycle 2	High 2				Ebb 2				Low 2				Flood 2			
Depth	22.697	19.104	14.719	11.606	22.385	19.478	17.258	13.574	21.836	19.56	16.207	13.421	22.257	21.098	17.557	15.512
Cast	c8-1	c8-2	c8-3	c8-4	c9-1	c9-2	c9-3	c9-4	c10-1	c10-2	c10-3	c10-4	c11-1	c11-2	c11-3	c11-4
U308	1.876	1.876	1.876	1.869	1.870	1.861	1.916	1.874	1.856	1.789	1.916	1.912	1.862	1.846	1.856	1.866
U409	8.297	8.297	8.297	8.311	8.316	8.314	8.359	8.307	8.302	8.189	8.359	8.367	8.308	8.299	8.308	8.299
Pyrite	19.112	18.983	16.028	17.307	19.150	19.059	19.213	17.314	19.136	18.714	19.117	17.307	19.142	19.044	16.136	17.306
Sulfur	5.835	5.705	4.105	9.739	5.829	5.700	5.983	9.743	5.815	5.503	5.838	9.739	5.821	5.685	4.085	9.735
Orpiment	10.600	9.081	4.281	21.508	10.681	9.392	10.989	21.502	10.667	8.962	10.554	20.940	10.673	9.377	4.589	21.494
Fe(OH)2	3.587	3.717	3.962	-6.077	3.614	3.767	3.384	-6.077	3.600	3.845	3.577	-6.077	3.606	3.752	4.049	-6.077
$CoFe_2O_4$	15.249	15.388	15.883	-4.079	15.285	15.579	14.856	-4.122	15.271	15.662	15.243	-4.268	15.277	15.564	16.198	-4.265
Magnetite	11.005	11.398	12.134	-17.884	11.099	11.547	10.405	-17.883	11.084	11.787	10.985	-17.883	11.091	11.539	12.462	-17.883
Lepidocrocite	1.621	1.752	1.997	-8.011	1.651	1.801	1.420	-8.010	1.636	1.881	1.614	-8.010	1.643	1.793	2.099	-8.011
Geothite	2.501	2.632	2.877	-7.131	2.531	2.681	2.300	-7.130	2.516	2.761	2.494	-7.130	2.523	2.673	2.979	-7.131
Hematite	7.402	7.664	8.155	-11.861	7.460	7.759	7.000	-7.131	7.445	7.922	7.387	-11.861	7.452	7.751	8.365	-11.861
Ferrihydrite	-0.199	-0.068	0.177	-9.831	-0.138	-0.071	-0.400	-11.861	0.135	0.061	-0.206	-9.830	-0.137	-0.074	0.272	-9.830
Maghemitite	-0.402	-0.140	0.351	-19.663	-0.275	-0.142	-0.804	-9.830	0.258	0.118	-0.417	-19.665	-0.274	-0.148	0.554	-19.665
Magnesioferrite	1.804	2.068	2.564	-17.538	0.135	0.431	1.402	-19.664	1.027	2.323	1.789	-17.539	0.115	0.431	1.040	-17.538
Uraninite	2.188	2.188	2.188	2.195	2.198	2.198	2.205	-17.538	2.190	2.162	2.205	2.209	2.178	2.198	2.185	2.194
CoS (alpha)	1.665	1.413	-0.182	5.519	1.655	1.519	1.828	5.563	1.647	1.222	1.683	5.329	1.635	1.519	-0.192	5.563
CoS (beta)	5.296	5.043	3.448	9.149	5.285	5.149	5.458	9.193	5.277	4.852	5.313	8.959	5.265	5.149	3.569	9.193
Chalcopyrite	13.881	14.112	15.957	0.390	13.913	14.192	13.502	0.347	13.905	14.501	13.841	0.316	13.893	14.192	16.101	0.347
Covellite	3.998	4.228	7.428	-3.835	3.985	4.246	3.665	-3.846	3.977	4.683	3.955	-3.859	3.965	4.246	7.443	-3.866
Greigite	13.401	13.274	7.610	0.179	13.529	13.453	13.411	0.192	13.521	12.873	13.411	0.180	13.509	13.453	7.987	0.192
Mackinawite	0.513	0.514	0.508	-5.195	0.560	0.578	0.467	-5.195	0.552	0.448	0.516	-5.195	0.540	0.578	0.543	-5.195
MnS	-2.391	-2.563	-4.158	1.552	-2.536	-2.454	-2.201	1.596	-2.293	-2.779	-2.346	0.042	-2.278	-2.454	-4.362	1.591
NiS (alpha)	0.592	0.487	-1.108	4.553	0.694	0.558	0.954	4.598	0.351	0.331	0.809	4.557	0.689	0.553	-1.215	4.593
NiS (beta)	7.792	7.687	6.092	11.753	7.894	7.758	8.154	11.798	7.551	7.531	8.009	11.757	7.889	7.753	6.172	11.793
NiS (gamma)	6.092	5.987	4.392	10.053	6.194	6.058	6.454	10.098	5.851	5.831	6.309	10.057	6.189	6.053	4.472	10.093
Galena	1.768	1.994	3.593	-3.469	1.761	1.892	3.061	-3.271	2.086	2.171	3.206	-2.448	1.756	1.887	3.483	-3.086
Barite	0.489	0.406	0.366	0.458	0.450	0.478	0.487	0.386	0.463	0.428	0.487	0.452	0.481	0.483	0.485	0.492

Table 4.6 - Average component abundance (%) of trace metals in the anoxic zone of water column calculated with MINEQL+. Average abundances over tidal cycles were first calculated at each depth of each tidal stage resulting in a tidal average, and then averaged over the two tidal cycles. Standard deviations (SD) were calculated using output results from both tidal cycles.

Ion	Species	% abundance	Log K	SD
Ba(2+)	Ba(2+)	99.6		0.00
Cu(2+)	Cu(HS)3(-)	100	25.1	0.00
U	U(OH)5(-)	99.9	-14.4	0.00
AsO3(3-)	H3AsO3	98.025	33	0.05
	H2AsO3(-)	2.05	24	0.10
Co(2+)	Co(2+)	68.863		1.14
	CoHCO3(-)	1.338	11.1	0.07
	CoCl(+)	16.325	-0.03	0.79
	CoSO4(aq)	13.065	1.15	0.66
CrO4(2-)	CrO4(2-)	70.83		2.79
	HCrO4(-)	2.95	5.94	0.15
	KCrO4(-)	4.4	-0.03	8.80
	NaCrO4(-)	22.48	0.13	3.64
Fe(2+)	Fe(2+)	61.4	0	24.41
	FeCl(+)	7.45	-0.8	9.91
	FeSO4(aq)	14.61	1.19	4.92
	Fe(HS)2(aq)	24.65	8.05	26.57
Mn(2+)	Mn(2+)	78.16	0	1.02
	MnCl	6.69	-0.4	0.36
	MnCl2(aq)	2.23	-0.5	3.34
	MnSO4(aq)	12.66	1.05	1.09
Ni(+)	Ni(+)	71.36	0	1.25
	NiHCO3(+)	2.18	11.3	0.12
	NiCl(+)	12.25	-0.16	0.81
	NiSO42(aq)	13.48	1.15	0.83
Pb(2+)	Pb(HS)2(aq)	80.98	14.4	13.14
	Pb(HS)3(-)	95.2	15.7	58.95

Table 4.7 - Average component abundance (%) of major constituents included in the model in the anoxic zone of water column calculated with MINEQL+. Average abundances over tidal cycles were first calculated at each depth of each tidal stage resulting in a tidal average, and then averaged over the two tidal cycles. Standard deviations (SD) were calculated using output results from both tidal cycles.

Ion	Species	% abundance	Log K	SD
Cl(-)	Cl(-)	99.9		0.00
Na(+)	Na(+)	99.9		0.00
NO3(-)	NO3(-)	99.9		0.00
Ca(2+)	Ca(2+)	81.506	0	0.86
	CaSO4(aq)	18	1.16	0.96
CO3(2-)	CaHCO3(+)	1.631	10.4	0.10
	H2CO3(aq)	4.667	15.8	0.08
	HCO3(-)	81.952	9.76	0.82
	MgHCO3(+)	4.848	10.2	0.32
	NaHCO3(aq)	5.729	9.23	0.62
K(+)	K(+)	97.425	0	0.19
	KSO42(-)	2.575	0.28	0.20
Mg(+)	Mg(+)	84.6	0	0.72
	MgSO42(aq)	15.2	1.11	0.74
PO4(3-)	CaHPO4 (aq)	3.96	13.3	0.18
	KHPO4(-)	3.716	11.8	7.43
	MgH2PO4 (+)	1.75	19.2	8.19
	MgHPO4 (aq)	27.93	13.2	2.22
	NaHPO4 (-)	23.34	12	5.66
	H2PO4(-)	7.255	18.3	8.44
	HPO4(2-)	28.675	11.6	4.90
SO4(2-)	SO4(2-)	60.1	0	5.77
	NaSO4(2-)	20.1	0.16	3.57
	CaSO42(aq)	3.6	1.21	0.33
	KSO4(2-)	0	0.25	11.50
	MgSO42(aq)	15.4	1.11	1.82
HS(-)	HS(-)	77.93	0	1.10
	H2S(aq)	26.86	6.74	0.58
	Cu(HS)3(-)	7.46	25	10.59
	PbH2S(aq)	2.35	14.4	13.32
	FeH2S(aq)	1.25	8.1	16.26

In contrast to Co and Ni, Cr, Pb, and to a lesser extent Cu are likely unreactive with respect to iron sulfide minerals due to their high rate of water exchange, and should preferentially form sulfide (Pb) or inorganic (S^{2-}) and organic (Cu) complexes, or precipitate as discrete metal sulfide phases (Morse and Luther, 1999). With the highest water exchange rate (Morse and Luther, 1999), and the highest concentrations in Chesapeake Bay sediments (Long and Morgan, 1990; Long et al., 1995; Long et al., 1996), it is not surprising to observe elevated levels of Pb_D released from sediments by tidal advection (Figure 4.11). Intriguingly, the release of As_D is decreased in the presence of sulfide during Tidal Cycle 2 (Figures 4.5, 4.7 and 4.12). Sulfur species complex arsenic under strongly reducing conditions (O'Day et al., 2004) and can co-precipitate with FeS to form arseno-pyrite (Bostick and Fendorf, 2003). This indicates that arsenic is efficiently removed from the water column of the Chesapeake Bay.

4.6 Conclusions

Using a combination of innovative and traditional analytical techniques, this study has documented the effect of tidal forcing on the distribution of trace metals at the oxic-anoxic interface. Simultaneously, dissolved sulfide diffuses into the oxycline to reduce Mn oxides and release dissolved trace metals in the anoxic waters. Measurements obtained during two successive tidal cycles show that the intensity of the flux of trace metals from the sediments is affected by tidal cycles.

Overall, the increase flux of some of the dissolved trace metals in the anoxic zone during Tidal Cycle 2 cannot be accounted for by excess reductive dissolution of

manganese oxides and must be a result from the advection of dissolved species due to the shear stress promoted by water flowing over the sediments at flood tide. The force of these pulses can cause resuspension of surficial sediments and/or more intense advective fluxes predominantly during flooding tides. However, sediment resuspension may not be essential to enrich bottom waters or else particulate levels would be higher near the SWI during Tidal Cycle 2 when the highest levels of dissolved species were observed. These data suggest that at least dissolved species diffuse and/or advect at the sediment-water interface during neap tides. The intensity of the flux of dissolved trace metals is controlled by their reactivity with sulfide and probably the iron sulfide mineral phases as well as the velocity of tidal flushing. Overall, this study demonstrates that the most dominant chemical processes affecting the distribution of trace metals during estuarine mixing in the Chesapeake Bay are sulfide related reductive dissolution and desorption, as well as, trace-metal sulfide interactions and pyritization. With sediment concentrations orders of magnitude greater than their aqueous counterparts, this research indicates that the sediment is only a temporary sink that continuously flushes metals concomitantly with Mn and H_2S into estuarine waters by tidally-driven advection. The significance of resuspension during spring tide and absence during neap tide should be investigated in detail in future research.

4.7 Acknowledgements

This research was supported by the National Science Foundation (EAR-0216368). We would like to offer our sincere gratitude to the crew and science team of the R/V Cape Henlopen, B. Lewis, G. Bristow and D. Meiggs for retrieving samples, and

dedicated members of both the Taillefert and Luther groups for their contribution and critiques.

4.8 Supplemental Information (Appendix D)

Vertical profiles of dissolved and particulate Mn, Co, As, and Ba from 2004 research cruise have been included in Appendix D as Figure D.1. Also included in Appendix D are interannual (2002 to 2004) depth profiles for dissolved uranium (Figure D.2), dissolved barium (Figure D.3), dissolved manganese (Figure D.4), dissolved cobalt (Figure D.5), dissolved nickel (Figure D.6), dissolved lead (Figure D.7), dissolved chromium (Figure D.8), dissolved copper (Dissolved D.9), dissolved arsenic (Figure D.10), and dissolved cadmium (Figure D.11). In addition, Tables D.1 and D.2 summarize the MINEQL+ input data used to calculate the saturation indices (Table 4.4 and 4.5) and species abundance provided in percentage (Table 4.6 and 4.7) of anoxic waters separated by tidal stage over the two consecutive tidal cycles.

CHAPTER 5

CONCLUSIONS

This dissertation demonstrates the importance of characterizing not only biological and chemical processes, but also physical processes, when investigating the distribution of trace metals in natural aquatic systems. This study also demonstrates the scope and versatility of voltammetric techniques in studying the cycling of redox species within riverine and estuarine settings *in situ* and *ex situ,* as well as in laboratory reactor environments. The main issues addressed in this thesis pertain to the following:

1. Speciation and partitioning of arsenic, iron, and manganese across the oxic-anoxic and water-sediment interfaces
2. Influence of arsenic loading on microbial processes in riverine sediment
3. Mechanisms behind the enrichment of redox sensitive species and trace metals in estuarine anoxic bottom waters

The major findings of this dissertation are summarized below:

5.1 Speciation and partitioning of arsenic, iron, and manganese across the oxic-anoxic and water-sediment interfaces

Despite global interest, details regarding the chemical and biological processes that dominate authigenic arsenic diagenesis and cycling were limited. A compilation of innovative analytical techniques was employed to determine the vertical transformation of major redox species and the speciation of As(III) and As(V) with a high spatial

resolution (i.e., < 5 mm) in two contaminated freshwater sediments. Porewater depth profiles illustrate the dominance of iron reduction processes on arsenic cycling. In fact, interannual results provide evidence of a significant correlation between the diagenetic processes involving iron and arsenic in the freshwater sediments studied. The sediment profiles suggest that iron oxide particles scavenge arsenic in the form of arsenate in the water column and settle to the sediment-water interface where they are reduced by indigenous iron reducing bacteria. As a result of microbial iron reduction, As(V) is released and accumulates in the porewaters near the sediment-water interface, where it diffuses back to the overlying waters. The diffusion of As(V) to the overlying water was much greater after a severe flood deposited fresh As-bearing particles to the surficial sediment.

Thermodynamics suggests that As(III) dominates in reducing conditions, however, As(III) was never found in the porewaters of any of the sediment cores at either freshwater site. Initially, this conundrum was attributed to asymmetry of the natural system and suggested that the abiotic reduction of As(V) is a slow process that was not occurring in these recently deposited sediments. This work was the first to implement a combination of voltammetric and ICP-MS techniques to determine arsenic diagenesis in a recently flooded freshwater sediment. The subsequent study tested the hypothesis that microbial and chemical reduction of As(V) is not significant in these sediments.

5.2 Influence of arsenic loading on microbial processes

Microcosm experiments confirm that any As(V) added to these sediments is immediately adsorbed in oxic conditions and released in anoxic conditions during the

microbial reduction of authigenic iron oxides. Incubations in the presence of ≤ 1 μM As(V) reveal that arsenate is released but not concomitantly reduced during this process. Curiously, microbial iron reduction is enhanced significantly when As(V) amendments are increased from natural levels to a threshold of approximately 2 to 6 μM, increasing the simultaneous formation of crystalline iron oxides and excess release of arsenate into porewaters. Above this threshold, however, the microbial reductive dissolution of iron oxides is inhibited by arsenate, and arsenite is produced, probably through a detoxification mechanism. These findings suggest that arsenic blocks ATP formation at concentrations as low as 0.1 μM As(V) and that indigenous iron-reducing bacteria are able to increase respiration rates to overcome this effect up to a threshold approximately one order of magnitude above natural levels. However, if As(V) inputs to sediments rise by one order of magnitude above the current porewater content (i.e. 200 nM), iron respiration will be inhibited and As(III) produced in significant quantities. The present river waters contain in average about 40 nM of As(V) in the dissolved phase that can be delivered to the sediments, especially after flood events. If the loading of As(V) to these sediments persists or increases, the currently abundant amorphous iron oxides will be transformed into more stable iron oxides with lower adsorption capacity for As(V). Compounded with the production of As(III), if the toxicity threshold is exceeded, these sediments may be a non-point source of both As(V) and As(III) to the overlying waters, including the drinking water reservoir of West Point Lake. The incubation study shows that even low inputs of arsenic to riverine sediments may affect microbial processes, the stability of iron oxides and, indirectly, the cycling of arsenic. This work demonstrated that arsenic levels have a strong impact on biogeochemical processes in natural sediments

even at low levels, and to prevent hazardous conditions, it is necessary to maintain the concentration of arsenate in these porewaters below the estimated threshold of 2 to 6 μM. Finally, this study was the first time iron recrystallization was linked to arsenic concentrations.

5.3 Mechanisms behind the enrichment of redox sensitive species and trace metals in estuarine anoxic bottom waters

In marine environments, salinity gradients driven by physical mixing processes can affect both chemical processes (e.g. speciation and partitioning) and biological processes (e.g., benthic and planktonic community structure and function). A combination of *in situ* measurements with discrete water sampling was utilized to determine the influence of tidal variations on the cycling of trace metals under changing redox conditions during two consecutive tidal cycles in the Chesapeake Bay (MD) during the peak anoxic/hypoxic season. *In situ* profiles show that the physico-chemical conditions of the water column are affected over tidal cycles. During the peak anoxia season, a combination of redox transformations and tidally-influenced flushing from sediments consistently promotes the accumulation of dissolved Mn and ΣH_2S in the suboxic zone. Under oxic conditions, trace metals may adsorb onto settling Mn-oxides that are deposited to sediments where they can be re-cycled to the overlying water by physical advective or diffusive forces. However, as the tides progress from high to low, both buoyant oxic and saline suboxic waters flow seaward resulting in vertical mixing of oxic and anoxic waters that shifts the oxycline up in the water column expanding the anoxic zone. At the next flood tide, the oxycline is lowered in the water column when

denser bottom waters flowing landward pull oxygen down deeper into the water column. Simultaneously, the landward flow of seawater above the sediment causes shear stress forces that advect dissolved species, including sulfides, manganese, and trace metals, upward into the bottom waters. Estuarine circulation relies on river flow to converge buoyant freshwater- typically high in $Ba_{D,}$ with saline ocean water- enriched with U_D, and establish the density gradient. The distribution of uranium and barium during both tidal cycles indicates that buoyant freshwater and denser oceanic water are mixing in the Chesapeake Bay, but that sediment-water interactions result in an excessive input of dissolved $\sum H_2S$, Mn, Cr, Ba, U, Cu, and Pb to the overlying waters at neap tide. This research suggests that the selective enrichment of Cr_D, Cu_D and Pb_D concentrations in the bottom waters of the Chesapeake Bay is controlled by a combination of tidally-driven advective flushing of chemical reserves stored in Chesapeake Bay sediments, regardless of resuspension, and reactivity with dissolved sulfides. In turn, the As_D directly precipitates with sulfide while Ni_D and Co_D adsorb or co-precipitate with iron sulfide minerals. This work is the first to successfully demonstrate that the enrichment of trace metals in anoxic bottom water and overlying oxic water is attributed to the tidal flushing of surface porewaters that are caused by shifting spring-neap tidal currents.

5.4 Future Research

In this dissertation, it is demonstrated that the behavior of trace metals in both freshwater and marine systems is complicated by the interdependent physical, chemical, and biological processes affecting their transformations. As a result, several questions developed from this work need to be investigated further.

For example, the hypothesis that arsenic indirectly restricts ATP formation by microorganisms should be tested with model organisms, such as *Shewanella* and *Geobacter* species, under a larger range of environmental conditions. The main obstacle to this investigation will be the ability for these microorganisms to grow on high levels of As(V) (Newman et al., 1998).

Similarly, sulfide effects on the solubility of As(III) should be determined utilizing synthetic sulfide-bearing minerals such as pure orpiment. The uptake of arsenic in anoxic environments is strongly correlated with the formation of iron sulfide minerals, including pyrite. However, the contributions of precipitation, co-precipitation, and adsorption mechanisms on sulfide minerals has not been resolved (Belzile, 1988; Bostick and Fendorf, 2003). The formation of intermediate complexes in the presence of excess sulfide, and their effects on the solubility of As(III) in the presence and absence of these excess sulfides remains uncertain. For example, using ion chromatography with conductivity detection Rochette et al. (2000) observed an unknown intermediate species beyond the retention times for sulfite, sulfate, thiosulfate, thiocyanate and arsenate. Based on mass balance of arsenite, arsenate, and total dissolved arsenic, this peak was interpreted to be thioarsenate ($H_2AsO_3S^-$), dithioarsenate ($H_2AsO_2S_2^-$) or thioarsenite ($H_3AsO_2S{\cdot}S$). Advanced analytical techniques including a combination of electrochemistry, HPLC-ICP-MS, and possibly Capillary Electrophoresis could be used to better characterize the compositional of As_xS_y, and $As_xS_yO_z$ complexes.

The sulfide research will carry over into the marine environment where knowledge regarding the composition of particles (metal oxide and organic matter) and quantification of their effects on trace metal distribution over short term and long term

tidal cycles in the Chesapeake Bay is lacking. Since the study of the distributions and partitioning of trace metals in estuaries is a central interest to the understanding of their global cycling and transport (Chiffoleau et al., 1994), this will be the focus of some future work. Finally, the quantification of sediment resuspension and its contribution to trace metal accumulation is essential to predict and simulate the effects of perturbations such as increases in sea level. If seasonal eutrophication and hypoxia persists in conjunction with a rise in sea level, then the cyclic pulses of dissolved trace metals from the abundant sediment reservoir will impact a larger area of the Bay. In addition to composition, the partitioning (distribution coefficients), and bioavailability of SPM and surficial sediments should be determined in natural samples, with isotherm calculations in accordance to Turner and Millward (2002). In addition, although metal sulfide clusters (nanoparticles) may be important transporters of trace metals, their formation and subsequent influence at the site should be investigated in future studies.

In summary, my future research direction will be to demonstrate the physiological, ecological, and toxicological effects of the chemical speciation of metals (especially arsenic) and to determine the factors dominating their transformations in both freshwater and marine systems.

APPENDIX A

OVERVIEW OF METHODOLOGY AND APPLCIATIONS

Voltammetric Measurements

In voltammetry, a potential is applied as a function of time between a working and a reference electrode. The current resulting from the oxidation or reduction of chemical species at each potential (Table A.1) is read at a counter electrode. Results are presented as current potential versus current scans, for each dissolved species (Figure A.1). The specific voltammetric techniques used in this study included linear sweep voltammetry (LSV) for O_2 and H_2O_2 determination and cathodic square wave voltammetry (CSWV) for Mn(II), Fe(II), soluble-Fe(III), and ΣH_2S =($H_2S + HS^- + S^{2-} + S^0 + S_x^{2-}$). All voltammetric measurements were conducted in unacidifed, unfiltered water without dilution.

Table A.1: Voltammetric half reactions and their reduction potentials at the Hg-plated gold wire surface (Brendel and Luther 1995).

Reactions	**E_p (V)**
$O_2 + 2H^+ + 2e^- + Hg \rightarrow H_2O_2(Hg)$	-0.30
$H_2O_2(Hg) + 2H^+ + 2e^- \rightarrow 2H_2O(Hg)$	-1.30
$HS^- + Hg \rightarrow HgS + H^+ + 2e^-$	< -0.60 (adsorption)
$HgS + H^+ + 2e^- \leftrightarrow HS^- + Hg$	-0.60
$Fe^{2+} + Hg + 2e^- \leftrightarrow Fe(Hg)$	-1.43
$org.Fe^{3+} + e^- + Hg \leftrightarrow Fe^{2+}(Hg)$	-0.2 to –0.9 (organic ligand dependent)
$Mn^{2+} + Hg + 2e^- \leftrightarrow Mn(Hg)$	-1.55

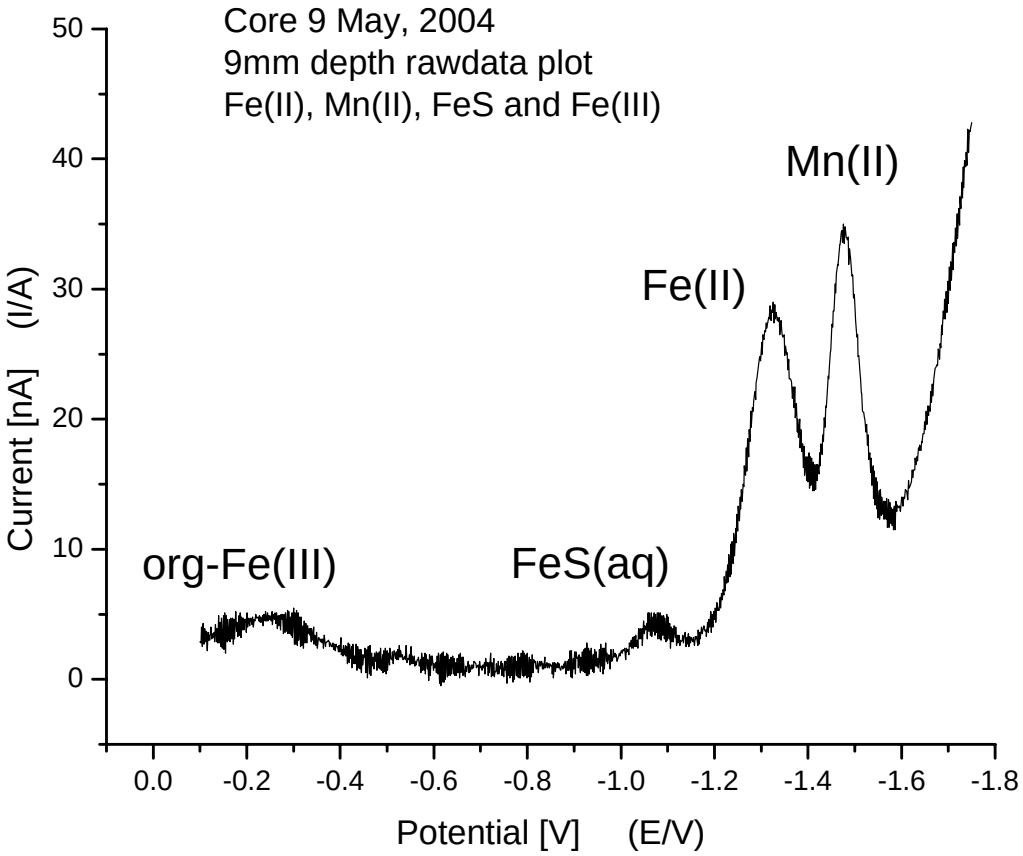

Figure A.1- Sample voltammogram from one of the freshwater depth profiles. Only Fe(II), Mn(II), $FeS_{(aq)}$ and organic-Fe(III) were detected at this depth and location. All four species of interest are labeled at their corresponding potentials.

Microelectrodes consist of a 100 μm diameter Au wire housed in a 4 mm diameter glass shaft with a tip of 5 cm length and <1 mm diameter or 3 mm PEEK ™ tubing connected via copper conducting wire to a potentiostat. The Au surface is polished with 15, 6, 1, ¼ μm diamond paste, plated with Hg to provide an electro-active mercury film, and then polarized. Once plated, each electrode is polarized at -0.9 v for ninety seconds to form a good amalgam between the Au and Hg (Brendel and Luther, 1995). Finally, electrodes were tested for quality and calibrated. A platinum wire was used as a counter electrode and a Ag/AgCl as reference electrode. The quality of Au/Hg microelectrodes issued in this study were tested by measuring dissolved O_2 solutions of similar ionic strength as freshwater and seawater (Figure A.2).

For sediments profiles, microelectrodes were calibrated for O_2 *in situ* using a single point calibration. Temperature and salinity was used to quantify the current intensity on the overlying waters. The potential was applied, with a conditioning step of 10 s at -0.1 V, then scanned from -0.1 V to -1.8 V at a rate of 200 mV s^{-1}. The conditioning step cleaned the electrode surface between measurements to avoid memory effects (Brendel and Luther 1995). Au/Hg microelectrodes were then calibrated for Mn(II) and Mn sensitivities were used to quantify Fe(II) and $\sum H_2S$ according to the Pilot Ion Method (Brendel and Luther, 1995).

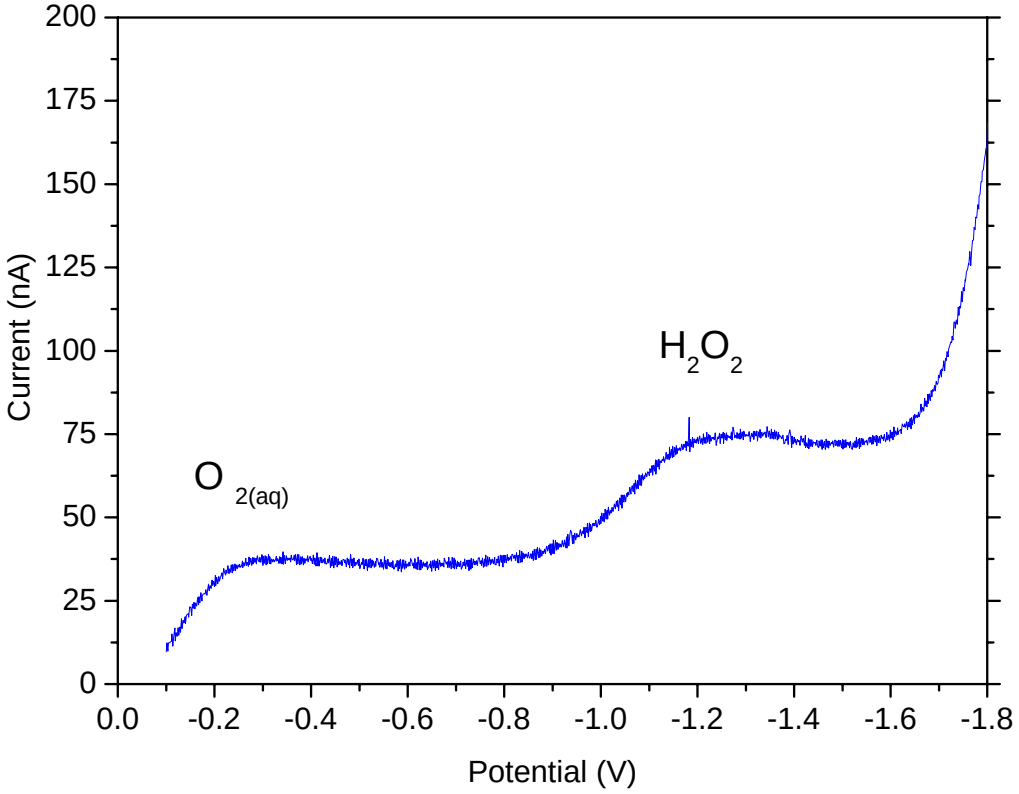

Figure A.2- Sample voltammogram for linear sweep oxygen calibration. The O_2 and H_2O_2 peaks are clearly distinct.

Mn(II) calibration of the microelectrodes was conducted in degassed water with a stock solution of 0.1 M $MnCl_2 \cdot 4H_2O$ (Fisher) in MilliQ water (Figure A.3). Mn(II) voltammograms were obtained at the same potential range, scan rate, and conditioning step as the O_2 calibration runs. In seawater, the slope of the Fe(II) calibration curve is equivalent to 0.36 times the Mn(II) calibration slope, and the CSWV sulfide calibration slope equals 12.6 times the Mn(II) calibration slope.

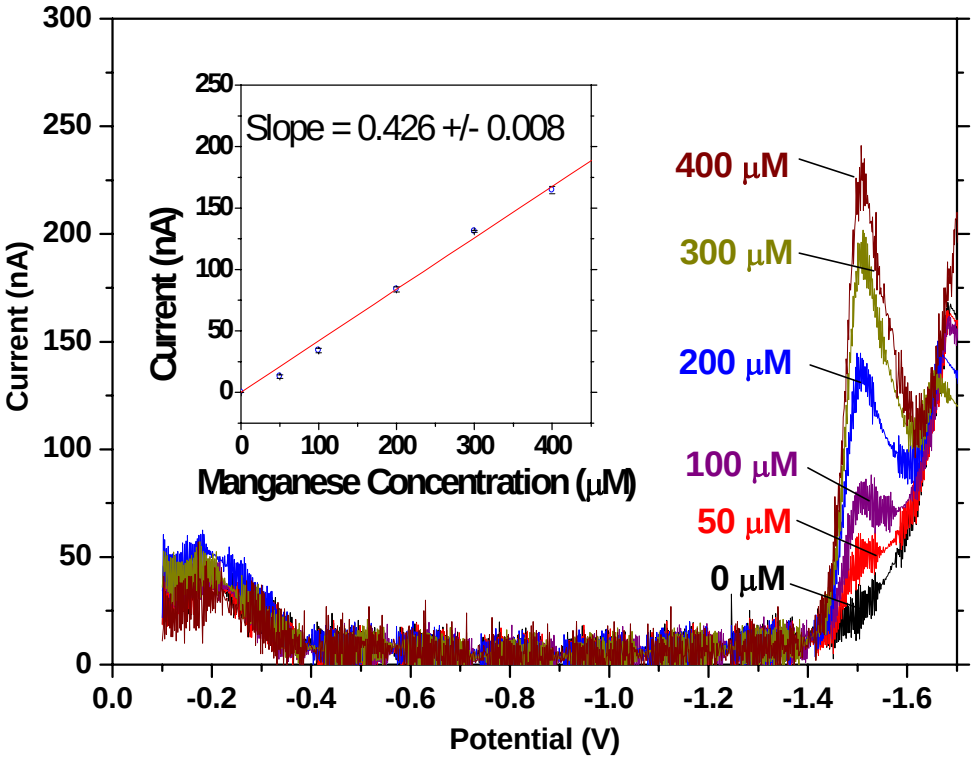

Figure A.3- Raw voltammograms from Mn calibration and corresponding calibration curve in the inset. The detection limit of Mn(II) in seawater is ~10 μM. Mn calibration range from 0 to 400 μM.

APPENDIX B

SUPPLEMENTAL INFORMATION FOR CHAPTER 3

Figures are provided in Appendix B to demonstrate non-amended reactors followed a zero-order rate law (Figure B.1) while reactors with up to 10 μM As(V) added followed first-order rate laws (Figure B.2) represented by the data from the 1 μM triplicate reactors of Placid Cove sediments. Figure B.3 represents the composite of the correlation between Fe(II) and As(V) concentrations released over time in triplicate reactors. These slopes were used to calculate the potential binding sites occupied on Fe-oxides.

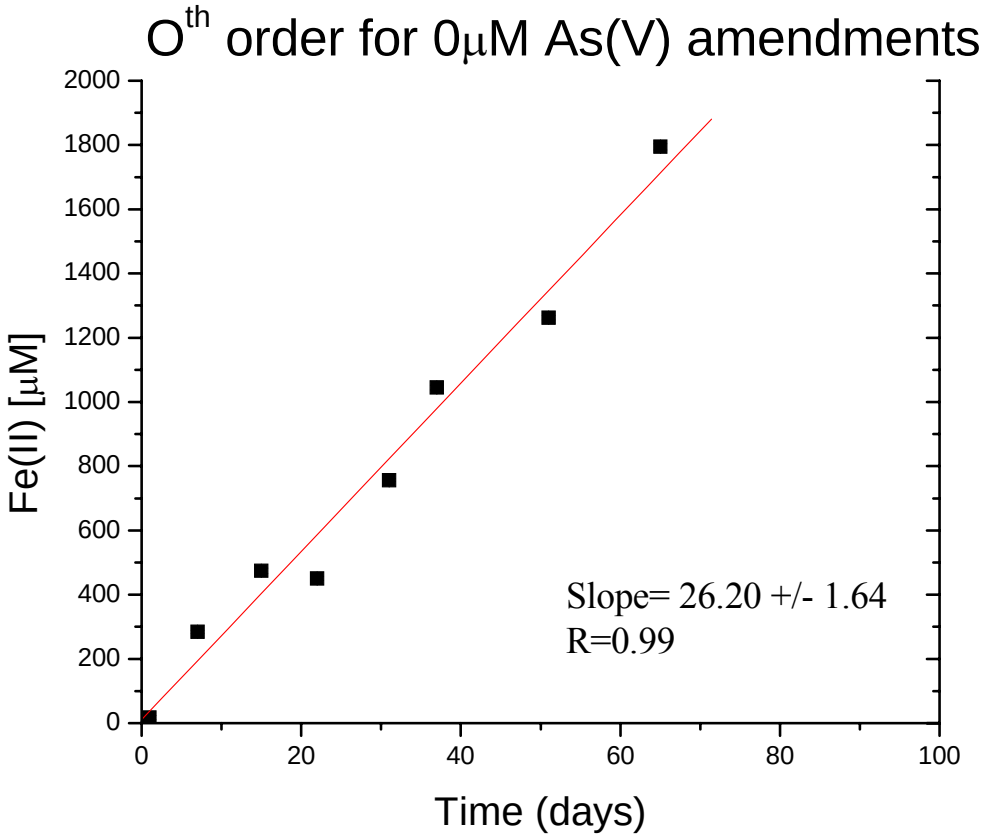

Figure B.1- Concentration of Fe(II) produced in porewaters over time in triplicate reactors amended with 0 μM As(V) an example of zero order kinetics.

a)

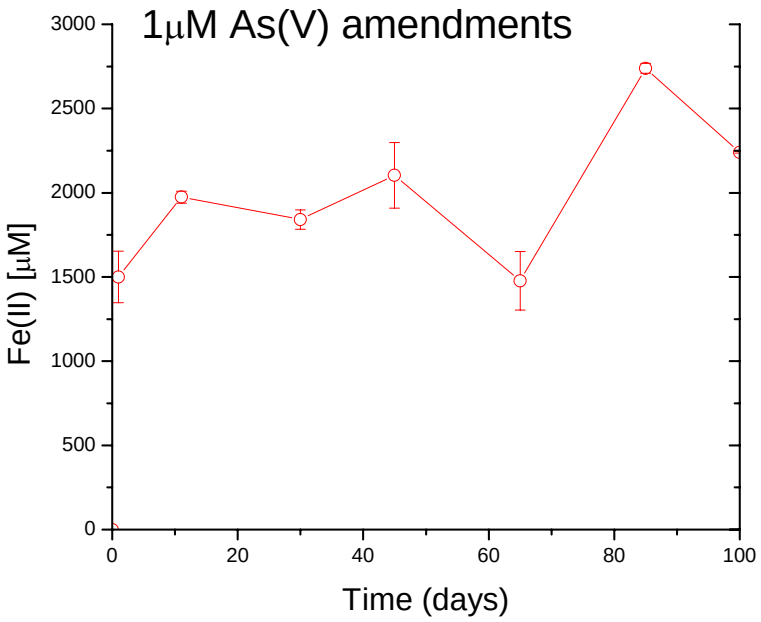

b)

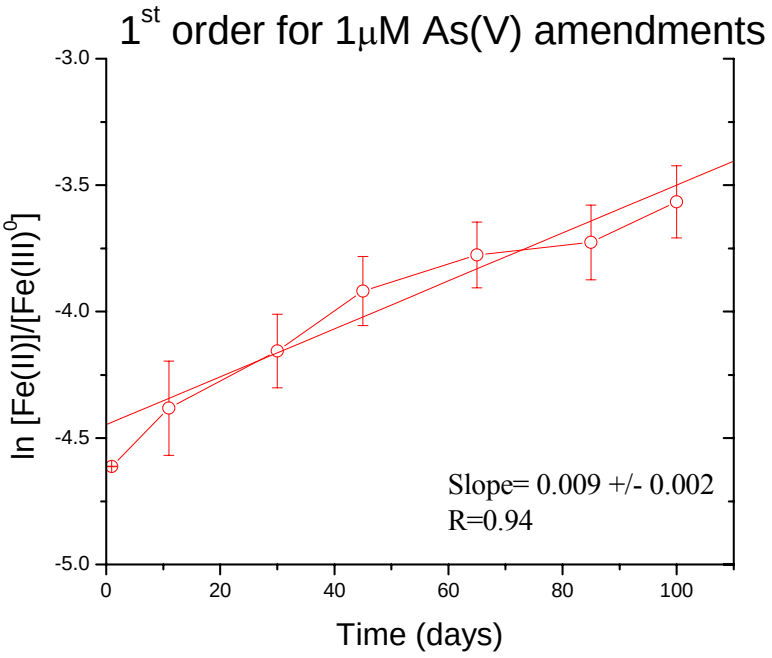

Figure B.2- a) concentration of Fe(II) produced in porewaters over time in triplicate reactors amended with 1 μM As(V) does not fit zero order kinetics, b) $\ln[Fe(II)]/[Fe(III)]^0$ over time represents first order kinetics. $[Fe(III)^0]$ is the initial $Fe(OH)_{3(s)}$ concentration of sediment sections from vertical depth profiles.

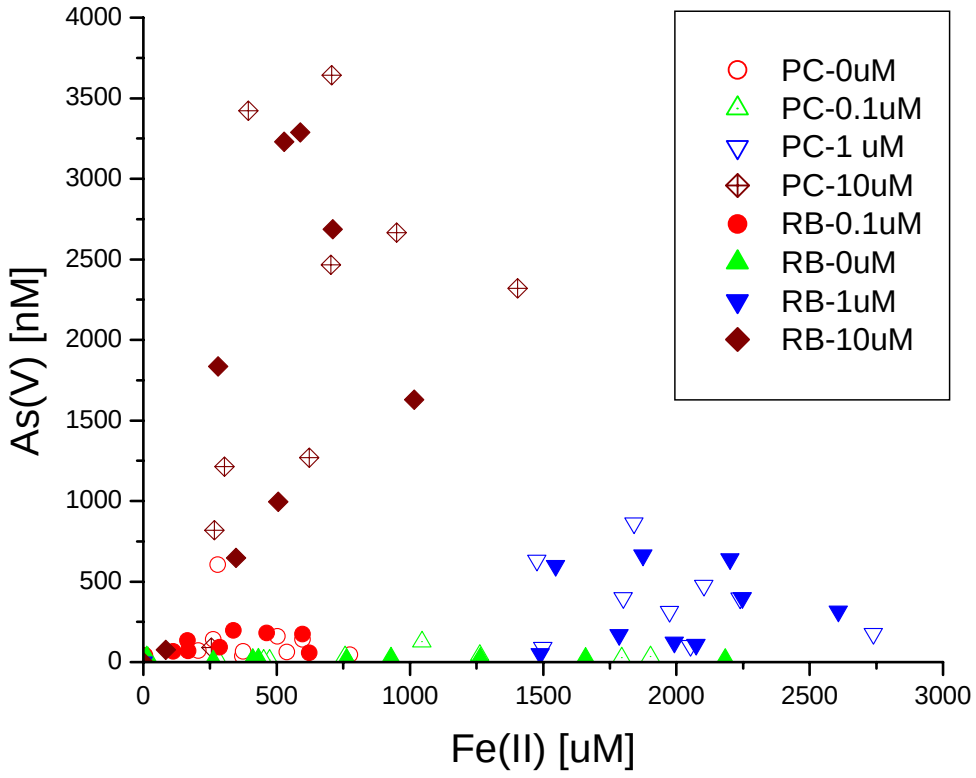

Figure B.3- Composite comparison of Fe(II) and As(V) concentrations released over time in triplicate reactors.

The Dzombak and Morel (1990) adsorption model with MINEQL+ of As(V) to $Fe(OH)_{3(s)}$ assumes 5 mmol/mole of high-binding sites (500:100,000) and 0.2 mol/mole of low affinity sites (20:100). From the slopes, a As:Fe ratio of 2 to 6: 100,000 in the 0 and 0.1 μM amended reactors are obtained for both the Placid Cove (PC) and River Bend (RB) sediments, and are similar to ratios calculated from depth profiles discussed in section 2.5 of this thesis. An As:Fe ratio of 10:100,000 was calculated for PC 1μM and 15:100,000 for RB 1μM amended sediments. An increase of As(V) up to 10 μM resulted in a As:Fe ratio of 187:100,000 and 320:100,000 in PC and RB sediment porewaters, respectively.

APPENDIX C

DESCRIPTION OF KINETIC MODEL

A Matlab ™ code was created to optimize for both R_{max} and K_{app} by fitting experimental data from individual incubations with the integrated Michaelis-Menten kinetics equation (Equation 3) in Chapter 3 of this dissertation using a non-linear least squares optimization function. Results of R_{max} and K_{app} were summarized in Appendix C (Table C.1). Initial guesses of both R_{max} and K_{app} are input along with the temporal evolution of Fe(II) from individual reactors with different As(V) amendments to integrate the differential equation using a 4th Runge Kutta (ODE45 function). The results of the integrated equation are then compared to the experimental data using a non-linear least square optimization function which minimizes the residual between the data and the modeled curve: $F = \sqrt{\sum_i (Fe^{2+}_{\exp} - Fe2match)^2}$. If the residual is greater than a tolerance value, or if the variation of the optimized parameter is smaller than a preset tolerance, the optimization stops. Figures C.1 and C.2 illustrate the accuracy of the interpolated data used to calculate and Figure C.3 illustrates the results of the optimization model.

Abbreviated Matlab™ script:

```
t =  (0:1:max(time))';     % extend time to single days
Fe2exp = c410um(:,1)*1e-6;      %M, import Fe(II) datafile per reactor and convert concentration
                                from uM to M during incubations
FeT = max(Fe2exp);      % enter total iron, compared to maximum of Fe(II) produced
Fe2match = interp1(time,Fe2exp,t);      % match experimental data, interpolation to match
                                        number of data points as t (time)
b= length(Fe2match);            %FeT = Fe(III)0 = Fe(II) adsorbed from HCl-extraction corrected
                                for volume only, input data is not corrected for wet sediment
                                volume or sediment density
FeT= 0.032;      %M for River Bend (RB), 0.046 M Placid Cove (PC)

Rmax= 5*1e-5;            % [M] conc,initial guess for Rmax= 24 e-6M or 24.74 uM/d PC and
                         24.27uM/d RB from slope of line 0 uM amended
Kapp = 8e-3;    % initial guess for Kapp
X0 = [Kapp Rmax];       % vector first guess of the parameters to optimize [M]
LB = [1e-5 0];
UB = [1e-1 1e-3];
f0 = 0;      % initial concentration of Fe(II) =0

%Optimize Kapp & Rmax to minimize the least square difference between the data
          % Use a least square non linear method
 [X,RESNORM,RESIDUAL,EXITFLAG,OUTPUT] = lsqnonlin('Fe2opt',X0,LB,UB);
RESNORM
RESIDUAL

%%%%%%%%%%%%%%%%%%%%%%%%%%%%%%%%%%%%
%         2nd - Optimization Subroutine : Kapp & Rmax
%      Call Runge Kutta 2nd Subroutine to calculate Fe(II) production
%        'RKFe2fun.m'
% %%%%%%%%%%%%%%%%%%%%%%%%%%%%%%%%%%%%
function F = Fe2opt(X)
global FeT X1 tspan f0 Fe2cal Fe2match %Fe2exp time
% Runge Kutta
X1=X;
[t,f] = ode45('RKFe2fun',tspan,f0);    % calls Runge Kutta subroutine
Fe2cal=f;
   F= norm((f- Fe2match)*10);  % minimization function (where F=0 perfect fit)

%%%%%%%%%%%%%%%%%%%%%%%%%%%%%%%%%%%%
%         3rd  Subroutine function: Runge Kutta
%         'Fe2opt.m'
%% %%%%%%%%%%%%%%%%%%%%%%%%%%%%%%%%%%%
function RKFe2fun1= RKFe2fun(t,f)
global FeT X1   % for Fe2Kapp1umopt.m
X=X1;
RKFe2fun1 = X(2)*(FeT-f)./(X(1)+FeT-f);          % integrate with respect to [Fe(II)]
```

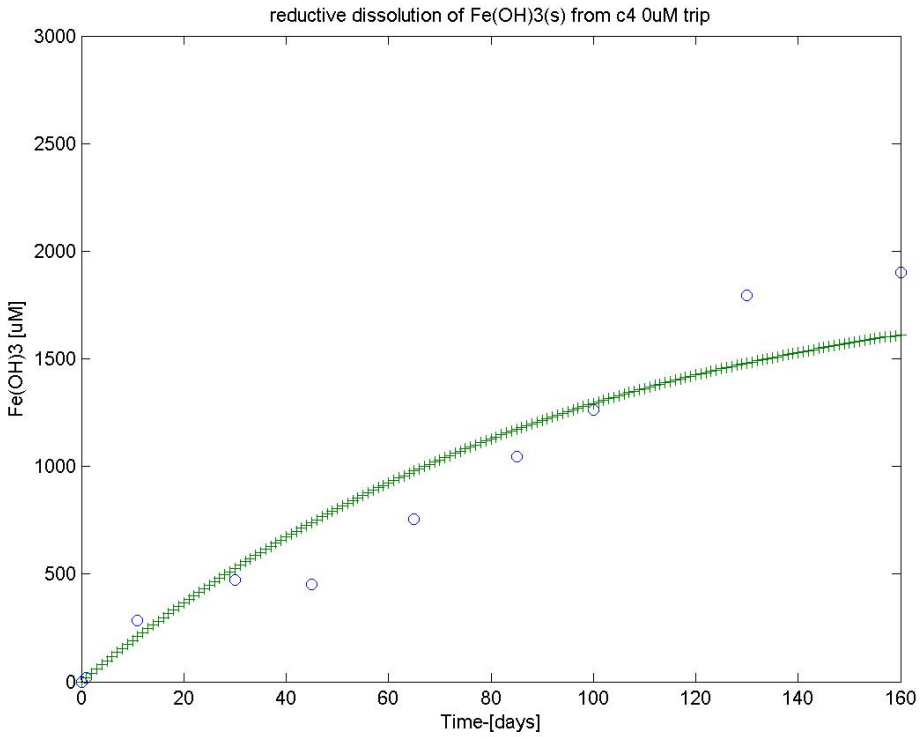

Figure C.1- Example of output from the Matlab script used to calculate R_{max} and K_{app} from an incubation with unamended sediments from PC site. Scatter points show experimental data. Green (+) shows the fitted curve.

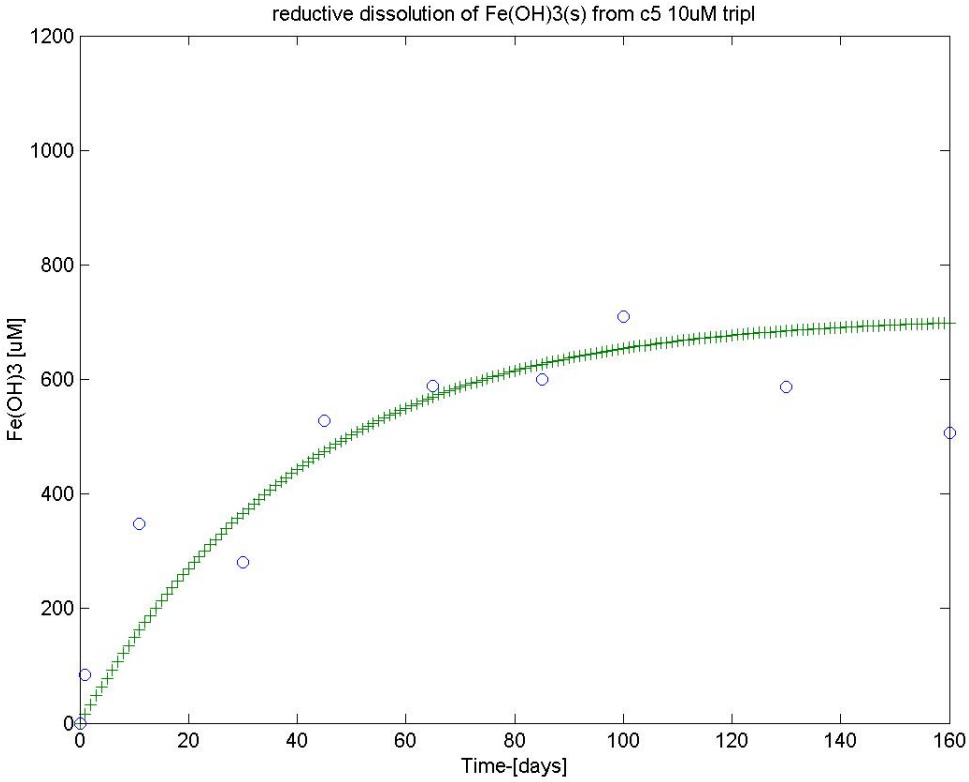

Figure C.2- Example of output from the Matlab script used to calculate R_{max} and K_{app} from an incubation amended with 10 μM As(V) sediments from RB site. Scatter points show experimental data. Green (+) shows the fitted curve.

Table C.1 –Maximum rate (R_{max}) and apparent Michaelis-Menten kinetics constant (K_{app}) for the reductive dissolution of authigenic iron oxides calculated from incubations performed with PC and RB sediments at different As(V) amendments. Correlation coefficients (R^2) between the fraction of As(V) released and Fe(II) produced initially and through steady-state (SS). Parameters represent averages and standard deviations of triplicate incubations for each treatment. Details of the calculations are provided in the text.

Incubation ID	Depth Incubated [mm]	$Fe(OH)_{3(s)}$ [μmol/g]	R_{max} [μM d^{-1}]	K_{app} [mM]	R^2 initial	R^2 SS
PC -0 μM	**0-15**	**178.8 ±20.2**	**100**	**0.17 ±0.10**	**0.941**	**0.892**
PC-0.1μM	**0-38**	**144.04±26.36**	**100**	**3.10 ±0.28**	**0.950**	**0.856**
PC-1μM	**0-38**	**144.04±26.36**	**300**	**3.60 ±0.20**	**0.862**	**0.539**
PC-10μM	**0-38**	**144.04±26.36**	**100**	**8.53 ±0.90**	**0.942**	**0.887**
RB –0 μM	**55-78**	**126±22.73**	**100**	**0.80 ±0.05**	**0.924**	**0.924**
RB-0.1μM	**55-112**	**120.5±23.9**	**100**	**0.83±0.10**	**0.959**	**0.901**
RB-1μM	**55-112**	**120.5±23.9**	**700**	**1.32 ±0.10**	**0.830**	**0.592**
RB-10μM	**55-112**	**120.5±23.9**	**100**	**4.70 ±0.30**	**0.992**	**0.920**

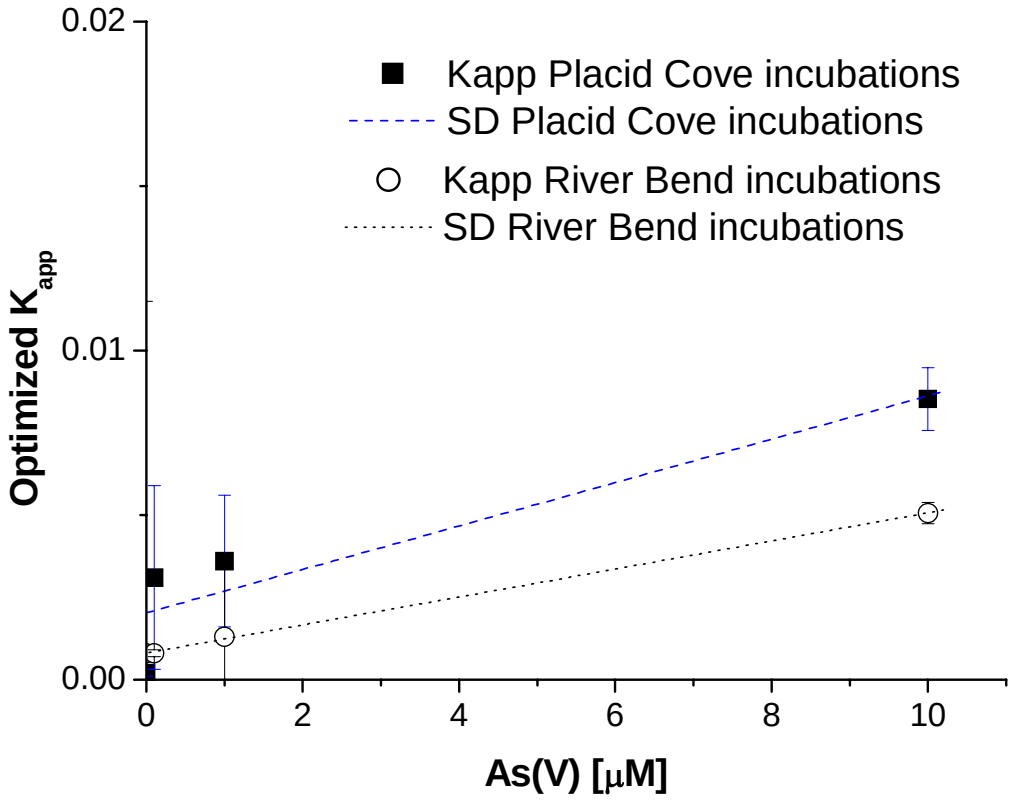

Figure C.3- As(V) amendment concentrations versus K_{app} results of optimization model. Standard deviations include replicate model outputs of triplicate incubation reactor series. Placid Cove: R= 0.933, SD= 0.001, m= 6.7E-4; River Bend: R= 0.999, SD= 5.95E-4, m= 4.25E-4.

APPENDIX D

SUPPLEMENTAL INFORMATION CHAPTER 4

Vertical profiles of dissolved and particulate Mn, Co, As, and Ba from 2004 research cruise have been included in Appendix D as Figure D.1. Also included in Appendix D are interannual (2002 to 2004) depth profiles for dissolved uranium (Figure D.2), dissolved barium (Figure D.3), dissolved manganese (Figure D.4), dissolved cobalt (Figure D.5), dissolved nickel (Figure D.6), dissolved lead (Figure D.7), dissolved chromium (Figure D.8), dissolved copper (Dissolved D.9), dissolved arsenic (Figure D.10), and dissolved cadmium (Figure D.11). In addition, Tables D.1 and D.2 summarize the MINEQL+ input data used to calculate the saturation indices (Table 4.4 and 4.5) and species abundance provided in percentage (Table 4.6 and 4.7) of anoxic waters separated by tidal stage over the two consecutive tidal cycles.

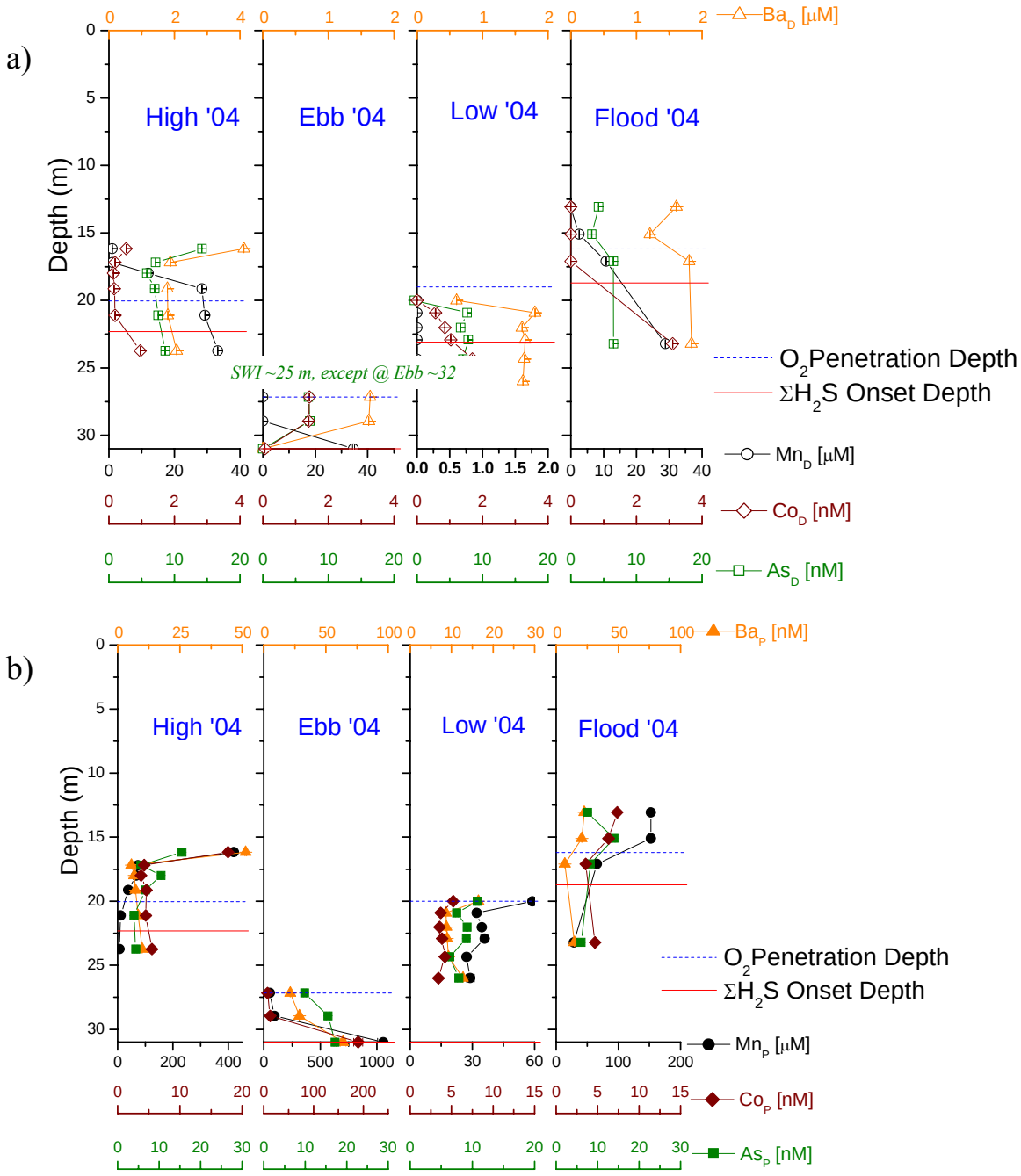

Figure D.1- 2004 Vertical Profile of Dissolved and Particulate Ba, Mn, Co, and As. a) Dissolved concentrations are depicted as Ba_D [nM] in open orange triangles, Mn_D [μM] in open black circles, Co_D [nM] in open brown diamonds, and As_D [nM] in open green squares. b) Particulate are depicted as Ba_P [nM] in solid orange triangles, Mn_P [μM] in solid black circles, Co_P [nM] in solid brown diamonds, and As_P [nM] in solid green squares. Oxygen penetration depth was determined from CTD data and is marked with a blue dashed line. ΣH_2S–onset depth was determined voltammetrically and is marked with a solid red line.

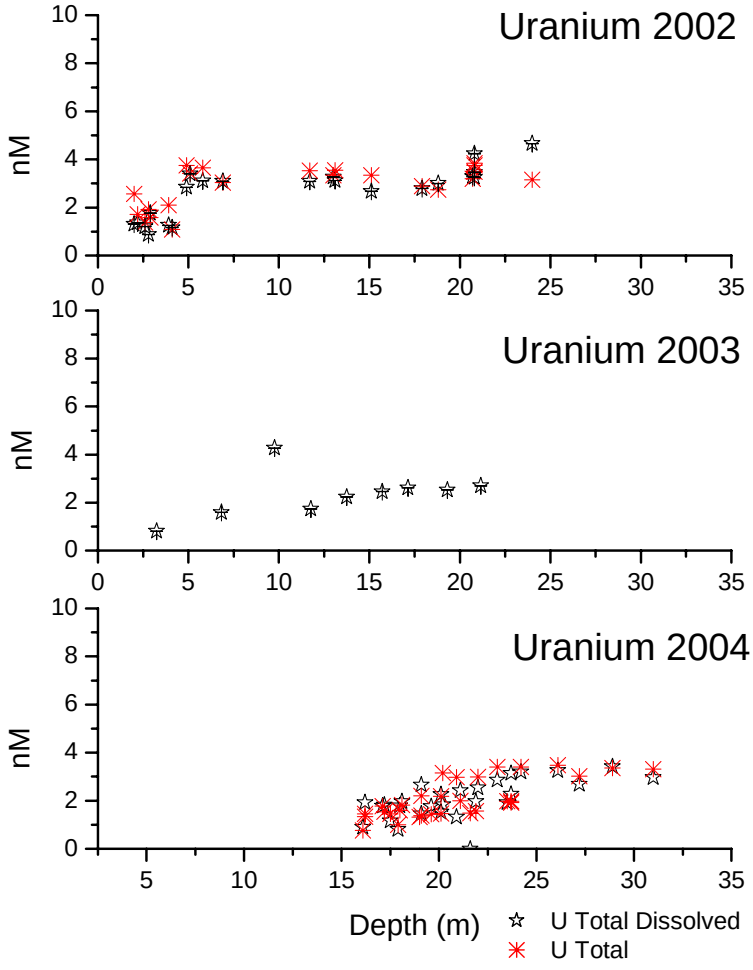

Figure D.2- Composite depth profiles of total dissolved uranium (black symbol) and total uranium (red symbol) from 2002 to 2004 reported in nM.

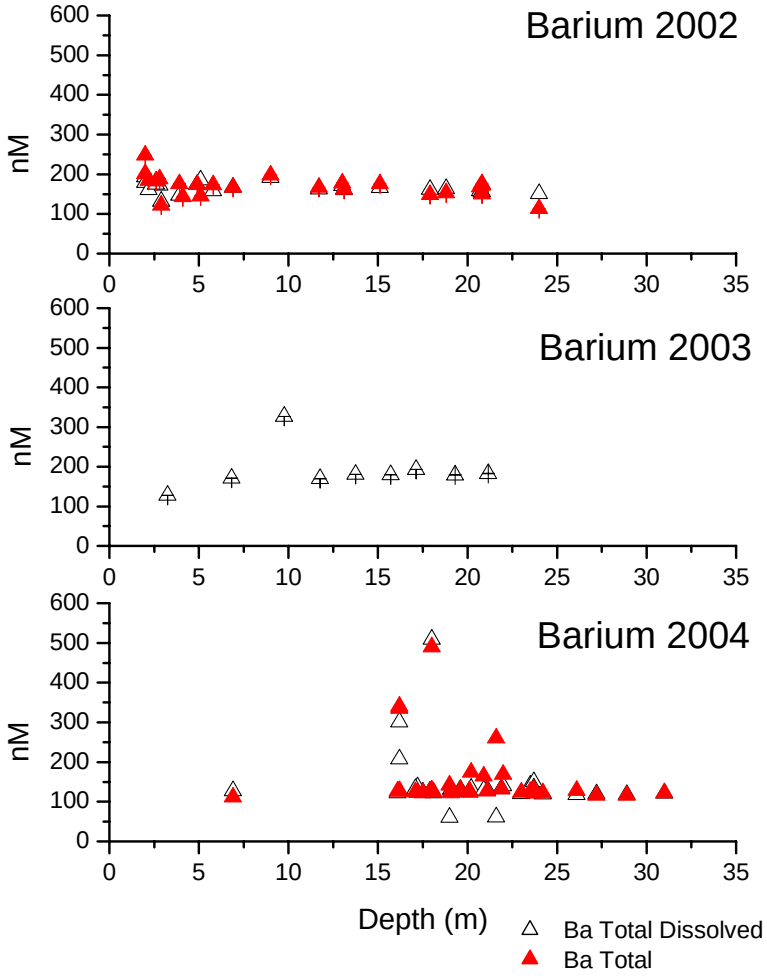

Figure D.3- Composite depth profiles of total dissolved barium (black symbol) and total barium (red symbol) from 2002 to 2004 reported in nM.

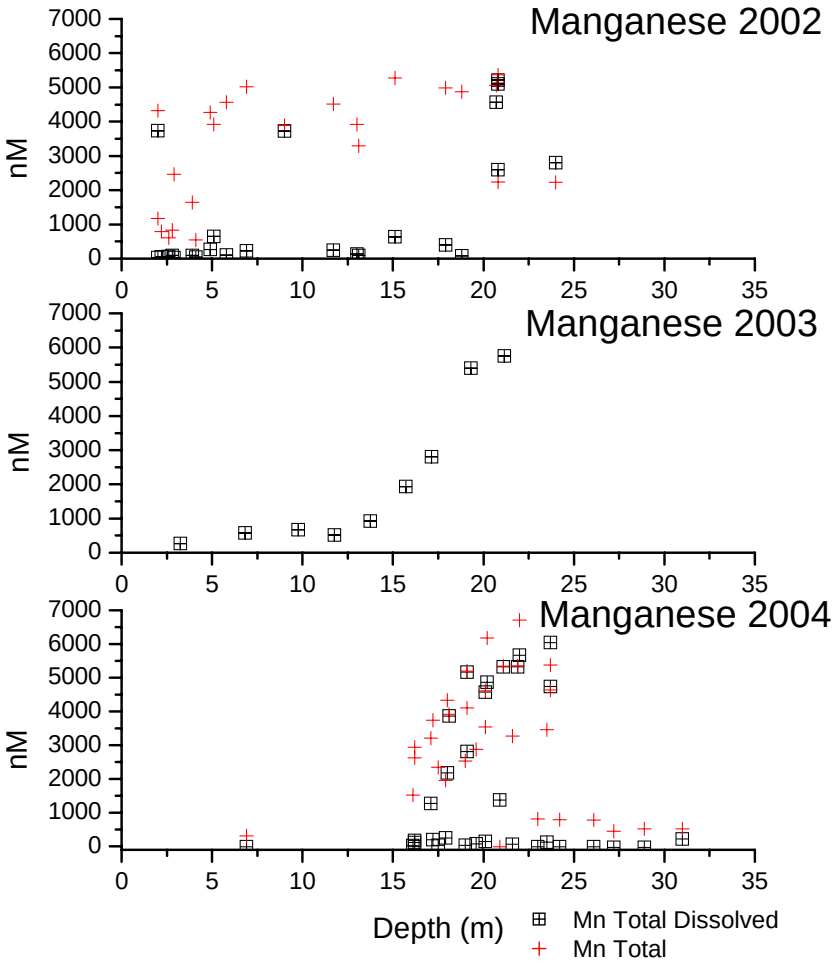

Figure D.4- Composite depth profiles of total dissolved manganese (black symbol) and total manganese (red symbol) from 2002 to 2004 reported in µM.

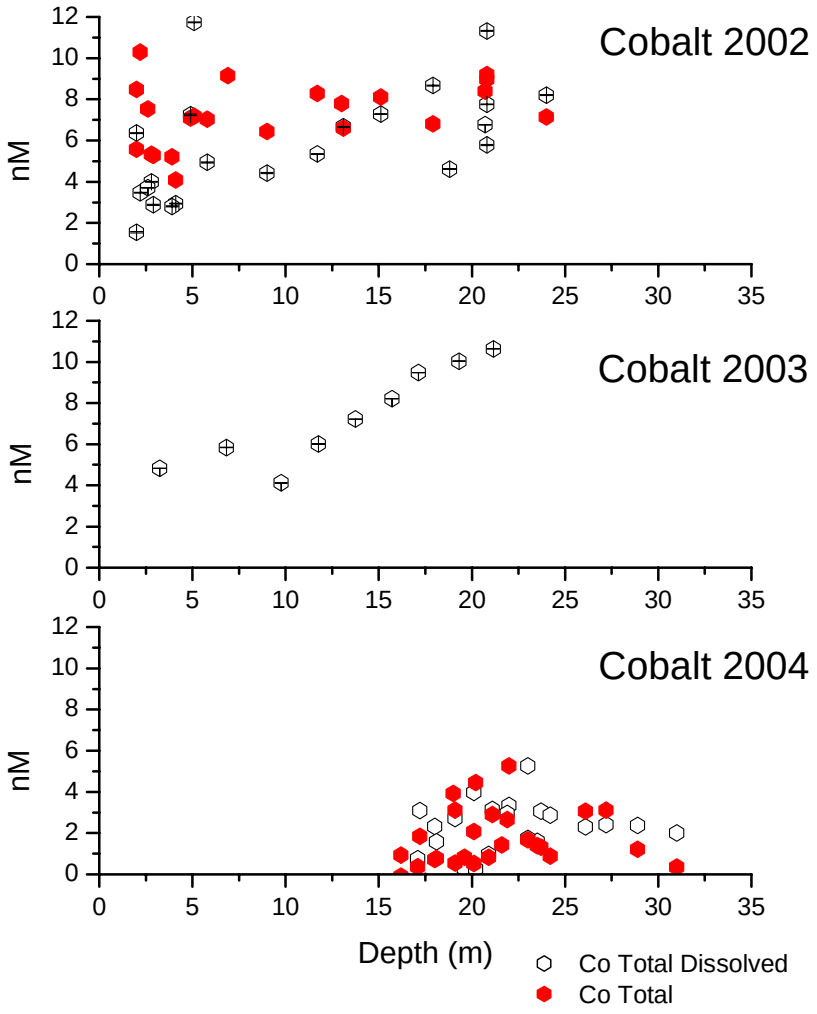

Figure D.5- Composite depth profiles of total dissolved cobalt (black symbol) and total cobalt (red symbol) from 2002 to 2004 reported in nM.

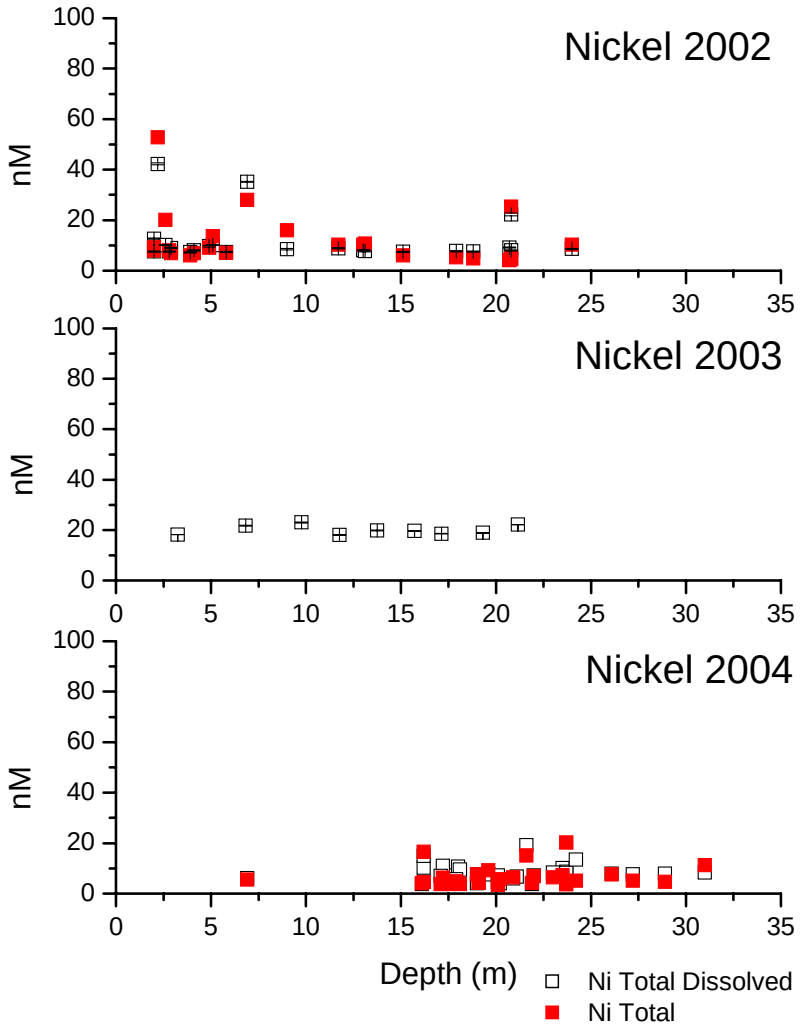

Figure D.6- Composite depth profiles of total dissolved nickel (black symbol) and total nickel (red symbol) from 2002 to 2004.

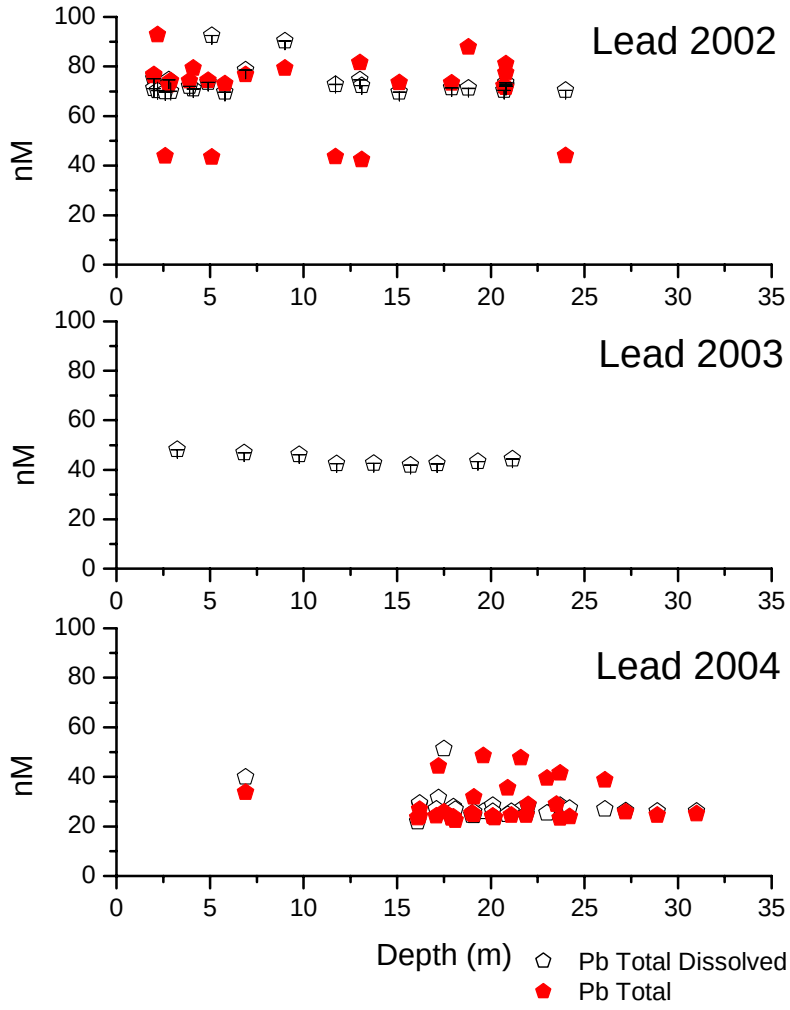

Figure D.7- Composite depth profiles of total dissolved lead (black symbol) and total lead (red symbol) from 2002 to 2004 reported in nM.

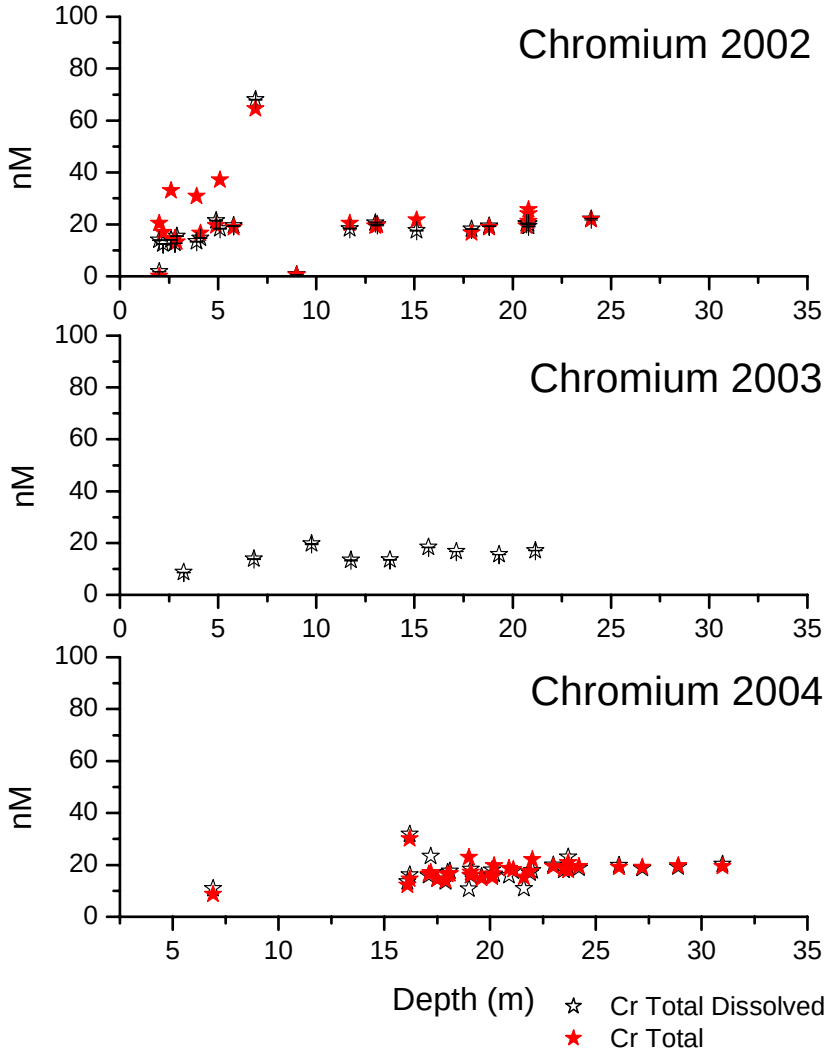

Figure D.8- Composite depth profiles of total dissolved chromium (black symbol) and total chromium (red symbol) from 2002 to 2004 reported in nM.

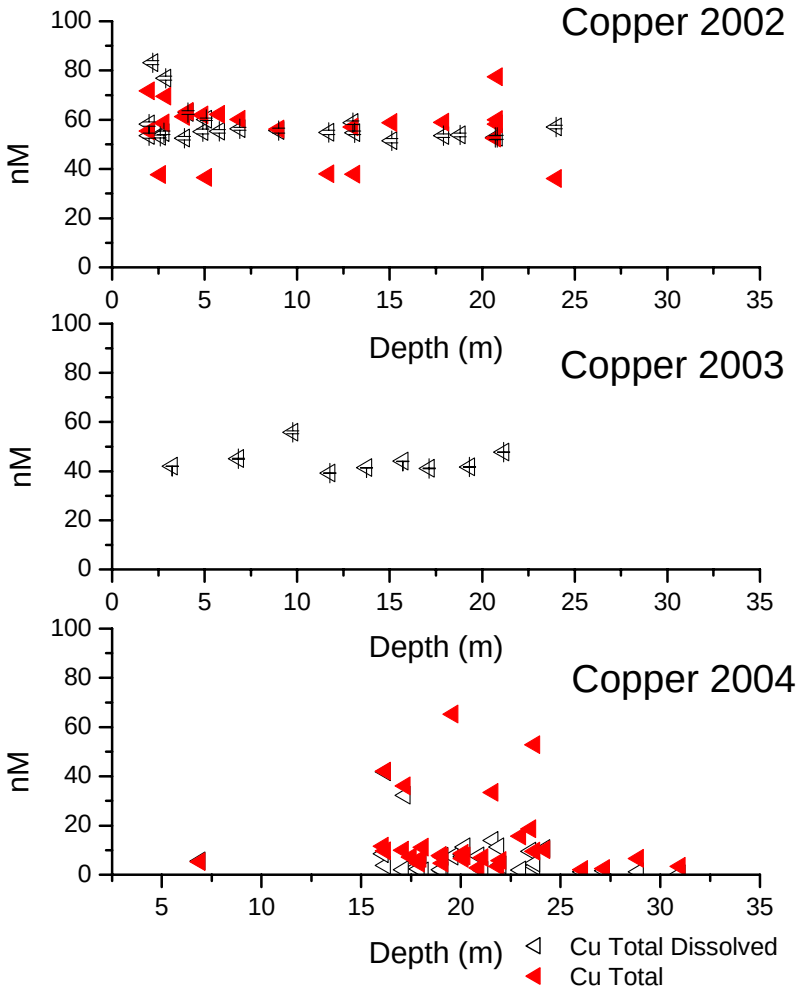

Figure D.9- Composite depth profiles of total dissolved copper (black symbol) and total copper (red symbol) from 2002 to 2004 reported in nM.

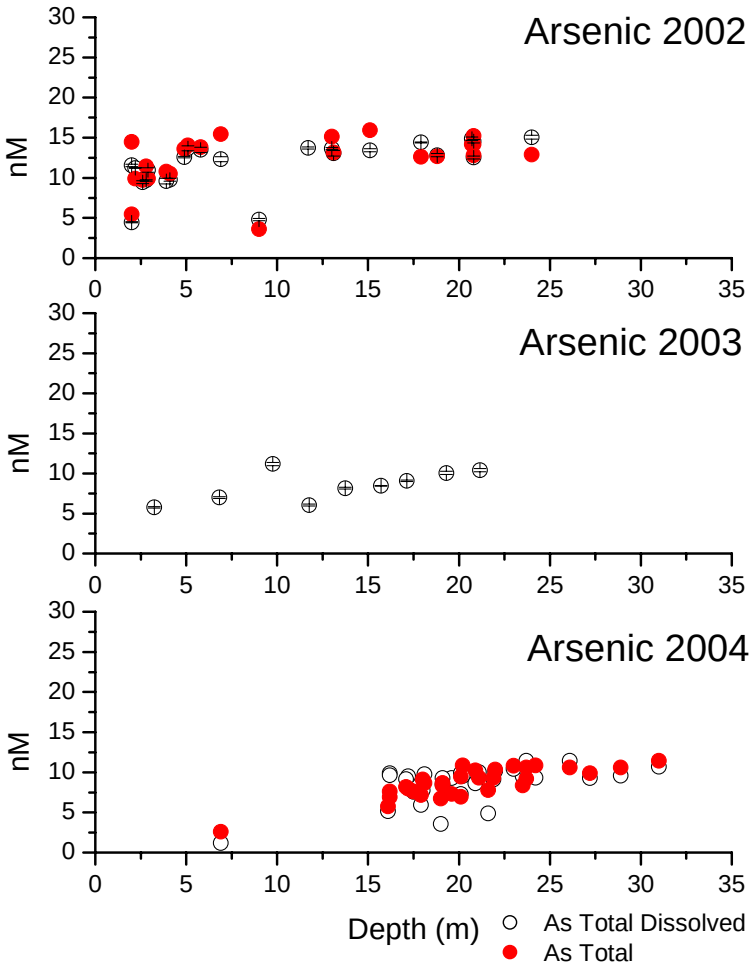

Figure D.10- Composite depth profiles of total dissolved arsenic (black symbol) and total arsenic (red symbol) from 2002 to 2004 reported in nM

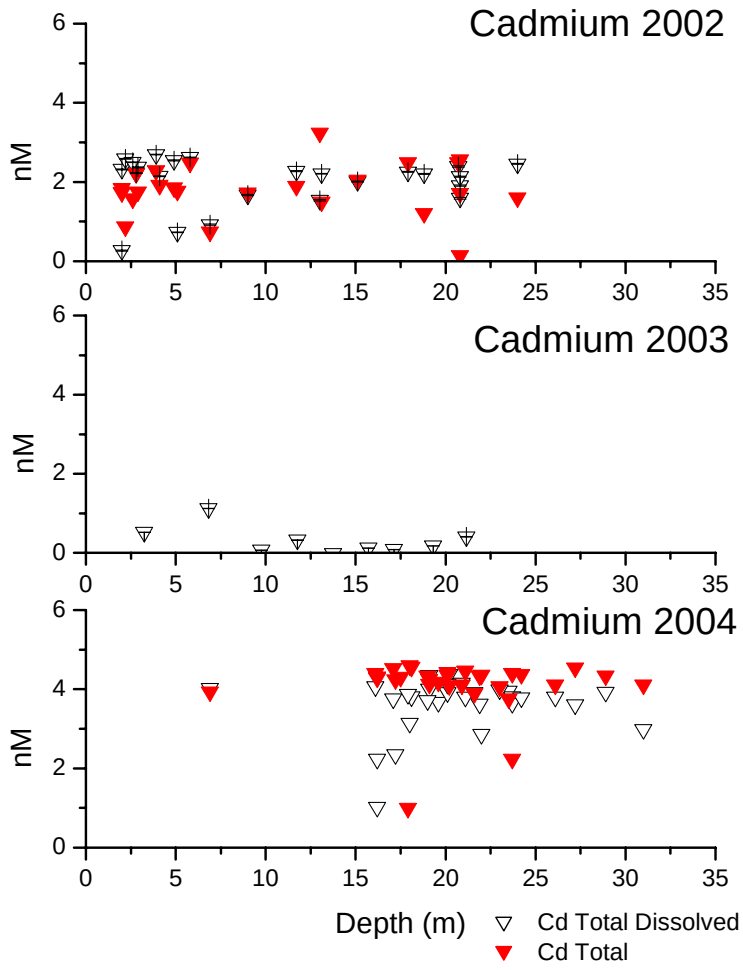

Figure D.11- Composite depth profiles of total dissolved cadmium (black symbol) and total cadmium (red symbol) from 2002 to 2004 reported in nM

Table D.1 Input concentrations of major constituents (Cl, Na, Ca, Mg, and K) as a function of depth used to calculate component concentrations and solid saturation indices with MINEQL+ in the suboxic zone during Tidal Cycle 1 and 2. Cast ID corresponds to cast number and discrete sample.

		Depth	Salinity	Cl	Na	K	Ca	Mg	SO_4^{2-}	SO_4^{2-}	HS
		m	0/00	M	M	M	M	M	M	Log K	Log K
	Charge:			-1	1	1	1	1	-2		
Tidal Cycle 1	**Cast ID:**										
High 1	c3-f1	22.546	19.104	0.287	0.2866	0.008	0.0056	0.0287	0.0154	1.814	4.69
	c3-f2	20.576	18.967	0.285	0.2845	0.0079	0.0055	0.0285	0.0152	1.817	4.78
	c3-f3	18.656	17.908	0.269	0.2686	0.0075	0.0052	0.0269	0.0144	1.842	4.883
	c3-f4	17.305	17.34	0.26	0.2601	0.0072	0.0051	0.0261	0.0139	1.856	0
Ebb 1	c4-f1	22.173	18.828	0.282	0.2824	0.0078	0.0055	0.0283	0.0151	1.82	4.447
	c4-f2	20.264	18.786	0.282	0.2818	0.0078	0.0055	0.0283	0.0151	1.821	4.832
	c4-f3	18.284	18.539	0.278	0.2781	0.0077	0.0054	0.0279	0.0149	1.827	4.987
	c4-f4	16.125	17.937	0.269	0.2691	0.0075	0.0052	0.027	0.0144	1.841	5.983
Low 1	c5-f1	22.07	18.322	0.275	0.2748	0.0076	0.0054	0.0276	0.0147	1.832	5.588
	c5-f2	20.086	17.863	0.268	0.2679	0.0074	0.0052	0.0269	0.0144	1.843	5.783
	c5-f3	18.202	17.602	0.264	0.264	0.0073	0.0051	0.0265	0.0141	1.849	6.114
	c5-f4	15.458	16.884	0.253	0.2533	0.007	0.0049	0.0254	0.0136	1.867	6.469
	c5-f5	13.366	16.28	0.244	0.2442	0.0068	0.0048	0.0245	0.0131	1.883	0
Flood 1	c6-f1	22.042	17.685	0.265	0.2653	0.0074	0.0052	0.0266	0.0142	1.847	5.293
	c6-f2	20.054	16.952	0.254	0.2543	0.0071	0.005	0.0255	0.0136	1.866	5.492
	c6-f3	18.446	16.445	0.247	0.2467	0.0069	0.0048	0.0247	0.0132	1.879	5.527
	c6-f4	15.405	15.658	0.235	0.2349	0.0065	0.0046	0.0235	0.0126	1.9	0
Tidal Cycle 2											
High 2	c8-f1	22.697	18.794	0.282	0.2819	0.0078	0.0055	0.0283	0.0151	1.821	3.913
	c8-f2	19.104	18.608	0.279	0.2791	0.0078	0.0054	0.028	0.015	1.825	4.036
	c8-f3	14.719	16.83	0.252	0.2525	0.007	0.0049	0.0253	0.0135	1.869	5.638
	c8-f4	11.606	14.491	0.217	0.2174	0.006	0.0042	0.0218	0.0116	1.934	0
Ebb 2	c9-f1	22.385	19.092	0.286	0.2864	0.008	0.0056	0.0287	0.0153	1.814	4.224
	c9-f2	19.478	18.594	0.279	0.2789	0.0077	0.0054	0.028	0.0149	1.826	4.05
	c9-f3	17.258	18.511	0.278	0.2777	0.0077	0.0054	0.0278	0.0149	1.828	3.76
	c9-f4	13.574	17.088	0.256	0.2563	0.0071	0.005	0.0257	0.0137	1.862	4.408
	c9-f5	11.36	15.292	0.229	0.2294	0.0064	0.0045	0.023	0.0123	1.91	0
Low 2	c10-f1	21.836	18.725	0.281	0.2809	0.0078	0.0055	0.0282	0.015	1.823	4.287
	c10-f2	19.56	18.431	0.276	0.2765	0.0077	0.0054	0.0277	0.0148	1.829	4.236
	c10-f3	16.207	18.33	0.275	0.275	0.0076	0.0054	0.0276	0.0147	1.832	3.905
	c10-f4	13.421	17.902	0.269	0.2685	0.0075	0.0052	0.0269	0.0144	1.842	4.17
	c10-f5	11.028	16.417	0.246	0.2463	0.0068	0.0048	0.0247	0.0132	1.88	4.799
	c10-f6	7.557	14.403	0.216	0.216	0.006	0.0042	0.0217	0.0116	1.937	0
Flood 2	c11-f1	22.257	18.869	0.283	0.283	0.0079	0.0055	0.0284	0.0152	1.819	4.63
	c11-f2	21.098	18.654	0.28	0.2798	0.0078	0.0055	0.0281	0.015	1.824	4.511
	c11-f3	17.557	17.529	0.263	0.2629	0.0073	0.0051	0.0264	0.0141	1.851	4.906
	c11-f4	15.512	17.261	0.259	0.2589	0.0072	0.005	0.026	0.0139	1.858	5.336
	c11-f5	13.45	16.835	0.253	0.2525	0.007	0.0049	0.0253	0.0135	1.869	0
Avgerage Seawater Concentration=				0.48	0.59	0.015	0.011	0.054	0.029		

Table D.2 Input concentrations of trace metals as a function of depth used to calculate component concentrations and solid saturation indices with MINEQL+ in the suboxic zone during Tidal Cycle 1 and 2. Cast ID corresponds to cast number and discrete sample. Inputs held constant: pH 7.45, Fe(II) at 4E-6 M, NO_3^{2-} at 6.92E-5 M, PO_4^{3-} at 3.26E-7 M, and HCO_3^- at 0.0012 M assumed closed to the atmosphere.

		Depth	Salinity	HS	Cr	Mn	Co	Ni	Cu	As	Ba	Pb	U
		m	0/00	uM	nM	nM	nM	nM	nM	nM	nM	nM	nM
	Charge:			-1	3	2	2	2	1	3	2	2	6
Tidal Cycle 1	**Cast ID:**												
High 1	c3-f1	22.546	19.104	20.4	7	350	1	12	10	2	28	19	0.72
	c3-f2	20.576	18.967	16.6	36	7329	2	39	6	12	194	4	6.33
	c3-f3	18.656	17.908	13.1	24	2609	3	34	15	14	179	19	5.61
	c3-f4	17.305	17.34	0	32	697	3	23	12	12	219	14	6.09
Ebb 1	c4-f1	22.173	18.828	35.7	42	6765	3	41	10	15	198	9	7.39
	c4-f2	20.264	18.786	14.72	30	5958	7	15	7	14	173	4	6.09
	c4-f3	18.284	18.539	10.31	34	7652	3	9	7	17	206	3	7.19
	c4-f4	16.125	17.937	1.04	30	8033	8	32	22	19	210	8	6.98
Low 1	c5-f1	22.07	18.322	2.58	35	7618	3	31	17	14	197	10	6.02
	c5-f2	20.086	17.863	1.65	61	14596	5	81	15	28	353	12	11.88
	c5-f3	18.202	17.602	0.77	34	7577	3	13	10	15	208	3	5.93
	c5-f4	15.458	16.884	0.34	34	3103	3	41	25	15	232	19	5.66
	c5-f5	13.366	16.28	0	33	486	3	25	15	14	237	13	5.35
Flood 1	c6-f1	22.042	17.685	5.09	32	6936	3	14	9	15	222	3	6.12
	c6-f2	20.054	16.952	3.22	33	6055	3	25	8	15	219	2	5.92
	c6-f3	18.446	16.445	2.97	32	520	3	13	10	15	240	4	6.00
	c6-f4	15.405	15.658	0	32	576	3	16	10	16	239	7	5.61
Tidal Cycle 2													
High 2	c8-f1	22.697	18.794	122.3	67	12550	4	22	15	11	342	36	10.52
	c8-f2	19.104	18.608	92.15	56	11114	3	20	14	3	289	38	8.64
	c8-f3	14.719	16.83	2.3	64	11365	4	23	15	4	366	45	8.29
	c8-f4	11.606	14.491	0	48	418	2	21	15	4	335	39	5.82
Ebb 2	c9-f1	22.385	19.092	59.75	68	11302	4	68	21	8	323	51	9.64
	c9-f2	19.478	18.594	89.11	71	12632	4	31	22	11	346	41	10.95
	c9-f3	17.258	18.511	173.7	71	12313	4	33	24	11	349	45	10.14
	c9-f4	13.574	17.088	39.08	53	8293	3	28	22	1	286	50	7.29
	c9-f5	11.36	15.292	0	50	465	3	22	16	8	386	37	7.32
Low 2	c10-f1	21.836	18.725	51.68	75	13187	4	30	19	9	361	54	11.09
	c10-f2	19.56	18.431	58.11	59	10712	3	25	16	5	289	43	9.37
	c10-f3	16.207	18.33	124.4	67	13393	4	36	14	10	334	101	10.33
	c10-f4	13.421	17.902	67.6	66	13190	3	18	13	10	334	36	10.02
	c10-f5	11.028	16.417	15.87	63	1673	3	21	19	7	404	39	9.04
	c10-f6	7.557	14.403	0	52	374	2	22	14	2	364	38	6.89
Flood 2	c11-f1	22.257	18.869	23.42	70	12658	4	20	13	12	335	40	11.41
	c11-f2	21.098	18.654	30.85	73	12590	3	18	12	17	328	33	10.55
	c11-f3	17.557	17.529	12.42	63	16258	3	18	12	14	365	39	9.94
	c11-f4	15.512	17.261	4.61	66	13548	3	20	14	10	337	36	9.10
	c11-f5	13.45	16.835	0	65	9293	3	21	13	11	391	34	9.77

REFERENCES

Adelson, J. M., Helz, G. R., and Miller, C. V., 2001. Reconstructing the rise of recent coastal anoxia; molybdenum in Chesapeake Bay sediments. *Geochimica Et Cosmochimica Acta* **65**, 237-252.

Aggett, J. and O' Brien, G.A, 1985. Detailed model for the mobility of arsenic in lacutrine sediments based on measurements in Lake Ohakuri. *Environmental Science & Technology* **19**, 231-238.

Ahmann, D. K., Hemond, H.F., Lovely, D.R., Morel, F.M.M, 1997. Microbial Mobilization of arsenic from sediments of the Aberjona Watershed. *Environmental Science & Technology* **31**, 2923-2930.

Anderson, R. F., Fleisher, M. Q., and Lehuray, A. P., 1989. Concentration, oxidation-state, and particulate flux of uranium in the Black-Sea *Geochimica Et Cosmochimica Acta* **53**, 2215-2224.

Andreae, M. O., 1979. Arsenic speciation in seawater and interstitial waters: The influence of biological-chemical interactions on the chemistry of a trace element. *Limnology and Oceanography* **24**, 440-452.

Antelo, J., Avena, M., Fiol, S., Lopez, R., and Arce, F., 2005. Effects of pH and ionic strength on the adsorption of phosphate and arsenate at the goethite-water interface *Journal of Colloid and Interface Science* **285**, (2) 476-486.

Appelo, C. A. J., Van Der Weiden., M.J.J., Tournassat, C., Charlet, L., 2002. Surface Complexation of ferrous iron and carbonate on ferrihydrite and the mobilization of arsenic. *Environmental Science & Technology* **36,** 3096-3103.

Bailey, J. E. and Ollis, D. F., 1986. *Biochemical Engineering Fundamentals*. McGraw-Hill Science.

Balistrieri, L. S., Murray, J. W., and Paul, B., 1992. The biogeochemical cycling of trace-metals in the water column of Lake Sammamish, Washington-Response to seasonally anoxic conditions. *Limnology and Oceanography* **37**, 529-548.

Belzile, N., 1988. The Fate of Arsenic in Sediments of the Laurentian Trough. *Geochimica Et Cosmochimica Acta* **52**, 2293-2302.

Belzile, N. and Tessier, A., 1990. Interactions between Arsenic and Iron Oxyhydroxides in Lacustrine Sediments. *Geochimica Et Cosmochimica Acta* **54**, 103-109.

Boicourt, W., 1992. Influences of circulation processes on dissolved oxygen in Chesapeake Bay In: Smith, D. E., Leffler, M., and Mackiernan, G. (Ed.),*Oxygen Dynamics in the Chesapeake Bay: A Synthesis of Recent Research* Maryland and Virginia Sea Grant Colleges, College Park, MD.

Bonneville, S., Van Cappellen, P., and Behrends, T., 2004. Microbial reduction of iron(III) oxyhydroxides: effects of mineral solubility and availability. *Chemical Geology* **212**, 255-268.

Borole, D. V., Krishnaswami, S., and Somayajulu, B. L. K., 1977. Investigation of dissolved uranium, silicon, and on particulate trace-elements in estuaries *Estuarine and Coastal Marine Science* **5**, 743-754.

Borole, D. V., Krishnaswami, S., and Somayajulu, B. L. K., 1982. Uranium isotopes in rivers, estuaries and adjacent coastal sediment of western India-their weathering, transport and oceanic budget. *Geochimica Et Cosmochimica Acta* **46**, 125-137.

Bose, P. and Sharma, A., 2002. Role of iron in controlling speciation and mobilization of arsenic in subsurface environment. *Water Research* **36**, 4916-4926.

Bostick, B. C., and Fendorf, S., 2003. Arsenite sorption on triolite (FeS) and pyrite (FeS_2). *Geochimica Et Cosmochimica Acta* **67**, 909-921.

Bratton, J. F., Colman, S. M., and Seal, R. R., 2003. Eutrophication and carbon sources in Chesapeake Bay over the last 2700 yr: Human impacts in context. *Geochimica Et Cosmochimica Acta* **67**, 3385-3402.

Breitburg, D. L., Sanders, J. G., Gilmour, C. C., Hatfield, C. A., Osman, R. W., Riedel, G. F., Seitzinger, S. B., and Sellner, K. G., 1999. Variability in responses to nutrients and trace elements, and transmission of stressor effects through an estuarine food web. *Limnology and Oceanography* **44**, 837-863.

Brendel, P. J. and Luther, G. W., 1995. Development of a Gold Amalgam Voltammetric Microelectrode for the Determination of Dissolved Fe, Mn, O2, and S in Porewaters of Marine and Fresh-Water Sediments. *Environmental Science & Technology* **29**, 751-761.

Bristow, G. and Taillefert, M., 2007, A Matlab-based software to integrate voltammetric scans and associated parameters from electrochemical analyzers. *Computers and Geosciences,* In Press.

Bruland, K. W., 1980. Oceanographic distribution of cadmium, zinc, nickel, and copper in the North Pacific *Earth and Planetary Science Letters* **47**, 176-198.

Bruland, K. W., Donat, J. R., and Hutchins, D. A., 1991. Interactive influences of bioactive trace-metals on biological production in oceanic waters *Limnology and Oceanography* **36**, 1555-1577.

Burdige, D. J., 1991. The Kinetics of Organic-Matter Mineralization in Anoxic Marine-Sediments. *Journal of Marine Research* **49**, 727-761.

Burdige, D. J., 2001. Dissolved organic matter in Chesapeake Bay sediment pore waters. *Organic Geochemistry* **32**, 487-505.

Burdige, D. J. and Homstead, J., 1994. Fluxes of Dissolved Organic-Carbon from Chesapeake Bay Sediments. *Geochimica Et Cosmochimica Acta* **58**, 3407-3424.

Burgess, J., 1988. Ions in Solution: Basic Principles of Chemical Interactions. Ellis Horwood-Wiley, New York, 191.

Burton, E.D., Bush, R.T., and Sullivan, L.A., 2006. Sedimentary iron geochemistry in acidic waterways associated with coastal lowland acid sulfate soils. *Geochimica Et Cosmochimica Acta* **70** (22), 5455-5468.

Caccia, V. G. and Millero, F. J., 2003. The distribution and seasonal variation of dissolved trace metals in Florida Bay and adjacent waters. *Aquatic Geochemistry* **9**, 111-144.

Caccia, V. G., Millero, F. J., and Palanques, A., 2003. The distribution of trace metals in Florida Bay sediments. *Marine Pollution Bulletin* **46**, 1420-1433.

Canuel, E. A., 2001. Relations between river flow, primary production and fatty acid composition of particulate organic matter in San Francisco and Chesapeake Bays: a multivariate approach. *Organic Geochemistry* **32**, 563-583.

Chant, R. J., 2002. Secondary circulation in a region of flow curvature: Relationship with tidal forcing and river discharge. *Journal of Geophysical Research-Oceans* **107**.

Charlet, L., Bosbach, D., and Peretyashko, T. 2002. Natural attenuation of TCE, As, Hg linked to the heterogeneous oxidation of Fe(II): an AFM study. *Chemical Geology* **190**, 303-319.

Chiffoleau, J. F., Cossa, D., Auger, D., and Truquet, I., 1994. Trace-metal distribution, partition and fluxes in the Seine Estuary (France) in low discharge regime. *Marine Chemistry* **47**, 145-158.

Chiu, V. Q. and Hering, J. G., 2000. Arsenic adsorption and oxidation at manganite surfaces. 1. Method for simultaneous determination of adsorbed and dissolved arsenic species. *Environmental Science & Technology* **34**, 2029-2034.

Chow, S. and Taillefert, M., 2005. Biogeochemical cycling of arsenic at the sediment-water interface of a recently flooded freshwater sediment. In: *Advances in Arsenic Research: Integration of experimental and observational studies and implications for mitigation*. O'Day, P. A., Vlassopoulos, D., Meng, X., and Benning, L. (Ed.) ACS Symposium Series 915, 220-234.

Coffey, M., Dehairs, F., Collette, O., Luther, G., Church, T., and Jickells, T., 1997. The behavior of dissolved barium in estuaries. *Estuarine Coastal and Shelf Science* **45**, 113-121.

Cooper, D. C. and Morse, J. W., 1998. Biogeochemical controls on trace metal cycling in anoxic marine sediments. *Environmental Science & Technology* **32**, 327-330.

Cullen, W. R. and Reimer, K.J., 1989. Arsenic speciation in the environment. *Chemistry Reviews* **89**, 713-764.

Cutter, G. A., 1991. Trace-Elements in Estuarine and Coastal Waters - United-States Studies from 1986-1990. *Reviews of Geophysics* **29**, 639-644.

DeGroot, A..J, Salomons, W., Allersma, E., 1976. *Processes affecting heavy metals in estuarine sediments*. Estuarine Chemistry Series, Academic Press, New York, 131-157.

Dixit, S. and Hering, J. G., 2003. Comparison of arsenic(V) and arsenic(III) sorption onto iron oxide minerals: Implications for arsenic mobility. *Environmental Science & Technology* **37**, 4182-4189.

Doucet, C., Dutheil, D., Petit, I., Zhang, K., Eugene, M., Touchard, G., Wahl, A., Seguin, F., Milinkevitch, S., Hauet, T., and Mauco, G., 2004. Influence of colloid, preservation medium and trimetazidine on renal medulla injury. *Biochimica Et Biophysica Acta-General Subjects* **1673**, 105-114.

Driehaus, W., Seith, R., and Jekel, M., 1995. Oxidation of arsenic(III) with manganese oxides in water treatment. *Water Resources* **29**, 297-305.

Dzombak, A. M., and Morel F.M.M, 1990. *Surface Complexation Modeling: Hydrous Ferric Oxide*. John Wiley & Sons, New York.

Feeney, R. and Kounaves, S.P., 2000. On-site analysis of arsenic in groundwater using a microfabricated gold ultramicroelectrode array. *Analytical Chemistry* **72**, 2222-2228.

Ferguson and Gavis, J., 1972. A review of the arsenic cycle in natural waters. *Water Research* **6**, 1259-1274.

Fischer, H. B., List, E. J., Koh, R. C. Y., Imberger, J., and Brooks, N. H., 1979. *Mixing in inland and coastal waters.* Academic Press, Inc., San Diego, California.

Fisher, T. R., Hagy, J. D., and Rochelle-Newall, E., 1998. Dissolved and particulate organic carbon in Chesapeake Bay. *Estuaries* **21**, 215-229.

Froelich, P. N., Klinkhammer, G. P., Bender, M. L., Luedtke, N. A., Heath, G. R., Cullen, D., Dauphin, P., Hammond, D., Hartman, B., and Maynard, V., 1979. Early oxidation of organic- matter in pelagic sediments of the Eastern Equatorical Atlantic-suboxic diagenesis. *Geochimica Et Cosmochimica Acta* **43**, 1075-1090.

Fugate, D.C., and Chant, R.J., 2005. Near-bottom shear stresses in a small, highly stratified estuary. Journal of Geophysical Research **110**, C03022, doi: 10.1029/2004JC002563.

Fugate, D. C., Friedrichs, C. T., and Sanford, L. P., 2007. Lateral dynamics and associated transport of sediment in the upper reaches of a partially mixed estuary, Chesapeake Bay, USA. *Continental Shelf Research* **27**, 679-698.

Glazer, B. T., Luther, G. W., Konovalov, S. K., Friederich, G. E., Nuzzio, D. B., Trouwborst, R. E., Tebo, B. M., Clement, B., Murray, K., and Romanov, A. S., 2006a. Documenting the suboxic zone of the Black Sea via high-resolution real-time redox profiling. *Deep-Sea Research Part II-Topical Studies in Oceanography* **53**, 1740-1755.

Glazer, B. T., Luther, G. W., Konovalov, S. K., Friederich, G. E., Trouwborst, R. E., and Romanov, A. S., 2006b. Spatial and temporal variability of the Black Sea suboxic zone. *Deep-Sea Research Part II-Topical Studies in Oceanography* **53**, 1756-1768.

Goh, K. H. and Lim, T. T., 2005. Arsenic fractionation in a fine soil fraction and influence of various anions on its mobility in the subsurface environment. *Applied Geochemistry* **20**, 229-239.

Goodrich, D. M. and Blumberg, A. F., 1991. The fortnightly mean circulation of Chesapeake Bay *Estuarine Coastal and Shelf Science* **32**, 451-462.

Guo, T., DeLaune, R. D., and Patrick, J., W.H., 1997. The influence of sediment redox chemistry on chemically active forms of arsenic, cadmium, chromium, and zinc in estuarine sediment. *Environment International* **23**, 305-316.

Guo, X. Y. and Valle-Levinson, A., 2007. Tidal effects on estuarine circulation and outflow plume in the Chesapeake Bay. *Continental Shelf Research* **27**, 20-42.

Hansel, C. M., Benner, S. G., and Fendorf, S., 2005. Competing Fe(II)-induced mineralization pathways of ferrihydrite. *Environmental Science & Technology* **39**, 7147-7153.

Harrington, J. M., Fendorf, S. E., and Rosenzweig, R. F., 1998. Biotic generation of arsenic(III) in metal(loid)-contaminated freshwater lake sediments. *Environmental Science & Technology* **32**, 2425-2430.

Harris, R. L., Helz, G. R., and Cory, R. L., 1975. Processes Affecting Vertical Distribution of Trace Components in Chesapeake Bay. In: *Marine Chemistry in the Coastal Environment.* Church, T.M. (Ed). ACS Symposium Series 18, 176-185.

Hartwell, S. I. and Hameedi, J., 2007. Magnitude and Extent of Contaminated Sediment and Toxicity in Chesapeake Bay. NOAA/National Ocean Service/National Centers for Coastal and Ocean Science/Center for Coastal Monitoring and Assessment/ Coastal & Oceanographic Assessments Status and Trends Team, Sliver Spring, MD.

Herszage, J. and Afonso, M. D., 2003. Mechanism of hydrogen sulfide oxidation by manganese(IV) oxide in aqueous solutions. *Langmuir* **19**, 9684-9692.

Hoeft, S. E., Lucas, F., Hollibaugh, J. T., and Oremland, R. S., 2002. Characterization of microbial arsenate reduction in the anoxic bottom waters of Mono Lake, California. *Geomicrobiology Journal* **19**, 23-40.

Holdren, G. R., Bricker, O. P., and Matisoff, G., 1975. Model for Control of Dissolved Manganese in Interstitial Waters of Chesapeake Bay. In: *Marine Chemistry in the Coastal Environment.* Church, T.M. (Ed). ACS Symposium Series 18, 364-381.

Horneman, A., Van Geen, A., Kent, D. V., Mathe, P. E., Zheng, Y., Dhar, R. K., O'Connell, S., Hoque, M. A., Aziz, Z., Shamsudduha, M., Seddique, A. A., and Ahmed, K. M., 2004. Decoupling of As and Fe release to Bangladesh groundwater under reducing conditions. Part 1: Evidence from sediment profiles. *Geochimica Et Cosmochimica Acta* **68**, 3459-3473.

Huddlestun, P. F., 1988. A revision of the lithostratigraphic units of the coastal plain of Georgia-The Miocene Through Holocene. Georgia Department of Natural Resources, Environmental Protection Division, Georgia Geological Survey, Atlanta.

Hussain, N., Church, T. M., and Kim, G., 1999. Use of Rn-222 and Ra-226 to trace groundwater discharge into the Chesapeake Bay. *Marine Chemistry* **65**, 127-134.

Hyacinthe, C., Anschutz, P., Carbonel, P., Jouanneau, J. M., and Jorissen, F. J., 2001. Early diagenetic processes in the muddy sediments of the Bay of Biscay. *Marine Geology* **177**, 111-128.

Jain, A., Raven, K. P., and Loeppert, R. H., 1999. Arsenite and arsenate adsorption on ferrihydrite: surface charge reduction and net OH- release stoichiometry. *Environmental Science & Technology* **1999**, 1179-1184.

Jain, C. K. and Ali, I., 2000. Arsenic: Occurrence, toxicity and speciation techniques. *Water Research* **34**, 4304-4312.

Janssen, F., Faerber, P., Huettel, M., Meyer, V., and Witte, U., 2005. Pore-water advection and solute fluxes in permeable marine sediments (I): Calibration and performance of the novel benthic chamber system Sandy. *Limnology and Oceanography* **50**, 768-778.

Jay, D. A. and Smith, J. D., 1990. Circulation, density distribution and neap-spring transitions in the Columbia River Estuary *Progress in Oceanography* **25**, 81-112.

Jin, Q. S. and Bethke, C. M., 2005. Predicting the rate of microbial respiration in geochemical environments. *Geochimica Et Cosmochimica Acta* **69**, 1133-1143.

Johnson, D. L. and Pilson, M. E. Q., 1975. Oxidation of arsenite in seawater. *Environmental Letters* **8**, 157-171.

Jonas, R. B., 1997. Bacteria, dissolved organics and oxygens consumption in salinity stratified Chesapeake Bay, an anoxia paradigm. *American Zoologist* **37**, 612-620.

Jones, C. A., Langner, H. W., Anderson, K., McDermott, T. R., and Inskeep, W. P., 2000. Rates of microbially mediated arsenate reduction and solubilization. *Soil Science Society of America Journal* **64**, 600-608.

Jones, S. E., Jago, C. F., Bale, A. J., Chapman, D., Howland, R. J. M., and Jackson, J., 1998. Aggregation and resuspension of suspended particulate matter at a seasonally stratified site in the southern North Sea: physical and biological controls. *Continental Shelf Research* **18**, 1283-1309.

Kastler, J. A. and Wiberg, P. L., 1996. Sedimentation and boundary changes of Virginia salt marshes. *Estuarine Coastal and Shelf Science* **42**, 683-700.

Kemp, W. M., Boynton, W. R., Adolf, J. E., Boesch, D. F., Boicourt, W. C., Brush, G., Cornwell, J. C., Fisher, T. R., Glibert, P. M., Hagy, J. D., Harding, L. W., Houde, E. D., Kimmel, D. G., Miller, W. D., Newell, R. I. E., Roman, M. R., Smith, E.

M., and Stevenson, J. C., 2005. Eutrophication of Chesapeake Bay: historical trends and ecological interactions. *Marine Ecology-Progress Series* **303**, 1-29.

Kim, G., Hussain, N., Scudlark, J. R., and Church, T. M., 2000. Factors influencing the atmospheric depositional fluxes of stable Pb, Pb-210, and Be-7 into Chesapeake Bay. *Journal of Atmospheric Chemistry* **36**, 65-79.

Kneebone, P. E., O'Day, P. A., Jones, N., and Hering, J. G., 2002. Deposition and fate of arsenic in iron- and arsenic-enriched reservoir sediments. *Environmental Science & Technology* **36**, 381-386.

Knight, M. A. and Pasternack, G. B., 2000. Sources, input pathways, and distributions of Fe, Cu, and Zn in a Chesapeake Bay tidal freshwater marsh. *Environmental Geology* **39**, 1359-1371.

Koh, C. H., Khim, J. S., Araki, H., Yamanishi, H., Mogi, H., and Koga, K., 2006. Tidal resuspension of microphytobenthic chlorophyll a in a Nanaura mudflat, Saga, Ariake Sea, Japan: flood-ebb and spring-neap variations. *Marine Ecology-Progress Series* **312**, 85-100.

Kostka, J. E., Haefele, E., Viehweger, R., and Stucki, J. W., 1999. Respiration and dissolution of iron(III) containing clay minerals by bacteria. *Environmental Science & Technology* **33**, 3127-3133.

Kostka, J. E. and Luther, G. W., 1994. Partitioning and speciation of solid-phase iron in salt-marsh sediments. *Geochimica Et Cosmochimica Acta* **58**, 1701-1710.

Kuwabara, J. S. and Baker, J. E., 1993. Trace Contaminants and Nutrients in Estuaries - the Importance of Process Interdependence. *Estuaries* **16**, 383-384.

Lawson, N. M., Mason, R. P., and Laporte, J. M., 2001. The fate and transport of mercury, methylmercury, and other trace metals in Chesapeake Bay tributaries. *Water Research* **35**, 501-515.

Lee, B. G. and Fisher, N. S., 1993. Microbially mediated cobalt oxidation in seawater revealed by radiotracer experiments. *Limnology and Oceanography* **38**, 1593-1602.

Lesley, M. P., 2002. The Flux and fate of metalloids from coal fired power plants to rivers. Masters of Science in Geochemistry, Georgia Institute of Technology.

Lewis, B., Glazer, B. T., Montbriand, P. J., Luther, G. W. I., Nuzzio, D. B., Deering, T., Ma, S. F., and Theberge, S., 2007. Short-term and interannual variability of redox-sensitive chemical parameters in hypoxic/anoxic bottom waters of the Chesapeake Bay. *Marine Chemistry* **105**, 296-308.

Li, H. and Smart, R. B., 1996. Determination of sub-nanomolar concentration of arsenic(III) in natural waters by square wave cathodic stripping voltammetry. *Analytica Chimica Acta* **325**, 25-32.

Li, M., Zhong, L. J., and Boicourt, W. C., 2005. Simulations of Chesapeake Bay estuary: Sensitivity to turbulence mixing parameterizations and comparison with observations. *Journal of Geophysical Research-Oceans* **110,** C12004, doi:10.1029/2004JC002585.

Li, Y. H., Burkhardt, L., and Teraoka, H., 1984. Desorption and Coagulation of Trace-Elements During Estuarine Mixing. *Geochimica Et Cosmochimica Acta* **48**, 1879-1884.

Lienemann, C. P., Taillefert, M., Perret, D., and Gaillard, J. F., 1997. Association of cobalt and manganese in aquatic systems: Chemical and microscopic evidence. *Geochimica Et Cosmochimica Acta* **61**, 1437-1446.

Lin, J., Xie, L., Pietrafesa, L. J., Shen, J., Mallin, M. A., and Durako, M. J., 2006. Dissolved oxygen stratification in two micro-tidal partially-mixed estuaries. *Estuarine Coastal and Shelf Science* **70**, 423-437.

Luther, G. W., Church, T. M., and Powell, D., 1991. Sulfur speciation and sulfide oxidation in the water column of the Black-Sea. *Deep-Sea Research Part a-Oceanographic Research Papers* **38**, S1121-S1137.

Luther, G. W., Ferdelman, T., and Tsamakis, E., 1988. Evidence suggesting anaerobic oxidation of the bisulfide ion in Chesapeake Bay *Estuaries* **11**, 281-285.

Luther, G. W., Glazer, B. T., Hohmann, L., Popp, J. I., Taillefert, M., Rozan, T. F., Brendel, P. J., Theberge, S. M., and Nuzzio, D. B., 2001. Sulfur speciation monitored *in situ* with solid state gold amalgam voltammetric microelectrodes:

polysulfides as a special case in sediments, microbial mats and hydrothermal vent waters. *Journal of Environmental Monitoring* **3**, 61-66.

Luther, G. W., Glazer, B. T., Ma, S., Trouwborst, R. E., Moore, T. S., Metzger, E., Kraiya, C., Waite, T. J., Druschel, G., Sundby, B., Taillefert, M., Nuzzio, D. B., Shank, T. M., Lewis, B. L., and Brendel, P. J., 2007. Use of voltammetric solid-state (micro)electrodes for studying biogeochemical processes: Laboratory measurements to real time measurements. doi:10.1016/j.marchem.2007.03.002. *Marine Chemistry*

Luther, G. W., Nuzzio, D. B., and Wu, J. F., 1994. Speciation of Manganese in Chesapeake Bay Waters by Voltammetric Methods. *Analytica Chimica Acta* **284**, 473-480.

Luther, G. W. and Rickard, D. T., 2005a. Metal sulfide cluster complexes and their biogeochemical importance in the environment. *Journal of Nanoparticle Research* **7**, 389-407.

Luther, G. W. and Rickard, D. T., 2005b. Metal sulfide cluster complexes and their biogeochemical importance in the environment. *Journal of Nanoparticle Research* **7**, 713-733.

Luther, G. W., Rickard, D. T., Theberge, S., and Olroyd, A., 1996. Determination of metal (Bi)Sulfide stability constants of Mn2+, Fe2+, Co2+, Ni2+, Cu2+, and Zn2+ by voltammetric methods. *Environmental Science & Technology* **30**, 671-679.

Luther, G. W., Theberge, S. M., Rozan, T. F., Rickard, D., Rowlands, C. C., and Oldroyd, A., 2002. Aqueous copper sulfide clusters as intermediates during copper sulfide formation. *Environmental Science & Technology* **36**, 394-402.

Luther, G. W., Wu, J. F., and Cullen, J. B., 1995. Redox Chemistry of Iodine in Seawater - Frontier Molecular-Orbital Theory Considerations, *Advances in Chemistry* Series 244, 135-155.

Ma, S.F., Noble, A., Butcher, D., Trouwborst, R.E., and Luther, G.W., 2006. Removal of H_2S via an iron catalytic cycle and iron sulfide precipitation in the water column of dead end tributaries. *Estuarine Coastal and Shelf Science* **70**, 461-472.

MacCrehan, W. and Shea, D., 1995. Temporal relationship of thiols to inorganic sulfur compounds in anoxic Chesapeake Bay sediment porewater. In: *Geochemical*

Transformations of Sedimentary Sulfur. ACS Symposium Series 612, Washington, D.C., 294-310.

Madigan, M. T., Martinko, J. M., and Parker, J., 2003. *Brock Biology of Microorganisms*.10th Ed. Prentice Hall, Pearson Education, Inc., Upper Saddle River, NJ.

Manning, B. A. and Goldberg, S., 1996. Modeling arsenate competitive adsorption with phosphate and molybdate on oxide minerals. *Soil Science Society of America Journal* **60**, 121-131.

Manning, B. A. and Martens, D.A., 1997. Speciation of Arsenic(III) and Arsenic(V) in sediment extracts by high-performance liquid chromatography-hydride generation atomic adsorption spectrophotometry. *Environmental Science & Technology* **31**, 171-177.

Martino, M., Turner, A., Nimmo, A., and Millward, G. E., 2002. Resuspension, reactivity and recycling of trace metals in the Mersey Estuary, UK. *Marine Chemistry* **77**, 171-186.

Marvin-DiPasquale, M. C., Boynton, W. R., and Capone, D. G., 2003. Benthic sulfate reduction along the Chesapeake bay central channel. II. Temporal controls. *Marine Ecology-Progress Series* **260**, 55-70.

Marvin-DiPasquale, M. C. and Capone, D. G., 1998. Benthic sulfate reduction along the Chesapeake Bay central channel. I. Spatial trends and controls. *Marine Ecology-Progress Series* **168**, 213-228.

Mason, R. P., Kim, E. H., and Cornwell, J., 2004. Metal accumulation in Baltimore Harbor: current and past inputs. *Applied Geochemistry* **19**, 1801-1825.

Matisoff, G., Bricker, O. P., Holdren, G. R., and Kaerk, P., 1975. Spatial and Temporal Variations in Interstitial Water Chemistry of Chesapeake Bay Sediments. In: Marine Chemistry in the Coastal Environment. Church, T.M. (Ed) ACS Symposium Series 18, 343-363.

McBride, B. C. and Wolfe, R. S., 1971. Biosynthesis of dimethylarsine by methaanobacterium. *Biochemistry* **10**, 4312-4317.

Meng, X. G., Jing, C. Y., and Korfiatis, G. P., 2003. A review of redox transformation of arsenic in aquatic environments. In: *Biogeochemistry of Environmentally*

Important Trace Elements. Cai, Y and Braids, O.C. (Ed). ACS Symposium Series 835, 70-83.

Meng, X.G., Korfiatis, G.P. Bang, S.B, and Bang, K.W., 2002. Combined effects of anions on arsenic removal by iron hydroxides. *Toxicology Letters* **133**, 103-111.

Millero, F. J., 2000. Effect of changes in the composition of seawater on the density-salinity relationship. *Deep-Sea Research Part I-Oceanographic Research Papers* **47**, 1583-1590.

Millero, F. J. and Hawke, D. J., 1992. Ionic Interactions of Divalent Metals in Natural-Waters. *Marine Chemistry* **40**, 19-48.

Mok, W. M. and Wai, C. M., 1990. Distribution and mobilization of arsenic and antimony species in the Coeur D'Alene River, Idaho. *Environmental Science & Technology* **24**, 102-108.

Moore, J. N., Ficklin, W. H., and Johns, C., 1988. Partitioning of arsenic and metals in reducing sulfidic sediments *Environmental Science & Technology* **22**, 432-437.

Morris, A. W., Bale, A. J., and Howland, R. J. M., 1982. The dynamics of estuarine manganese cycling. *Estuarine Coastal and Shelf Science* **14**, 175-192.

Morse, J. W. and Luther, G. W., 1999. Chemical influences on trace metal-sulfide interactions in anoxic sediments. *Geochimica Et Cosmochimica Acta* **63**, 3373-3378.

Mucci, A., Boudreau, B., and Guignard, C., 2003. Diagenetic mobility of trace elements in sediments covered by a flash flood deposit: Mn, Fe and As. *Applied Geochemistry* **18**, 1011-1026.

Mukhopadhyay, R., Rosen, B., Phung, L.T., and Silver, S., 2002. Microbial arsenic: from geocycles to genes and enzymes. *FEMS Microbiology Reviews.* **26**, 311-325.

Murphy, J., and Riley, J.P., 1962. A modified single solution method for the determination of phosphate in natural waters. *Analytica Chimica Acta* **27**, 31-36.

Newman, D. K., Ahmann, D., and Morel, F. M. M., 1998. A brief review of microbial arsenate respiration. *Geomicrobiology* **15**, 255-268.

O'Day, P. A., Vlassopoulos, D., Root, R., and Rivera, N., 2004. The influence of sulfur and iron on dissolved arsenic concentrations in the shallow subsurface under changing redox conditions. *Proceedings of the National Academy of Sciences of the United States of America* **101**, 13703-13708.

Ona-Nguema, G., Morin, G., Juillot, F., Calas, G., and Brown, G. E., 2005. EXAFS analysis of arsenite adsorption onto two-line ferrihydrite, hematite, goethite, and lepidocrocite. *Environmental Science & Technology* **39**, 9147-9155.

Oremland, R. S., Dowdle, P. R., Hoeft, S., Sharp, J. O., Schaefer, J. K., Miller, L. G., Blum, J. S., Smith, R. L., Bloom, N. S., and Wallschlaeger, D., 2000. Bacterial dissimilatory reduction of arsenate and sulfate in meromictic Mono Lake, California. *Geochimica Et Cosmochimica Acta* **64**, 3073-3084.

Oremland, R. S., Hoeft, S. E., Santini, J. A., Bano, N., Hollibaugh, R. A., and Hollibaugh, J. T., 2002. Anaerobic oxidation of arsenite in Mono Lake water and by facultative, arsenite-oxidizing chemoautotroph, strain MLHE-1. *Applied Environmental Microbiology* **68**, 4795-4802.

Oremland, R. S. and Stolz, J. F., 2003. The ecology of arsenic. *Science* **300**, 939-944.

Oremland, R. S. and Stolz, J. F., 2005. Arsenic, microbes and contaminated aquifers. *Trends in Microbiology* **13**, 45-49.

Ouvrard, S., de Donato, P., Simonnot, M. O., Begin, S., Ghanbaja, J., Alnot, M., Duval, Y. B., Lhote, F., Barres, O., and Sardin, M., 2005. Natural manganese oxide: Combined analytical approach for solid characterization and arsenic retention. *Geochimica Et Cosmochimica Acta* **69**, 2715-2724.

Owens, M. and Cornwell, J. C., 1995. Sedimentary evidence for decreased heavy-metals inputs to the Chesapeake Bay. *Ambio* **24**, 24-27.

Pierce, M. L. and Moore, C. B., 1982. Adsorption of arsenite and arsenate on amorphous iron hydroxide. *Water Research* **16**, 1247-1253.

Postma, D., 1985. Concentrations of Mn and separation from Fe in sediments 1.1 Kinetics and stoichiometry of the reaction between birnessite and dissolved Fe(II) at 10-degrees-C *Geochimica Et Cosmochimica Acta* **49**, 1023-1033.

Poulton, S. W., 2003. Sulfide oxidation and iron dissolution kinetics during the reaction of dissolved sulfide with ferrihydrite. *Chemical Geology* **202**, 79-94.

Poulton, S. W., Krom, M. D., and Raiswell, R., 2004. A revised scheme for the reactivity of iron (oxyhydr)oxide minerals towards dissolved sulfide. *Geochimica Et Cosmochimica Acta* **68**, 3703-3715.

Precht, E., Franke, U., Polerecky, L., and Huettel, M., 2004. Oxygen dynamics in permeable sediments with wave-driven pore water exchange. *Limnology and Oceanography* **49**, 693-705.

Preda, M. and Cox, M. E., 2002. Trace metal occurrence and distribution in sediments and mangroves, Pumicestone region, southeast Queensland, Australia. *Environment International* **28**, 433-449.

Price, N. M. and Morel, F. M. M., 1991. Colimitation of phytoplankton growth by nickel and nitrogen. *Limnology and Oceanography* **36**, 1071-1077.

Pritchard, D. W., 1952. Salinity distribution and circulation in the Chesapeake Bay estuarine system. *Journal of Marine Research* **11**, 106-123.

Rickard, D. and Luther, G.W., 2003. Aqueous metal sulfide clusters in marine sediments: Implications for transport, mineral formation and ecology. *Geochimica Et Cosmochimica Acta* **67**, A398-A398.

Rickard, D. and Luther, G. W., 2006. Metal sulfide complexes and clusters. *Sulfide Mineralogy and Geochemistry*. Reviews in Mineralogy & Geochemistry 61, 421-504.

Rickard, D. and Luther, G. W., 2007. Chemistry of iron sulfides. *Chemical Reviews* **107**, 514-562.

Rickard, D., Morse, J. W., and Luther, G. W., 2004. Clusters, nanoparticles and the solubility constant. *Geochimica Et Cosmochimica Acta* **68**, A222-A222.

Riedel, G. F., Sanders, J. G., and Osman, R. W., 1999. Biogeochemical control on the flux of trace elements from estuarine sediments: effects of seasonal and short-term hypoxia. *Marine Environmental Research* **47**, 349-372.

Rochette, E. A., Bostick, B. C., Li, G. C., and Fendorf, S., 2000. Kinetics of arsenate reduction by dissolved sulfide. *Environmental Science & Technology* **34**, 4714-4720.

Roden, E. E. and Tuttle, J. H., 1992. Sulfide Release from Estuarine Sediments Underlying Anoxic Bottom Water. *Limnology and Oceanography* **37**, 725-738.

Roden, E. E. and Tuttle, J. H., 1993. Inorganic Sulfur Cycling in Mid and Lower Chesapeake Bay Sediments. *Marine Ecology-Progress Series* **93**, 101-118.

Roden, E. E. and Tuttle, J. H., 1996. Carbon cycling in mesohaline Chesapeake Bay sediments .2. Kinetics of particulate and dissolved organic carbon turnover. *Journal of Marine Research* **54**, 343-383.

Roden, E. E., Tuttle, J. H., Boynton, W. R., and Kemp, W. M., 1995. Carbon Cycling in Mesohaline Chesapeake Bay Sediments POC Deposition Rates and Mineralization Pathways. *Journal of Marine Research* **53**, 799-819.

Roman, M., Zhang, X., McGilliard, C., and Boicourt, W., 2005. Seasonal and annual variability in the spatial patterns of plankton biomass in Chesapeake Bay. *Limnology and Oceanography* **50**, 480-492.

Rue, E. L., Smith, G. J., Cutter, G. A., and Bruland, K. W., 1997. The response of trace element redox couples to suboxic conditions in the water column. *Deep-Sea Research Part I-Oceanographic Research Papers* **44**, 113-134.

Ryu, J., Gao, S., Dahlgren, R.A., Zierenberg, R.A., 2002. Arsenic distribution, speciation and solubility in shallow groundwater of Owens Dry Lake, California. *Geochimica Et Cosmochimica Acta* **66**, 2981-2994.

Sadiq, M., 1997. Arsenic chemistry in soils: An overview of thermodynamic predictions and field observations. *Water Air and Soil Pollution* **93**, 117-136.

Saltikov, C. W., Wildman, R. A., and Newman, D. K., 2005. Expression dynamics of arsenic respiration and detoxification in Shewanella sp strain ANA-3. *Journal of Bacteriology* **187**, 7390-7396.

Sarin, M. M. and Church, T. M., 1994. Behavior of Uranium During Mixing in the Delaware and Chesapeake Estuaries. *Estuarine Coastal and Shelf Science* **39**, 619-631.

Schubel, J. R., 1968. Turbidity Maximum of Northern Chesapeake Bay. *Science* **161**, 1013-1015.

Schubel, J. R. and Kana, T. W., 1972. Agglomeration of Fine-Grained Suspended Sediment in Northern Chesapeake Bay. *Powder Technology* **6**, 9-16.

Schubel, J. R. and Pritchard, D. W., 1985. Responses in the Milieu and Biology of Upper Chesapeake Bay to Variations in Discharge of the Susquehanna River. *Estuaries* **8**, A53-A53.

Schubel, J.R. 1986. Responses of Upper Chesapeake Bay to Variations in Discharge of the Susquehanna River. *Estuaries* **9**, 236-249.

Scott, M. J. and Morgan, J.J., 1995. Reactions at oxide surfaces: Part 1. Oxidation of As(III) by synthetic birnessite. *Environmental Science & Technology* **29**, 1898-1905.

Scudlark, J. R., Rice, K. C., Conko, K. M., Bricker, O. P., and Church, T. M., 2005. Transmission of atmospherically derived trace elements through an undeveloped, forested Maryland watershed. *Water Air and Soil Pollution* **163**, 53-79.

Shaw, D., 2006. Mobility of arsenic in saturated, laboratory test sediments under varying pH conditions. *Engineering Geology* **85**, 158-164.

Shaw, T. J., Moore, W. S., Kloepfer, J., and Sochaski, M. A., 1998. The flux of barium to the coastal waters of the southeastern USA: The importance of submarine groundwater discharge. *Geochimica Et Cosmochimica Acta* **62**, 3047-3054.

Shaw, T. J., Sholkovitz, E. R., and Klinkhammer, G., 1994. Redox Dynamics in the Chesapeake Bay - the Effect on Sediment-Water Uranium Exchange. *Geochimica Et Cosmochimica Acta* **58**, 2985-2995.

Sholkovitz, E. R., Shaw, T. J., and Schneider, D. L., 1992. The geochemistry of rare-earth elements in the seasonally anoxic water column and porewaters of Chesapeake Bay *Geochimica Et Cosmochimica Acta* **56**, 3389-3402.

Silver, S.and Phung, L.T., 1996. Bacterial heavy metal resistance: New surprises *Annual Review of Microbiology*, 50: 753-789.

Silver, S.and Phung, L.T., 2005. A bacterial view of the periodic table: genes and proteins for toxic inorganic ions. *Journal of Industrial Microbiology & Biotechnology*, 32 (11-12): 587-605.

Skrabal, S. A., Donat, J. R., and Burdige, D. J., 2000. Pore water distributions of dissolved copper and copper-complexing ligands in estuarine and coastal marine sediments. *Geochimica Et Cosmochimica Acta* **64**, 1843-1857.

Slotnick, M. J., Meliker, J. R., and Nriagu, J. O., 2006. Effects of time and point-of-use devices on arsenic levels in Southeastern Michigan drinking water, USA. *Science and the Total Environment* **369**, 42-50.

Smedley, P. L. and Kinniburgh, D. G., 2002. A review of the source, behavior and distribution of arsenic in natural waters. *Applied Geochemistry* **17**, 517-568.

Stolz, J. F. and Oremland, R. S., 1999. Bacterial respiration of arsenic and selenium. *FEMS Microbiology Review* **23**, 615-627.

Stookey, L. L., 1970. Ferrozine: a new spectrophotometric reagent for iron. *Analytical Chemistry* **42**, 779-782.

Strickland, J. D. H., 1952. The preparation and properties of silicomolybdic acid. *Journal of the American Chemical Society* **74**, 862-876.

Stumm, W., 1992. *Chemistry of the Solid-Water Interface*. Wiley-Interscience, New York.

Stumm, W. and Morgan, J. J., 1996. *Aquatic Chemistry Chemical Equilibria and Rates in Natural Waters*. John-Wiley and Sons, Inc, New York.

Taillefert, M., Hover, V. C., Rozan, T. F., Theberge, S. M., and Luther, G. W., 2002a. The influence of sulfides on soluble organic-Fe(III) in anoxic sediment porewaters. *Estuaries* **25**, 1088-1096.

Taillefert, M., MacGregor, B. J., Gaillard, J. F., Lienemann, C. P., Perret, D., and Stahl, D. A., 2002b. Evidence for a dynamic cycle between Mn and Co in the water column of a stratified lake. *Environmental Science & Technology* **36**, 468-476.

Taillefert, M., Rozan, T. F., Glazer, B. T., Herszage, J., Trouwborst, R. E., and Luther, G.W., 2002c. Seasonal Variations of Soluble Organic-Fe(III) in Sediment Porewawters as Revealed by Voltammetric Microelectrodes. In: *Environmental Electrochemistry*: *Analyses of Trace Element Biogeochemistry*. Rozan, T. and Taillefert, M. (Ed.), ACS Symposium Series 811, Washington, D.C., 247-264.

Tovar-Sanchez, A., Sanudo-Wilhelmy, S. A., and Flegal, A. R., 2004. Temporal and spatial variations in the biogeochemical cycling of cobalt in two urban estuaries: Hudson River Estuary and San Francisco Bay. *Estuarine Coastal and Shelf Science* **60**, 717-728.

Turner, A. and Millward, G. E., 2002. Suspended particles: Their role in estuarine biogeochemical cycles. *Estuarine Coastal and Shelf Science* **55**, 857-883.

Turner, A., Nimmo, M., and Thuresson, K. A., 1998. Speciation and sorptive behavior of nickel in an organic-rich estuary (Beaulieu, UK). *Marine Chemistry* **63**, 105-118.

Van den berg, C. M. G., 1993. Complex-Formation and the Chemistry of Selected Trace-Elements in Estuaries. *Estuaries* **16**, 512-520.

Violante A, and Pigna M. 2002. Competitive sorption of arsenate and phosphate on different clay minerals and soils *Soil Science Society Of America Journal* **66**, 6, 1788-1796.

Wilkin, R. T., Wallschlager, D., and Ford, R. G., 2003. Speciation of arsenic in sulfidic waters. *Geochemical Transactions* **4**, 1-7.

Williams, P. N., Price, A. H., Raab, A., Hossain, S. A., Feldmann, J., and Meharg, A. A., 2005. Variation in arsenic speciation and concentration in paddy rice related to dietary exposure. *Environmental Science & Technology* **39**, 5531-5540.

Williams, P. N., Raab, A., Feldmann, J., and Meharg, A. A., 2007. Market basket survey shows elevated levels of As in South Central U.S. processed rice compared to California: consequences for human dietary exposure. *Environmental Science & Technology* **41**, 2178-2183.

Xu, H., Allard, B., and Grimvall, A., 1988. Influence of pH and organic substance on the adsorption of As(V) on geologic materials. *Water Air Soil Pollution* **57**, 269-278.

Yan, X., Kerrick, R., and Hendry, M.J., 2000. Distribution of arsenic(III), Arsenic(V) and total inorganic arsenic in porewaters from a thick till and clay-rich aquitard sequence, Saskatchewan, Canada. *Geochimica Et Cosmochimica Acta* **62**, 2637-2648.

Zimmerman, A. R. and Canuel, E. A., 2001. Bulk organic matter and lipid biomarker composition of Chesapeake Bay surficial sediments as indicators of environmental processes. *Estuarine Coastal and Shelf Science* **53**, 319-341.

http://bicn.com/acic/ - (Accessed April, 25, 2005)
www.epa.gov\safewater- (Accessed April 25, 2005)
waterdata.usgs.gov./nwis (Accessed October, 1, 2007)